Advances in lithium-sulfur batteries

X. Zhang, H. Xie, C.-S. Kim, K. Zaghib, A. Mauger, C.M. Julien

Advances in Lithium–Sulfur Batteries

X. Zhang[1], H. Xie[2,*], C.-S. Kim[3], K. Zaghib[3], A. Mauger[4], C.M. Julien[4,*]

[1]SynPLi Consulting, 17300 Rochefort, France

[2]Northeast Normal University, National and Local United Engineering, Laboratory for Power Batteries, 5268 Renmin Str., Changchun, P.R. China

[3]Institut de Recherche d'Hydro-Québec (IREQ), 1800 Lionel-Boulet, Varennes, Québec, J3X 1S1, Canada

[4]Sorbonne Universités, UPMC Univ Paris 06, Institut de Minéralogie, de Physique des Matériaux et de Cosmochimie (IMPMC), CNRS UMR 7590, 4 place Jussieu, 75005 Paris, France

***Corresponding authors:** E-mail: xiehm136@nenu.edu.cn; Christian.Julien@upmc.fr

Keywords: Lithium-sulfur batteries; Polysulfides; Composite electrodes; Electrolyte; Separators; Mesopore structure

Abstract

This review is focused on the state-of-the-art of lithium-sulfur batteries. The great advantage of these energy storage devices in view of their theoretical specific capacity (2500 Wh kg^{-1}, 2800 Wh L^{-1}, assuming complete reaction to Li_2S) has been the motivation for a huge amount of works. However, these batteries suffer of disadvantages that have restricted their applications such as high electrical resistance, capacity fading, self-discharge, mainly due to the so-called shuttle effect. Strategies have been developed with the recent modifications that have been proposed as a remedy to the shuttle effect, and the insulating nature of the polysulfides. All the elements of the battery are concerned and the solution, as we present herewith, is a combination of modification of the cathode, of the separator, of the electrolyte, including the choice of binder, even though few binder-free architectures have now been proposed.

1. Introduction

Due to the rapid development in our societies, energy storage has become critical. In this context, lithium-ion batteries (LIBs) have enabled the commercialization of electric and plug-in hybrid cars. They are also used for current regulation and leveling, solving the intermittence problems of sustainable energy supply (windmills, photovoltaic plants) and integration on smart grids [1]. The huge advantage of the Li-S battery in view of its theoretical capacity (2500 Wh kg^{-1}, 2800 Wh L^{-1}, assuming complete reaction to Li_2S) [2] has been the motivation for a huge amount of works since its discovery. In addition, sulfur is very cheap. The concept of the Li-S battery dates from 1962 [3]. The first promising results were obtained in the late sixties with the use of organic electrolyte [4]. Unfortunately, this battery also suffers of disadvantages that have restricted its applications: high electrical resistance [5], capacity fading, self-discharge, mainly due to the so-called shuttle effect. All the reviews on Li-S batteries through the years have repeatedly reported these difficulties with which the community of researchers in electrochemistry struggle [6-10]. In addition, the problem of high resistance of the sulfur and the polysulfides has been solved by adding conductive elements, like carbon under different forms [11] in the cathode, at the expense of the amount of active material available for the electrochemical process [12]. Actually, if we add 40% of conductive carbon to the product, a figure that was still commonly met few years ago, the advantage with the lithium-ion batteries (LIBs) is small in terms of energy density and the volume density is even in favor of the LIBs [13]. Although these problems have never been completely solved, constant progress has been made, in particular in the recent years, giving hope today that these challenges will be met in the near future. It is the purpose of this work to review the results that have been obtained, mostly in the two last years, which justify this reasonable optimism. To limit the length of the review, attention is focused on the structural aspects and the electrochemical properties, but not on the synthesis aspects, which are detailed in the publications we have cited. In addition, we recommend the reading of a pertinent review on the atomic layer deposition applied to Li-S batteries that has been recently published [14].

In most cases, the capacities reported in the papers are reported by gram of sulfur (g_{sulfur}). However, this is not a value for a battery, not even for an electrode, but just for one component of an electrode. Such values are absolutely useless for a comparison between different composite concepts. Any useful comparison needs to refer to the energy density on cell level, and this information is rarely available. When available, we report it in this review; otherwise we do not mention the capacities in the original works since they are useless for a comparison between different composite concepts, and we

put the focus on the collection of the different approaches. Exceptions are results on which we wish to attract attention for their outstanding performance. Even though it does not permit any comparison with the performance at the cell level, the information available per gram of sulfur gives some insight on the ability of the composite to use all or a part of the sulfur in the cycling process.

The electrochemical reaction during the discharge proceeds approximately in three steps [15-16] illustrated in Fig. 1: (I) a reversible conversion of sulfur through stepwise reduction up to the formation of $S^0 \rightarrow S_4^{2-}$. These polysulfides are soluble, so that the reaction kinetics are fast. (II) a conversion of S_4^{2-}-polysulfides to solid Li_2S_2. This $S^{0.5-} \rightarrow S^-$ reduction is more difficult, because of the energy needed to nucleate the solid phase. (III) a conversion of solid Li_2S_2 to solid Li_2S. This is the most difficult step because of the sluggish diffusion of lithium in this solid environment [15, 17]. This decomposition in three steps is an approximation. In particular, electrochemical impedance spectroscopy [18] and in situ X-ray diffraction spectra [19] revealed that Li_2S appear immediately at the beginning of the lower plateau.

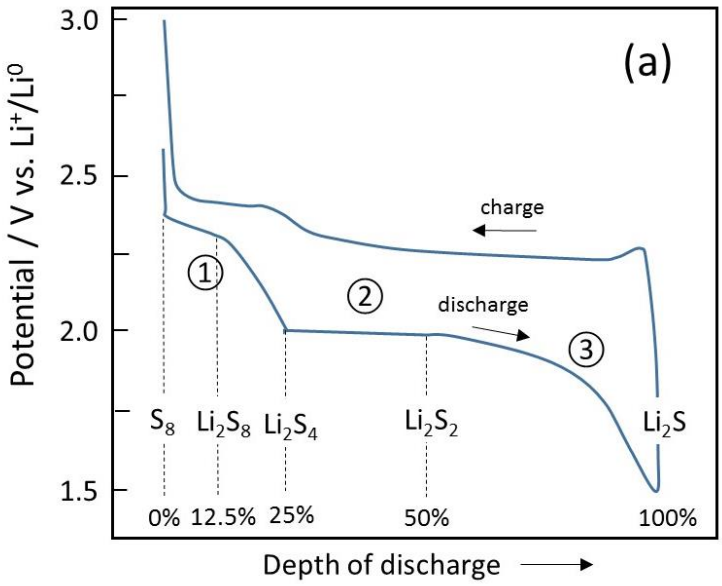

Figure 1. Discharge–charge profiles of a Li–S cell, illustrating regions (I) conversion of solid sulfur to soluble polysulfides; (II) conversion of polysulfides to solid Li_2S_2; (III) conversion of solid Li_2S_2 to solid Li_2S.

On the other hand, the charge process is such that all the polysulfides transform via charge

transfer following the most facile oxidation state S_8^{2-}. Upon cycling, the S_n^{2-} formed on oxidation of Li_2S_2 and Li_2S (or on reduction of S_8) react with them to form S_{n-x}^{2-} polysulfides at the anode side. They diffuse on the cathode side and are re-oxidized into S_n^{2-} species. This parasitic cyclic process decreases the active mass available in the discharge process and is responsible for an important decrease of the coulombic efficiency in the charge process [20]. A model of this internal shuttle effect has reproduced quantitatively the self-discharge, coulombic efficiency, thermal effects observed experimentally [21-22], giving evidence that this internal shuttle effect is responsible for these problems. More recently, a complete modeling of the batteries with S/C composite cathode could be made [23], while the self-discharge has been modeled in [24-25]. In addition, upon cycling, the reduction of the soluble polysulfides during discharges result in the formation of insoluble agglomerates of Li_2S_2 and Li_2S formed on the surface of cathode [26]. These agglomerates become an inert mass in the electrochemical process, which results in a capacity fading, and also in an increase of the impedance the battery, which reduces the rate capability. Another consequence of the redistribution of active materials associated to the nucleation phenomena is that the initial status of sulfur in the cathode is of limited importance if the redistribution of Li_2S is inevitable [27-29]. More details on the working mechanism and the limitation factors of Li-S batteries through the formation of the different polysulfides, the structural and morphological changes during cycling, have been obtained by different techniques: inductively coupled plasma, optical emission spectrometer (ICP-OES) measurement, liquid chromatography coupled with mass spectrometry (LC-MS) [30], transmission X-ray microscopy [31], in-situ electron microscopy [32] and UV/Vis *in Operando* Mode [32-33], in-situ X-ray diffraction [34].

Since the rapid dissolution of the soluble polysulfides formed at the higher plateau of the voltage curve are at the origin of the irreversible loss of active material, a strategy has been used [35]: terminate the recharge process at the start of the lower plateau, and limit the cycling process afterwards to this region of the lower plateau, corresponding to the redox reaction in the limited range of composition between Li_2S_4 and Li_2S. As we have already mentioned, Li_2S_4 is already soluble, but less than the longer-chain polysulfides so that the active material can hardly seep into the electrolyte. This improved the cycling life, since the capacity decreased only by 0.53% over 500 cycles with a coulombic efficiency close to 100%. Other strategies have been developed to keep a maximum of capacity by using the two plateaus: usually, the Li-S cells are cycled in the voltage range 2.8-1.5 V, unless $LiNO_3$ is added in the electrolyte for improving the coulombic efficiency, in which case the discharge is raised to 1.7 V to avoid the irreversible reduction of $LiNO_3$. In the following, we review

these strategies, together with the recent modifications that have been proposed as a remedy to the shuttle effect, and the insulating nature of the polysulfides. All the elements of the battery are concerned and the solution, as we shall see, is a combination of modification of the cathode, of the separator, of the electrolyte, including the choice of binder, even though few binder-free architectures have now been proposed. We have already mentioned that most of the papers report capacities per gram of sulfur (g_{sulfur}). In the same way, the C-rate is based on the theoretical capacity of sulfur (1675 mA g_{sulfur}^{-1}). Of course, the non-sulfur components contribute importantly to the power density and rate capability. Therefore, neither the value of the capacity not the values of the C-rate are meaningful, as these informations do not allow any comparison between different cell assembly nor even composite concepts. Again, only these data at the cell level would allow for such a comparison, and in that case, it would be impossible to separate the cell into components, since the cell performance depends on all of them: cathode, electrolyte, separator and anode. At the present state-of-the-art where so few data exist at the cell level, such a global approach is impossible, and we adopted the choice of separating the cell in its components by devoting different sections to them. This is actually the approach that is done in the publications, since their authors aim to find a solution for a cathode, in which case they chooses a conventional electrolyte, or they focus attention on the electrolyte, in which case they choose a conventional cathode, usually some kind of carbon more or less characterized. Nevertheless, we still report in different places the capacity retention, because it gives an information on the ability of the cell to suppress the internal shuttle effect (at least, a very good capacity retention over hundreds of cycles means that a solution has been found to reduce importantly the shuttle effect). And in this case, we also report the C-rate at which the capacity retention has been obtained, because the capacity retention depends on this parameter, even though this is always based on sulfur only, unless explicitly specified.

2. Carbon-sulfur electrodes

The problem of the low electrical conductivity of sulfur was addressed by adding conductive element. The first composites have been made by filling pores of bulk carbon with sulfur [36-37], with limited success. A substantial improvement has been obtained by using nano-structured carbonaceous materials, following the same strategy used with the preparation of anodes for Li-ion batteries extensively reviewed recently in a book [38]. One example is the use of multi-walled carbon nanotubes (MWCNT) [39-40] or nano-fibers [41] as conductive wires. An improvement of the cycling stability has been achieved with a MWCNT-core/sulfur-shell composite [42], although it is difficult to

understand why the aggregation phenomena the cathode can be reduced since the active element is in contact with the polymer. One possibility is that the interior of the cathode is inaccessible, as revealed by the low initial capacity, which may become more accessible upon cycling so that it postpones the capacity fading. The move up a notch has been made with interwoven C/S composites where sulfur is introduced inside the 3D-accessible channels of the CMK-3 carbon structure made from carbon tubes that are propped apart by carbon nano-fibers [43]. The sulfur is introduced from the melt by impregnation owing to capillary forces. This method permits the control of the sulfur mass so that the pore structure retains pathways for the electrolyte and Li^+ ions, while the residual pore structure buffers the volume change of the cathode during cycling. Indeed, the difference in density between sulfur (2.03 g cm^{-3}) and Li_2S (1.67 g cm^{-3}) implies an expansion during discharge and contraction during charge. In addition, the wall-structure of the CMK-3 carbon is conductive to Li-ion transport. The trapping of the intermediate polysulfides due to both the sluggish kinetics inside the framework and the sorption properties of carbon favors their full reduction to Li_2S and Li_2S_2 on discharge, or oxidation to S_8 on charge. As a result the capacity is increased. An even more complete reaction can be obtained by modifying the carbon surface with polyethylene glycol (PEG) polymer, which creates a chemical gradient that retards diffusion of the polysulfides into the electrolyte. The percentage of sulfur dissolution into the electrolyte was stabilized after few cycles to circa 25% and does not change after that for few tenth of cycles at low current density, showing a suppression of the internal shuttle effect at the time scale of the experiments. The good electrical contact evidenced by the reduced polarization is another proof of the inhibition that prevents the precipitation of resistive agglomerates on the external surface of the framework. The SEM images confirm this polymer protection. Following this work, CMK-3 was coated with another polymer: poly(3,4-ethyle-nedioxythiophene)-poly(styrene sulfonate) (PEDOT:PSS) [44] or wrapped in graphene [45-46] with similar results. Decoration with DNA, a CMK-3/S cathode showed a 70% capacity retention after 200 cycles at 0.1C [47].

The porosity is an important parameter. The pore size in [43] was 6.5 nm. Other attempts to use smaller pore size of 3 nm did not give any improvement [48] because the pores are completely filled, which blocks the transport. Actually, the electrochemical reactions mainly take place at the interface between sulfur and carbon framework [49-50]. Bimodal mesoporous carbon with 2.0 and 5.6 nm was used to regulate the conduction and increase the rate capability [51]. These works show the importance of the porosity of the carbon, which must have both meso- and micro-porosity. Another bimodal microporous (0.5 and 0.8 nm to 2.0 nm) carbon was used and also gave good results [52]. Although

mesopores may not trap the migrating polysulfides in their nanospace well, they have other benefits, like facilitating Li^+-ion transport [53] and sufficient electrolyte accessibility during high-rate electrochemical reactions [54]. Koh et al. have shown that nanoscale contact of sulfur and mesoporous carbon is not crucial, and that the improved performance of cells with C/S composites is primarily due to the ability of mesoporous carbon materials to serve as a reservoir for various active materials generated during charge and discharge [55].

Another parameter that plays an important role is the loading. The loading must be small enough to leave enough space in the structure for the transport of sulfur species. This has been evidenced in an experiment made on a S/C composite, where the sulfur was introduced into the micropores by wet-impregnation [56]: With two cells differing only by the sulfur loading to make possible a comparison, the first discharge capacity increased by almost a factor 2 (95% sulfur utilization) at current density 2500 mA g_{sulfur}^{-1} when the loading decreased from 51.5 wt.% to 11.7 wt.%. This was a good performance at this current density in 2009, but the capacity faded rapidly. A sulfur-impregnated mesoporous carbon spheres with hierarchical pores in the range of 3-30 nm, and sulfur loading ratio of 60 wt.% showed a 62% capacity retention after 100 cycles at 0.2C, and at 2C [57]. In an older work, C/S composites of a different nature have been considered, by coating sulfur with carbon [58], following the example of the carbon coating of lithium iron phosphate in the case of Li-ion batteries (see for instance [38]). With sulfur, however, the carbon layer was thicker (18 nm against 3-5 nm). At least it has the same positive effect by increasing the electrical conductivity, and a high initial capacity was found. However, the carbon-coating poses extra problems specific to the Li-S batteries. In particular the question of the prevention of the diffusion of intermediate polysulfides responsible for the internal shuttle effect and the poor cycling life was not addressed. Actually, the capacity retention was small. Therefore, the simple carbon coating that was so efficient to solve the problems of the cathodes for Li-ion batteries did not immediately solved the problem of the internal shuttle in the Li-S battery. More sophisticated carbon must be used, with control of both the porosity and conductivity.

Nano-structured carbon exists under many architectures ranging from 3D (aerogels), 2D (graphene), 1D (nanotubes, wires, fibers). All of them being very popular as additives in electrodes of batteries, and they have been reviewed in the context of the lithium batteries in [38]. In the case of the Li-S battery, the breakthrough for the carbon use is the work of Nazar with CMK-3 [43]. Soon after this work, first core-shell carbon structures were made through an aqueous solution route that allowed a 10 nm-thick uniform coat of sulfur on the carbon particles [59]. This method gave mitigate results, but

most importantly the capacity was stable for 50 cycles only. In another attempt, the core-shell composite was made using carbon-black, which is a cheap commercial product, owing to a precipitation method [60]. The use of carbon black reduced the size of the sulfur precipitates, and thus improved the electrochemical properties. A carbide-derived carbon (DUT-107) featuring a high surface area (2088 m^2 g^{-1}), high total pore volume (3.17 cm^3g^{-1}) and hierarchical micro-, meso- and macro-pore structure applied as a rigid scaffold for sulfur infiltration gave very good results [61]: in a full cell model system using a prelithiated hard carbon anode, the performance of DUT-107/S cathodes is demonstrated over 4100 cycles with a very low capacity decay of 0.0118% per cycle (see Fig. 2). Note in all this review, the surface areas are determined by the BET experiments, since this is the result reported in the literature, and the intrinsic property that characterize the material. It can thus be different from the electrochemical surface area. Application of polysulfide additive increases the capacity, although a slightly higher decay of 0.0125% per cycle is observed. Note these results have been obtained with high sulfur content (69.7 wt.% per total electrode). Hierarchically structured biomorphic carbide-derived carbon offered specific surface areas up to 1750 m^2 g^{-1}, micro-/meso-pore volumes up to 1.0 cm^3 g^{-1} and macro-pore volumes of 1.2 cm^3 g^{-1}. Owing to this pore system, stable capacities were obtained at current densities exceeding 20 mA cm^{-2} (2C) using amounts of electrolyte of 6.8 mL m g_{sulfur}^{-1} [62]. This is a progress with what could be achieved few years ago, even though already 5 mL per mg of sulfur reduce the gravimetric energy density on cell level down to 100 Wh kg^{-1}, well below the values for state of the art Li-ion batteries.

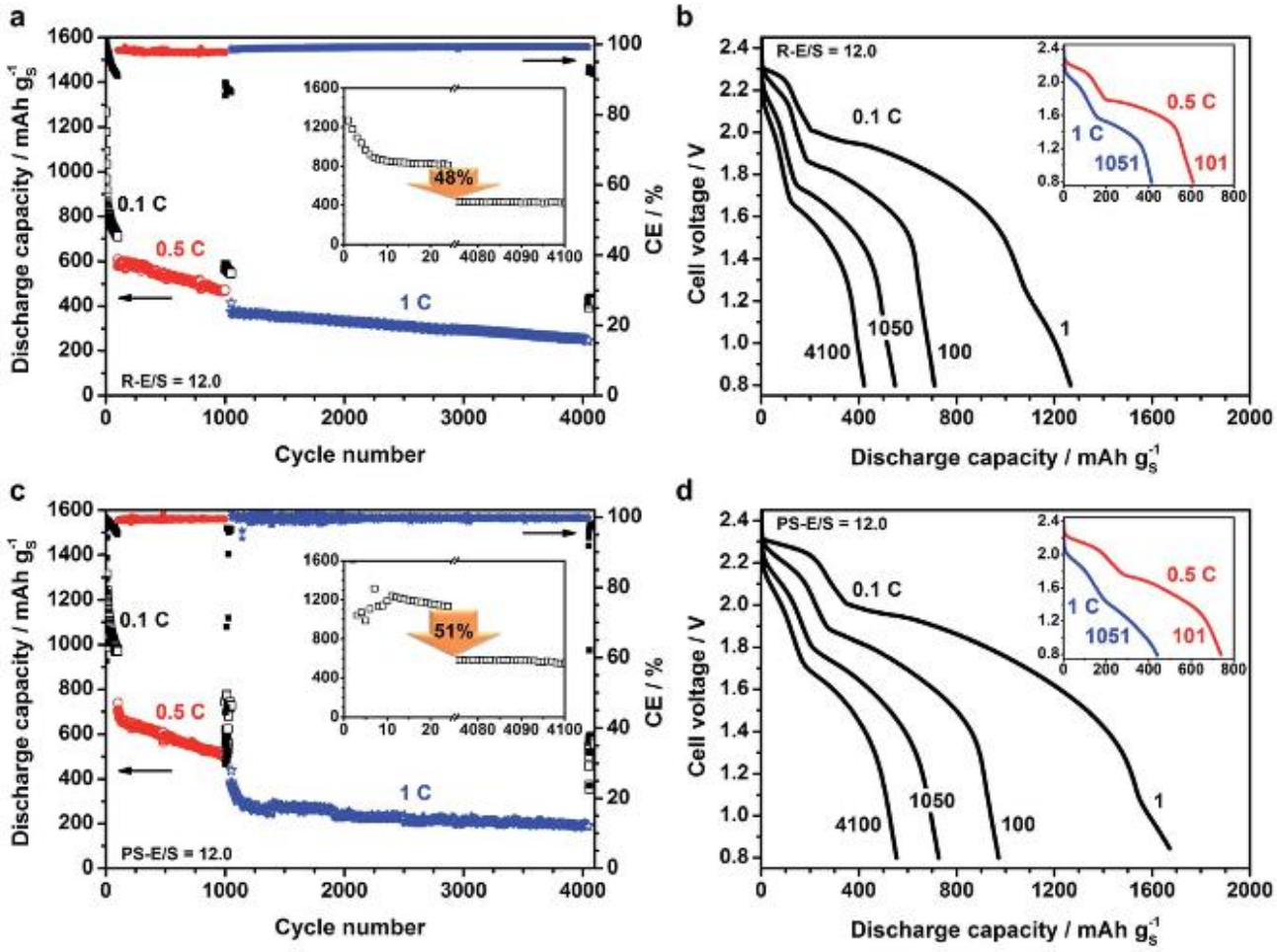

Figure 2. Electrochemical properties of carbon-sulfur electrodes. Cycling performance and corresponding discharge voltage profiles of DUT-107/S cathodes measured in a full cell setup [61]. The anode was made of prelithiated hard carbon anode (LiHC@GDL) with a stable areal capacity of ca. 3.0 mAh cm^{-2}, as a substitute for lithium metal. The electrolyte was 1 mol L^{-1} LiTFSI + 0.25 mol $LiNO_3$ in DME/DOL (a and b) and 0.8 mol L^{-1} LiTFSI + 0.25 mol $LiNO_3$ + 0.15 mol Li_2S_6 in DME/DOL (c and d), respectively. The amount of electrolyte was 12.0 mL per mg of sulfur (mg_{sulfur}). The insets in the cycling experiments compare the initial (cycles 1–24) and final (cycles 4076–4100) discharge capacities at 0.1C. CE= coulombic efficiency. Reproduced with permission from the Royal Society of Chemistry.

Hierarchical porous carbon nanostructure with intrinsic O- and N-dopants and an ultrahigh specific surface area of 1500 m^2 g^{-1} derived from crude soybeans used as a cathode after a sulfur loading of 5.5 mg cm^{-2} and a sulfur content of 80% displayed a specific capacity that corresponds to an areal capacity

of 5.2 mAh cm^{-2} [63]. An interesting comparison of the results obtained with different carbon blacks has been published [64]. As a result, these authors found that high surface area carbons can adsorb significant amounts of polysulfides and demonstrate high specific capacities, but they also produce brittle electrodes, so that a best compromise has been found by mixing high and low surface area carbon blacks. They also showed that a simple electrode composed of Ketjenblack EC-600JD, polymer binder and sulfur shows excellent cycling performance with high specific capacities and very good capacity retention even at 1C rate over 600 cycles. Mesoporous carbon materials (MCMs) with excellent electron conductivity and high surface area was also successfully synthesized with a narrow pore size distribution (0.5-2.0 nm) simply from waste litchi shells [65]. Used as the framework for a C/S composite cathode, the performance was good over 200 cycles at 0.5C. Layered carbide derived carbon with hierarchically porous structure with a sulfur loading of 50 wt.% showed a capacity retention of 59% at 0.5C after 200 cycles, and a capacity only twice smaller at 5C [66]. Porous carbon nanosheets with a high specific surface area (951 m^2 g^{-1}) and a dominant pore size of 2 nm/sulfur composites also gave good results, but the tests were limited to 50 cycles [67]. On another hand, carbonized porous aromatic framework (CPAF) nanobeads with 75 wt.% S showed at 0.2C (based on sulfur) a high initial capacity per gram of sulfur that was 83.4% of the theoretical value, and at 0.5C, it showed 0.074% decay rate per cycle over 1000 cycles [68] (see Fig. 3). This good result it attributed to some intrinsic properties of the CPAF: their high surface area (679.8 m^2 g^{-1} and 2.0 m^2 g^{-1} before and after sulfur loading), which provides the possibility of formation of an electrostatic charge-separation layer, the inherent optimized pore size that facilitates ion migration, the abundant micropores that can absorb and accommodate active materials, and the highly ordered structure that enables the formation of conductive paths. By using the sulfur-containing carbon precursor furfuryl mercaptan in varying amounts in the carbon precursor formulation, sulfur functionalities with different carbon/sulfur molar ratios were introduced. Such functionalized sulfur-doped ordered mesoporous carbons increased the capacity retention [69]. Engineered hollow core-shell interlinked carbon spheres that consist of a mesoporous shell, a hollow void, and an anchored carbon core delivered, with a sulfur loading of 70 wt.%, a stable capacity over 200 cycles 0.5C [70].

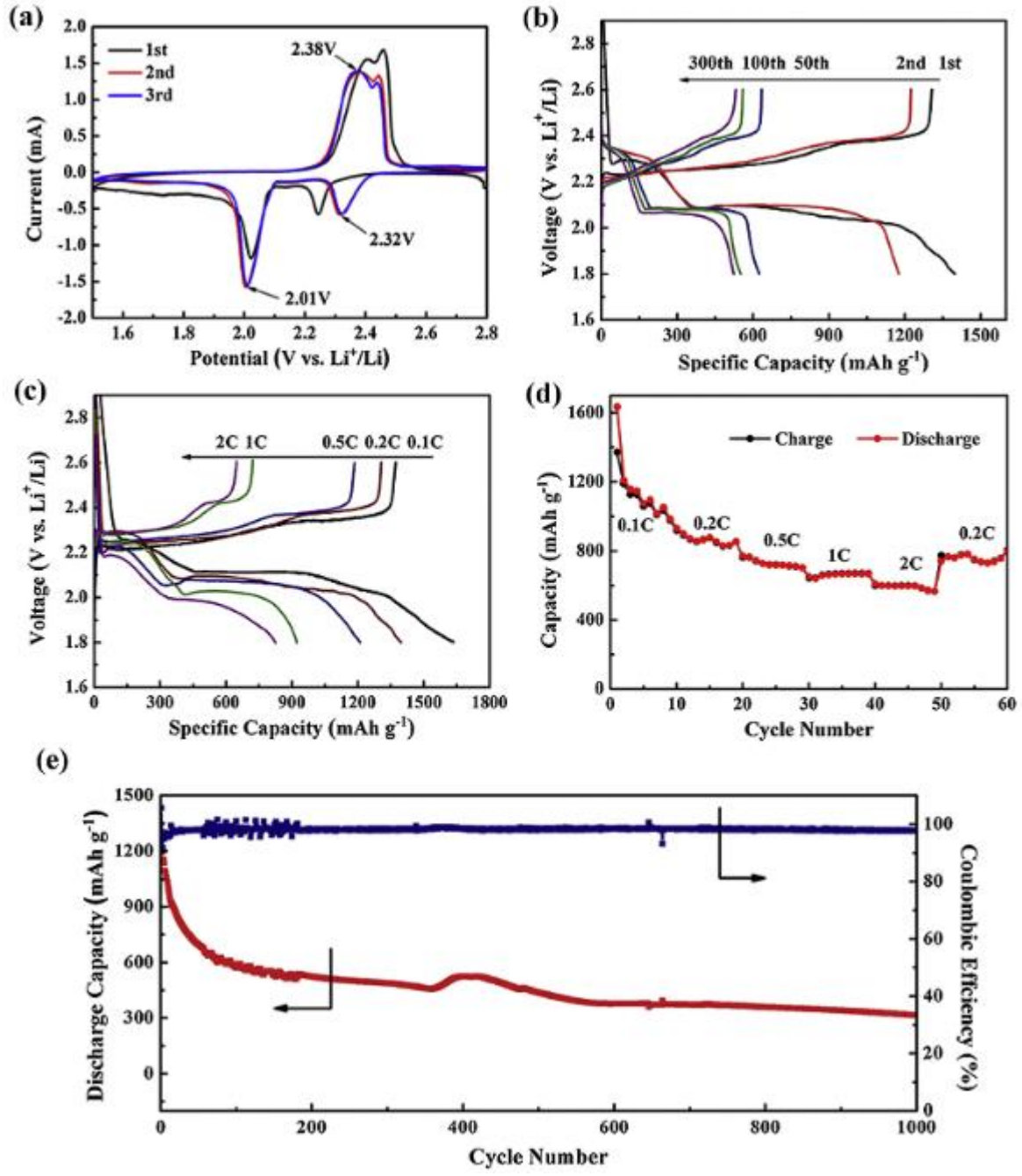

Figure 3. Electrochemical characterization of carbonized porous aromatic framework (SCPAF) electrode [68]. (a) CV profiles of SCPAF electrode at a sweep rate of 0.2 mV s^{-1}, (b) galvanostatic charge/discharge curves of SCPAF electrode at different cycle at 0.2C, c) charge/discharge curves of the SCPAF electrode at different rates, (d) rate capability of SCPAF composites, (e) cycling performance of SCPAF electrode at a rate of 0.5C. Reproduced with permission from Elsevier.

N-doped mesoporous carbon has been added to N-containing polymer as precursor [71]. The results show that N-doping has positive effects on the electrochemical properties of the composite with sulfur. The reasons are controversial, as the role played by nitrogen is not clear. Density functional calculations suggest that nitrogen enhances the oxygen-sulfur bonding, while it is suggested that the chemical interaction between sulfur and mesoporous carbon is responsible for the improvement. Note, however, that nitrogen doping is known to improve the conductivity of the carbon, and leads to a significant improvement with respect to non-doped carbon, when entering the composition of electrodes for Li-ion batteries, where there is no sulfur at all [38]. X-ray absorption near-edge structure (XANES) spectroscopy, however, has shown that a significant change in oxygen coordination structure is observed, whereas the carbon and nitrogen chemical environments remain unaltered, thus confirming the role of oxygen in the present case [72]. However, the influence of nitrogen doping on electrochemical performance of carbon/sulfur composites cathode has been studied deeply under the conditions of similar surface area and pore texture. This study presents the directly experimental demonstration that both nitrogen content and nitrogen group species play crucial roles on electrochemical performance of carbon/sulfur composites cathode [73]. The presence of hydrogen is also considered one of the reasons why the biomass carbon derived from mushroom is a promising matrix for sulfur [74]. Hollow carbon nanofiber@nitrogen-doped porous carbon (HCNF@NPC) coaxial-cable structure encapsulating sulfur as a composite cathode maintained a capacity retention rate of 63% after 200 cycles, even at a high current density [75]. Nitrogen and oxygen dual-doped porous carbon that possesses a hierarchical porous structure serving as a host for 64.5 wt.% sulfur content showed a capacity retention of 62% over 600 cycles at 1C [76].

Sulfur reacts with metals to form metal sulfides. Advantage of this reaction has been used to incorporate metal with carbon to stabilize the active materials within the porous carbon. In particular copper particles were incorporated by impregnation and synchro-dry technique [77]. The improvement of the properties of the cathode with this Cu/C composite as the sulfur host was remarkable, as the capacity was steadily maintained over 500 cycles. Recently, a composite electro-formation of a Cu foil with incorporated S-polythiophene particles with a sulfur loading of 0.29 mg cm^{-2} with high specific area and good porosity was tested as a binder-free and carbon-free cathode, but the results were not as good as the ones mentioned above [78]. With the addition of a small amount of selenium to form $S_{0.94}Se_{0.06}$/C composites the sulfur anode delivered a stable capacity over 500 cycles at current density 1 A g_{sulfur}^{-1}, and a good rate capability up to current density 20 A g_{sulfur}^{-1} [79].

Hierarchical porous carbon was synthesized in order to combining the advantages of microporous pores in regards to stability with large pores for rapid ion transport [80-81]. Also, nanospace of carbon substrates can swell the liquid electrolyte, which is a benefit for stabilizing the electrochemical reaction within the porous cathode [82-83]. A highly ordered mesoporous carbon (core)/microporous carbon (shell) was used to increase the capacity, and the loading in the particles by 60% [84], taking advantage of both micro- and mesopore: mesopore internal face to take sufficient sulfur, micropore at the external face because the carbonate particles like ethylene carbonate or dimethyl carbonate in the electrolyte are too big to penetrate into the micro-pores [85]. Therefore, the micro-pores act as a barrier to these carbonate molecules that deteriorate the battery via their irreversible reactions with the polysulfides. Taking advantage of the dual micro/meso porosity, but also of the stabilizing effect of TiO_2 on the polysulfides, a hybrid nanostructured microporous carbon-mesoporous carbon doped TiO_2/sulfur composite cathode with sulfur loading 61% retained 72% of the initial capacity with a columbic efficiency greater than 97% after 140 cycles at 0.1C. [86]. With a multi-chamber/micro/mesoporous carbon nanocube substrate, a high initial capacity of 1078 mAh g_{sulfur}^{-1} and a long cycle stability (loss of capacity of 7% after 1000 cycles) were recorded, owing to the presence of different nanosized pore structures [87] (see Fig. 4). Zhang et al. reported the good stability of sulfur confined in microporous carbon spheres up to 500 cycles, but only when the loading in sulfur was limited to 42 wt.%. The micro-pore size was about 0.7 nm [88]. Higher loading reduces the performance. Similar results were observed with other cathodes with sulfur in carbon micro-pores [89]. Recently, hierarchical porous carbons (HPCs) with extremely high surface areas of up to 2340 $m^2 g^{-1}$ with total pore volume of up to 3.8 $cm^3 g^{-1}$ were used as supports for sulfur for Li-S batteries. The hierarchical structure of the carbon originating from interconnected large mesopores (10-50 nm), small mesopores (2-10 nm) and micropores (<2 nm) made the total available surface area highly accessible, resulting in excellent electrode kinetics with a good capacity retention after 200 cycles up to 5C rates [90]. In addition, these authors demonstrated that a porosity-independent capacity fade is also systematically demonstrated in the presence of lithium nitrate electrolyte additive in the electrolyte, indicating effective elimination of capacity loss due to polysulfide shuttle.

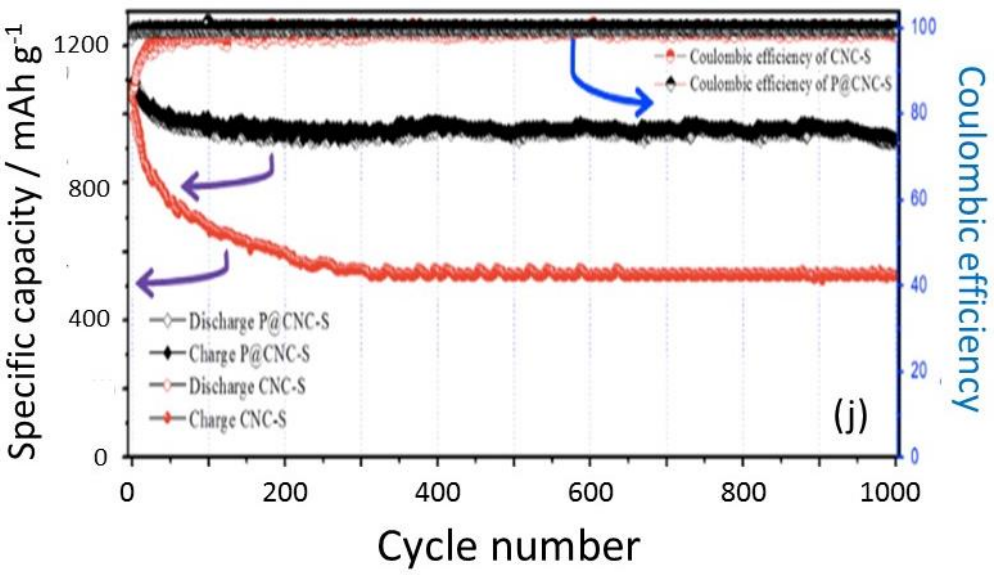

Figure 4. Cycling performances of multi-chambered micro/mesoporous carbon nanocube encapsulated sulfur non-coated (CNC-S) and coated with PEDOT (P@CNC-S) at 1C for 1000 cycles (1C=1673 mA g^{-1}) and their corresponding coulombic efficiencies [87]. The working electrodes were made from 80 wt.% of active materials, 10 wt.% of carbon black, and 10 wt.% of the binder polyvinylidene fluoride (PVDF) dissolved in N-methyl-2- pyrrolidone (NMP). Reproduced with permission from Elsevier.

Nitrogen-doped hierarchically porous coralloid carbon/sulfur delivered a high initial discharge capacity per gram of sulfur close to theoretical, which remained about 1.86 times as that of activated carbon after 50 cycles at current density 100 mA g_{sulfur}^{-1}, and the rate capability was good with only small capacity fade over 200 cycles up to a current density of 800 mA g_{sulfur}^{-1} [91]. Impregnation of sulfur in nitrogen-doped porous carbon shows interconnected sheet-like porous morphology with a large surface area of 1315 m^2 g^{-1}. As a cathode, it retained 68% of capacity after 100 cycles at 0.1C, and a good rate capability up to 5C [92].

Hollow carbon-sulfur composites were designed to combine the advantage of the conductivity of carbon and the hollow that gives some space to buffer the change of volume of the sulfur species during cycling [93,94]. An ultra-light flexible carbon foam (MFC) with a 3D interconnected hollow network was used as a host for sulfur loading of 75 wt.%. Reduced graphene oxide was used to decorate the MFC skeleton [95] in order to increase the conductivity. After the inevitable capacity

fading in the first few cycles, the capacity retention at 0.1C is over 95% after 100 cycles compared with the 20th cycle. The performance was attributed not only to the hollow structure and porosity, but also to the high content in N and O dopants in the carbon. N-doped hollow porous carbon microspheres loaded with 65 wt.% sulfur exhibited a capacity retention of 60% over 400 cycles at 0.1C [96].

Overall, the advances in the development of carbon substrates under different forms: 1D fibers [97-99] and nanotubes [100-101], 2D (graphene [102-105], or porous carbon [53, 94, 106-107], have increased the discharge capacity to 1500 mAh g_{sulfur}^{-1} and an enhancement in cycle life to 1000 cycles [101, 106]. The best results in terms of capacity versus loading have been obtained by combining the three kinds of carbons: zero-dimensional carbon nanoparticle, one-dimensional carbon nanotube, and two-dimensional graphene to obtain a nanocarbon−sulfur cathode material with ultrahigh sulfur loading of up to 90 wt.% realized in the form of sulfur nanolayer-coated three-dimensional (3D) conducting network. A specific capacity of 1115 mAh g^{-1} at 0.02C was obtained, and good rate performance of 551 mAh g^{-1} at 1C, where this time the data are per gram of the sulfur + carbon composite and not per gram of sulfur only [108]. Note the capacity mentioned at 0.02C actually amounts to 1239 mAh g_{sulfur}^{-1}, so that 100% of the sulfur was used. The mass loading of sulfur in cathodes was ∼2 mg cm^{-2}.

2.1. One-dimensional carbon

1D-carbon is attractive since it is flexible and conducting, and it is widely used as additive in electrodes of lithium-ion batteries at the laboratory scale. In Li-S batteries, the first attempts were not very successful because the content of the composite in sulfur was 30-33% only [97, 109]. Different morphologies of assembles of nanotubes have been chosen, like microspheres [110] or aligned forests [111]. In [111], the composite with 63% sulfur content delivered circa 750 mAh per gram of sulfur, i.e. 500 mAh per gram of electrode after 50 cycles. In [110], sulfur was uniformly coated on the surface of functional MWCNT to form a core–shell structure with a sulfur layer of thickness 10–20 nm. Then the intermediate composite was ball-milled to form interwoven and porous sphere architecture with large pores (around 1 to 5 μm). The composite as a cathode showed good capacity retention after 200 cycles up to a current density of 1 A g_{sulfur}^{-1}. At high concentration (68 wt.%) of sulfur, the polysulfides were successfully immobilized on the surface of functionalized CNTs using a fabrication method that combined solvent exchange at the surface and low-temperature treatments. As a cathode, a long cycle life exceeding 1300 cycles and a very low capacity decay rate (0.025% per cycle) at 0.33C rate were demonstrated [112]. The rate capability was also remarkable, with a good capacity retention over 500

cycles at 2C.

To increase the loading, sulfur was encapsulated in hollow carbon nanofibers 200-300 nm in diameter. Prepared from anodic Al_2O_3 template, the sulfur loading reached 75 wt.% [113]. Unfortunately, at the end of discharge, Li_2S_x detached from carbon matrix and first-principle calculations have confirmed that the binding energy between carbon and Li_2S_x is small [114]. This change in the bonding between carbon and sulfur species during cycling has been considered as the cause for the capacity fading, as 48.5% of the initial capacity was retained after 150 cycles at 0.5C. A better capacity retention, however was obtained by encapsulating sulfur into a hybrid porous carbon/carbon nanotube (CNT) substrate [115]. To overcome the problem mentioned above, amphiphilic polymers have been introduced: poly(vinylpyrrolidone) (PVP) and Triton X-100 [116]. The amphiphilic moieties act as anchoring centers to make polar Li_2S_x strongly bind to the carbon. As a result, a significant improvement of the capacity retention was achieved, as 80% of the initial capacity was now retained at the same rate of 0.5C. Nevertheless, the best results were obtained without the help of any polymer [117]. The synthesis process was as follows. (a) Anodic aluminum oxide (AAO) membranes were first prepared from aluminum discs by a two-step anodizing process to generate aligned pore channels. (b) Conformal carbon layers of ≈3 nm thick were then deposited on the surfaces of the pores in the membrane to form CNT structures by employing a chemical vapor deposition (CVD) process. (c) Sulfur infiltration via capillary force. (d) Next, platinum was sputtered onto the bottom side to seal the pores and function as a current collector, followed by a heat treatment at 400 °C. (e) Removal of the residual aluminum and AAO template via a wet etching. During 150 and 300 deep cycles at 0.5 and 20C (33.5 A g_{sulfur}^{-1} when converted in current density), high capacity retentions of 99.2% and 97.3% were observed with respect to their capacities in the second cycles. Even for 1000 cycles, when tested at 2 and 5C for charge and discharge, a capacity retention of 75.8% was observed. The results, which constitute actually one of the few best performance reported ever in terms of energy density and rate capability for a Li-S battery, shows that the process has avoided the problem of contact between Li_2S and carbon encountered in [113], without the need for a polymer. The success may come from the two-step anodization process used in [117] to generate aligned pore channels, as the anodization process is most critical because it determines the hollow dimensions of the CNTs and therefore the dimensions of the sulfur core in the final S@C electrode. The additional pore-widening step to increase the pore diameter to facilitate more effective sulfur infiltration was also crucial to explain the performance. Another difference is that a majority of sulfur adopted the uncommon

monoclinic phase rather than the typical orthorhombic phase owing to the heat treatment in confined nano-environment, which might also stabilize the anchoring of the polysulfides. Since then, a confirmation of the stabilization of the amorphous phase by C-S interaction was given reported by Jung and Han [118], who shows that the amorphous phase is stable if carbon atoms penetrate into the sulfur at elevated temperatures and the carbon density exceeds a threshold of $C_{0.3}S_8$.

It is not possible to infiltrate sulfur in the carbon nanotubes, because they are too thin (10-20 nm). The sulfur can only be deposited on their surface. We have already reported the beneficial effect of N and O heteroatoms in composites with mesoporous carbon, which help in the anchoring of carbon with sulfur species [71]. In the same way, N and O heteroatoms were introduced in carbon nanotubes [119-120]. A carbon-nanotube membrane realized a self-supporting composite electrode that can tolerate 10 MPa stress with 9% strain 12000 times and with a very good electrical conductivity of 800 S cm^{-1} [121]. These properties were attributed to the fact that the sulfur was in the tube wall. After a 100 cycle stability test, the capacity of sulfur at 1.5 A g_{sulfur}^{-1} is 653 and 524 mAh g_{sulfur}^{-1} (the overall capacities of the cathode are 150 and 262 mAh g^{-1}) for the sample with 23 wt.% and 50 wt.% of sulfur, respectively. The progress through the years with sulfur/ carbon nanotubes is constant. In 2012, such a composite delivered an initial capacity of 1352 mAh g^{-1} at 1C rate, retaining 915 mAh g^{-1} after 100 cycles, illustrating the beneficial effect of combing high surface area and high conductivity owing to intercalated nanotubes that form a percolating network through the structure [122]. The sulfur content was 40%, and the average energy density over 100 cycles was 852 Wh kg^{-1} based on the total mass of cathode. In 2013, enhanced sulfur content at 65 wt.% and average energy density over 100 cycles at 0.1 C at 1200 Wh kg^{-1} was reported, owing to the pre-oxidation of the carbon in HNO_3/H_2SO_4 to introduce the N and O hereoatoms mixture [123]. An increase of the proportion of sulfur in the electrode is beneficial to the tap density that is increased up to 1.98 g cm^{-3} for a sulfur loading of 90% obtained with nanotubes aligned through a solution-based process [99], leading to a volumetric energy density of 1116 mAh cm^{-3}. However, the rate capability is decreased with such high loadings. Instead of coating the carbon nanotubes, it is also possible to anchor sulfur nanoparticles on them to form a composite that delivered a high initial capacity, retaining 85% of it after 100 cycles at 1C-rate [124], a performance however smaller than the result obtained at the same C-rate in [122]. A freestanding bilayer carbon–sulfur (FBCS) where the top component is composed of interlacing multiwalled carbon nanotubes (MWCNT) and the bottom component is made up of a mixed layer of sulfur imbedded in MWCNT and N-doped porous carbon (NPC), after high sulfur loading level (3 mg cm^{-2}) displayed an excellent

capacity retention of 83.1% at 0.5C and 83.4% at 1C after 300 cycles [125].

Since a decade, it is possible to reach surface areas circa 1500 m^2 g^{-1} for carbon nanotubes [126] In practice, however, the surface area used for Li-S is the order of 100 m^2 g^{-1} with the pore size that permits the impregnation of sulfur. It is thus desirable to increase this surface area. Owing to water steam etching, carbon nanotubes with surface area 431 m^2 g^{-1} were obtained, which could be loaded with a content in sulfur of 70% [127]. Contrary to the general trend according to which more loading is associated to smaller rate capability [99], the performance at high C-rate was not degraded: at 5C rate, 70% capacity was retained after 250 cycles. Another approach was to coat the carbon nanotubes with a microporous carbon layer, although the mesoporous-microporous core-shell structure is more easily obtained with particles [84], as seen earlier in this review. Nevertheless, such a carbon nanotube morphology could be obtained with a surface area as large as 936 m^2 g^{-1} [128]. In this context, a complex structure was made in the following sequence. (a) acid-treated carbon nanotubes are coated with an amorphous SiO_2 layer; (b) an organo-silicon compound is added as the agent for pore creation and carbon precursor; (c) chemical treatment plus calcination at high temperature converts the organo-silicon layer into carbon; (d) SiO_2 is etched away. The final product is made of multi-walled carbon nanotubes encapsulated into hollow porous carbon nanotubes, with a surface area of 822.8 m^2 g^{-1} [129]. This structure combines all the beneficial effects of the good electrical conductivity associated to carbon, hamper the dissolution of lithium polysulfide owing to the mesoporous-microporous geometry discussed earlier in the context of carbon particles, and provides large pore volume for sulfur impregnation, with the hollow structure. As a cathode, this composite with 71 wt.% sulfur content (56 wt.%, taking into account the additives and binder) delivered an initial capacity close to theoretical at current density 500 mA g^{-1}. The rate capability was also remarkable up to current density of 6 A g^{-1}. After 200 cycles, the capacity remained high, with a low decay rate of 0.089% per cycle over 200 cycles at current density 2 A g^{-1}. Hierarchical microporous–mesoporous carbonaceous nanotubes (denoted as HMMCNT) that feature a thick microporous wall and inner hollow channel could deliver a high specific capacity with a decay rate of only 0.13% per cycle over 150 cycles at a high rate of 1600 mA g^{-1}, when the sulfur loading was 50 wt.% [130].

2.2. Two-dimensional carbon

2.2.1. Graphene oxide

Graphene oxide has been found of interest for Li-S batteries, because it can be wrapped around sulfur by the solution ionic strength engineering described in [131-132]. In ionic solutions, the graphene oxide crumples to minimize its surface energy. When sulfur particles are added in ionic solutions, the graphene oxide wraps the particles in the process, forming a core-shell structure. An electrode built according to this process showed a a capacity retention of 89% after 1000 cycles at 0.6C [131]. The same effect can be observed with ultra-thin graphite sheets that can easily wrap the sulfur particles [133].

One difficulty met with graphene oxide is that it is insulating, like sulfur, so that the addition of conductive agents is unavoidable, and can weight typically 20 wt.% [102]. Also, the graphene oxide surface is usually modified to immobilize the sulfur and a uniform deposition of sulfur on graphene, since the calculations of the electronic structure has shown that the bonding between sulfur and the residual oxygen functional groups on graphene oxide is weak [134]. This can be done by introducing hydroxyl groups [103], introducing $FeCl_3$ as an oxidizing agent [135], reducing the graphene oxide with H_2S [136], or introducing a polymer that contains hydroxyl groups and can interact with the hydroxyl groups on the surface of the graphene oxide [137], or a polymer that is soft enough to buffer the volume change during cycling, like polydopamine [138-139]. A cationic surfactant cetyltrimethyl ammonium bromide (CTAB) was also used successfully to insure a uniform deposition of sulfur on graphene oxide [140]. When combined with elastomer binder and ionic liquid electrolyte, and 20% conducting agents, the cell could retain a high capacity after 1500 cycles at C/20, and even after 150 cycles at 6C. The content in sulfur was high: 80% so that there was 56 wt.% of sulfur in the electrode, so that, even if the capacity is divided by approximately two when the total weight of the electrode is taken into account, it is superior to the weight density available with Li-ion technology ion.

Like in any type of carbon, N-doping of graphene oxide helps immobilizing the sulfur. As a result, it improved the cycling performance, raising the capacity retention over 2000 cycles at rate 2C [141]. Recently, a graphene oxide membrane was coated directly onto the sulfur cathode by a blade coating technique [142]. The GO membrane was in direct contact with an electrically conducting carbon-coated separator, so that the extremely ordered structure of the thin (~0.75 mm) membrane and its inherent surface could suppress a majority of polysulfides in the cathode. The capacity of 835 mAh $g_{electrode}^{-1}$ after 100 cycles at 0.5C was obtained with a high sulfur content of 80%. A hair-derived carbon/sulfur composite (sulfur loading of 69 wt.%) wrapped with reduced graphene oxide delivered an initial discharge capacity close to theoretical with good capacity retention after 300 cycles at a current density

of 0.2C. Its capacity retention at 2C was measured to be 62% with respect to the capacity achieved at 0.2C [143]. This performance was attributed to the inherent N-doping and the porosity of the hair-derived carbon.

2.2.2. Graphene

The advantage of graphene is that, contrary to graphene oxide, it is a good conductor so that we can expect the concentration of conductive additives needed to operate the cell can be decreased if not suppressed by using graphene. The graphene framework also functions as a supporting framework to store the sulfur [144-149]. Recently, it has been reported that the size of sulfur particles enveloped by graphene can be controlled by adjusting the ratios of a double solvent (CS_2/alcohol) [150].

The demonstration that graphene can be used with sulfur used solvothermal-derived porous graphene sheets [151]. Then different works brought successive improvements under the form of graphene-wrapped sulfur particles [152-154], sandwich-type composites [155-157] or sulfur-coated graphene sheets [158]. A homogenous deposition of sulfur on the graphene sheets was obtained by a two-step method with reduction and synchronous sulfur modification of graphene oxide by sulfide and sulfate [159] or by a hydrothermal route [160]. If needed, the conductivity can be increased by N-doping [161]. An example is provided by nitrogen-doped aligned carbon nanotube/graphene sandwiches that delivered a high initial discharge capacity with nearly 76% capacity retention after 80 cycles (ca. 880 mAh g^{-1}) at 1C rate [162]. Highly crumpled nitrogen-doped graphene sheets with ultrahigh pore volume (5.4 $cm^3\ g^{-1}$) have recently been used as both sulfur host and interlayer [163]. These wrinkled graphene sheets achieved a high capacity and exceptional cycling stability even at high sulfur content ($\geq$ 80 wt.%) and sulfur loading (5 $mg_{sulfur}\ cm^{-2}$). The high specific capacity together with the high sulfur loading push the areal capacity of sulfur cathodes to $\sim$5 mAh cm^{-2}.

Since the porosity in graphene (and in fact in any carbon framework for sulfur) is so important, efforts have been made to control it. In particular, the pore structure and morphology of graphene-based assemblies have been precisely tuned by combining evaporation drying and subsequent freeze-drying. The inherent pulling force ascribed to strong surface tension between water and graphene nanosheets during evaporation drying is used to tune the pore structure, and freeze-drying is then used to fix the pore structure without further changes [164].

Recently, instead of simply doping carbon with nitrogen, a carbon nitride has been chosen to form a graphene-like g-C_3N_4 nanosheets (GCN), a sheet-like material raising the nitrogen content to 56

wt.%, with high specific surface area of 209.8 m^2g^{-1}, as a host to anchor lithium polysulfides [165]. The composite with 70.4 wt.% sulfur loading exhibited an initial reversible capacity close to theoretical at 0.05C and a discharge capacity reduced by a factor 2 at 0.5C over 750 cycles. Nitrogen-doped hierarchical porous carbon nanosheets with surface loading of 59 wt.% showed an improved rate capability up to 4C. Over 500 charge/discharge cycles at 1C, it still retains a high discharge capacity with a capacity loss of only 0.051% per cycle [166]. This illustrates again the efficiency of the controlled porosity coupled with N-doping. A chemically activated graphene matrix co-doped with nitrogen and sulfur, with surface area (1012 $m^2 g^{-1}$) and a wide pore size distribution of 2 nm and 25–40 nm, used as a cathode after mass loading of sulfur of 1.5 mg cm^{-2}, exhibited a capacity loss of 0.056% per cycle over 600 cycles at 0.2C [167].

We have already mentioned, however, that graphene alone does work as well as we might have expected, and it is now understood that the problem comes from the fact that graphene is not naturally porous. Note, however, that graphene–sulfur composites by electrolytic exfoliation of graphite coupled with in situ sulfur electrodeposition delivered a good initial discharge capacity at 0.1 A g^{-1} over 60 cycles [168]. Many works were thus intended to increase this porosity, by chemical activation of KOH [169], or exfoliation of graphite through a micro-mechanical method assisted by sulfur [104]. The functionality is the same as in the case of carbon nanotubes: the pores act as a reservoir for polysulfides, while the electrons are drained to the collector by graphene [170-171]. Zhou et al. utilized a graphene foam electrode with a high areal capacity of 13.4 mAh cm^{-2} to host a high sulfur loading of 3.3–10.1 mg cm^{-2} [172] (see Fig. 5). The electrode with 10.1 mg cm^{-2} sulfur loading could deliver an extremely high areal capacity of 13.4 mAh cm^{-2}, and preserve stable cycling performance with 0.07% capacity decay per cycle over 1000 cycles under a large current density of 6 A g^{-1}.

A hollow graphene nano-shell diameter of 10–30 nm with a pore volume of 1.98 cm^3g^{-1} enabled an increase of the cycling life of the Li-S battery [173]. The very small pore size limited the diameter of the encapsulated sulfur. The advantage is that as much as 91% of the sulfur could be utilized at 0.1C rate. A stable coulombic efficiency of 95% was obtained without the addition of lithium nitrate after 1000 cycles at a 1C rate. The corresponding capacity fading rate was only 0.06% per cycle.

Recently, an integrated cathode–separator structure consisting of an active material coating (1.5–2.1 mg cm^{-2}) and a graphene coating (1.3 mg cm^{-2}) on a polypropylene separator opened a new Li–S cell configuration [174]. This cathode showed excellent rate capability up to 12 A g^{-1} due to the close contact and strong adhesion between sulfur and the graphene membrane.

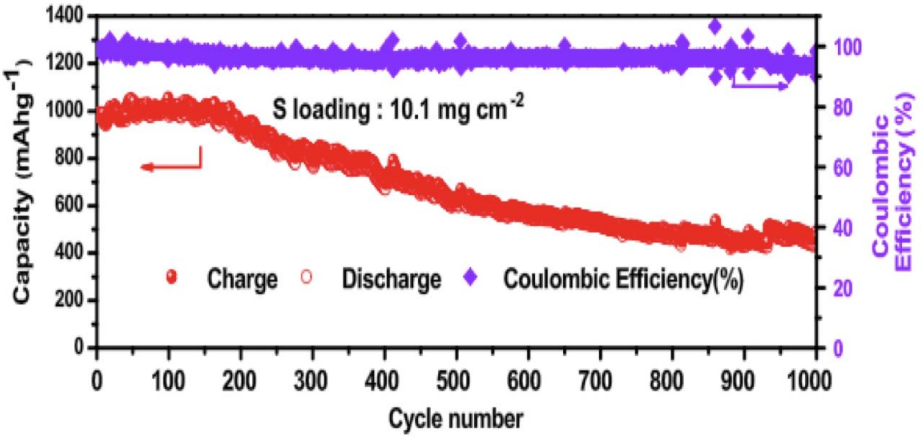

Figure 5. Cycling performance and Coulombic efficiency of the S-PDMS/GF electrode with a 10.1 mg cm^{-2} sulfur loading at 1500 mA g^{-1} for 1000 cycles [172]. Reproduced with permission from the Elsevier.

Another problem with graphene is the tendency of re-stacking. To avoid this effect, two graphene layers were separated by protuberances that avoided their stacking. The resulting surface area was 1628 m^2 g^{-1}, resulting in high energy density, and the large conductivity 438 S cm^{-1}, resulting in good rate capability. At rate 5C, half of the initial capacity was obtained after 1000 cycles [175]. Sulfur encapsulated in 3D hyper-branched hollow carbon nanorod retained 91% capacity after 500 cycles. Owing to the good conductivity of the nanorods, the rate capability was very good: At rate of 10C, the cathode still delivered a high capacity and 85.6% of it after 500 cycles.

2.2.3. Carbons assembled in 3D

Ultrathin 3D microporous carbon with uniform pore width from 5.8 to 6.8 Å (specific surface 701.4 m^2g^{-1} and micropore volume 0.3841 cm^3 g^{-1}) and thickness in approximately 50 nm, with loading of sulfur of 60%, retained a high capacity up to 3C [176]. A cathode was built with sulfur introduced into a 3D carbon replica framework with different pore sizes. The best results were obtained when the pore size of the carbon replica is 8.6 nm and the wall thickness is 4.7 nm [177]. A 3D nanostructure of graphene interconnected with hollow carbon spheres (3D rGO–HCS) as the sulfur host has been proposed [178]. The S@rGO–HCS nano-composite electrode, with a sulfur mass loading of 0.8–1.0 mg cm^{-2} showed a capacity of 93.9% after 100 cycles at 4C rate, and demonstrated a low capacity-decay rate of 0.052% per cycle after 400 cycles at 0.5C rate.

Hierarchical porous carbon rods constructed by vertically oriented porous graphene-like

nanosheets with a high specific surface area, ultra-large pore volume, and hierarchical porous structures was recently proposed by Zheng et al. [179]. When used as the active material for a sulfur cathode, the HPCR-S composite with 78.9 wt.% sulfur exhibited excellent rate performance up to 5 C, and cycling stability. Three-dimensional carbon nanotube/graphene–sulfur sponge with a high sulfur loading of 80.1% delivered a capacity for sulfur of 1217 mAh g_{sulfur}^{-1}; the corresponding capacity for the whole electrode (including the conductive additive and the binder) was 877 mAh g_{sulfur}^{1}. The capacity decay was only 0.08% per cycle, and the high-rate capacity up to 4C was 653 mAh g_{sulfur}^{-1} [180]. Super-aligned carbon nanotube/graphene (CNT/G) hybrid materials as a 3D conducting framework in which the sulfur was introduced achieved a high discharge capacity at 1 C with a capacity fade as low as 0.041% per cycle over 1000 charge–discharge cycles [181]. Carbon nanotubes and nanorods can be assembled into a cage in which the sulfur is encapsulated [101, 182]. Their size is very large compared to the previous core-shell structures already discussed, as they size up to 20 μm. This is favorable to the cycling life, because these cages afford 35% buffer space for volume expansion, but it costs volumetric density. A very stable discharge capacity was obtained over 500 cycles up to 10 C rate, with sulfur embedded in 3D hyper-branched hollow carbon nanorods [183]. Sulfur-impregnated 3D hierarchical porous nitrogen-doped aligned carbon nanotubes exhibited a high initial discharge capacity at 0.2 C after 200 cycles [184]. N-doped graphene foam prepared from a solvothermal process benefited from a high surface area (398 m^2g^{-1}) and conductivity (102 S m^{-1}) [185]. As a result, the cathode delivered a high initial capacity, and 92.5% of it was retained after 145 cycles at a current density of 600 mA g^{-1}. A 3D graphene-like material with high surface area of 2700 m^2 g^{-1} and large pore volume of 2.5 cm^3 g^{-1} was prepared owing to micro- and mesosized pores based on ion-exchange resin [186]. 84.5% of the initial capacity was retained after 300 cycles at 0.5 C. A cathode made of inter-penetrative composites of carbon nanotubes−reduced graphene oxide/sulfur with 53 wt.% sulfur exhibited a reversible capacity of 409 mAh per gram of electrode (much smaller than the 877 mAh per gram of electrode obtained in [179], however). In another work, a sulfur/ 3D graphene composite prepared by loading elemental sulfur into three-dimensional graphene reported a high capacity after 100 cycles at 0.1C rate with a Coulombic efficiency > 96%, as well as high rate capability up to 2C rate (3.35 A g^{-1}) with a loading of 73 wt.% sulfur [187]. Acetylene black/sulfur@graphene composite with three-dimensional sandwich structure prepared with a sulfur content of 54 wt.% via an *in situ* sulfur deposition showed a high sulfur utilization of 95.7% at a current density of 200 mA g^{-1} [188]. The acetylene was reported to play an important role by effective restraining for soluble polysulfides, and acting as a buffer for the volume

changes of sulfur during cycling. So far, carbon aerogels [189] did not achieve the performance of the 3D-carbons reviewed above [190].

3. Polymer additives to the cathode

As an alternative to carbon coating, sulfur has also been embedded within a conductive polymer since more than a decade [191-193]. However, at that time, the average potential was lowered to 1.6 V, while the average potential without the polymer is 2.15 V with respect to Li^+/Li, which suggests a large over-potential, and the internal shuttle effect was not solved either. The results of this approach were thus mitigated. Thinks improved importantly with the choice of polymers with specific properties.

3.1. Polypyrrole

Polypyrrole (PPy) is a conductive polymer, and can be naturally randomly mixed with sulfur to increase the conductivity, and it has another beneficial effect by absorbing partially the dissolved polysulfides [194-195]. The best results have been obtained with the tubular morphology [196-197]. Recently the addition of polypyrrole nanotubes interlayer was efficient to improve the sulfur utilization with high loading of sulfur (2.5–3 mg cm^{-2}) and suppress the corrosion reaction on the surface of the lithium anode [198]. As a result, a good initial discharge capacity over 300 cycles was reported.

An efficient S-core/PPy-shell structure was synthesized by using a cationic surfactant, decyltrimethylammonium bromide (DeTAB), to nucleate PPy on the surface of sulfur particles. A 70% reduction in discharge capacity at C/5 during the first three cycles, followed by a slow decrease of the capacity after 50 cycles, [199] shows that the PPy shell did not suppress entirely the shuttle. Nakamura et al. reported that the PPy coating of the sulfur suppressed the polysulfide dissolution, using an electrolyte consisting of 1.0 mol L^{-1} LiTFSI in a mixture of 1,2-dimethoxyethane (DME) and 1,3-dioxolane (DOL) [200], but the assertion is too optimistic, since the loss of capacity over 100 cycles is non-negligible.

3.2. Polyaniline

These results are not as good as the one obtained with the S-TiO_2 core-shell structure mentioned earlier, but in the last case, there was a hollow space in the core to buffer the volume change during cycling. A more significant comparison can be made with a hollow sphere of polyaniline (PANI), the sulfur being introduced inside the sphere by vapor phase infusion. Then the sulfur is stuck on the inner surface of

the PANI by the S-C bonds [201]. The initial discharge capacity was close to theoretical at 0.2C, 80% and 70% of it was maintained at 1C and at 5C, respectively. A serious capacity decay during the first 40 cycles is attributed to the dissolution of sulfur on the outer surface of the PANI hollow sphere for the sample, but after these cycles, the stability is remarkable, the capacity decay during 510–1000 cycles at 0.5C being as low as 0.016% per cycle. The electrochemical impedance spectroscopy (EIS) in this work illustrates how the reaction proceeds. Before discharge, the initial interfacial resistance is high (129 Ω), because of the insulating sulfur at the outer surface of the spheres. This resistance decreases in the first cycles, giving evidence of the dissolution of this sulfur under the form of soluble polysulfides. After these first cycles, the resistance increases again, due to the formation of aggregates at the outer surface. In the present case, however, the increase of the resistance was very slow, reaching 193 Ω after 200 cycles, proof that a stabilization of the morphology of the surface was achieved, with a controlled aggregation of the sulfur species. The performance of this cathode is also due to the fact that the amount of Li_2S inside the spheres, as determined by EIS, was small enough so that a void space remained even after lithiation. Therefore, the hollow structure gave room for the change of volume of the sulfur species inside the spheres during cycling. A ternary-layered nitrogen-doped graphene/sulfur/PANI showed improved the performance compared with the corresponding binary-layered nitrogen-doped graphene/sulfur (NGNS-S) [202]. The efficiency of the association graphene and PANI is also evidenced in a cathode made of sulfur loaded in curved graphene and coated with conductive PANI, which delivered an initial discharge capacity of 616 mAh g^{-1} on the basis of the cathode mass at 0.2C with a capacity retention of over 90% after 100 cycles [203]. Another ternary composite cathode PANI/sulfur/acetylene black (PANI@S-C), in which 12.5 wt.% PANI is uniformly coated onto the surface of a S-C composite powder to form a core/shell structure, retained half of its initial capacity after 100 cycles at 0.16 mA cm^{-2} [204]. Without the acetylene black additive, a sulfur-wrapped PANI nanofiber(average diameter of 70 nm) composite with a core–shell structure used as a cathode displayed a capacity retention of 88.3% after 100 cycles at 1C [205]. A lithiated polyethylene glycol (PEG) based surfactant tethered on ultra-small sulfur nanoparticles and wrapped up with PANI with high loading of 75% exhibited a high and stable capacity at the end of 100 cycles at a 1C current rate [206]. A hollow core-shell composite has been realized with another polymer: poly(vinylpyrrolidone) (PVP) [207]. In this case, the sulfur is located inside the vesicular micelle as a result of the preferential growth of sulfur on the hydrophobic part of the PVP. This cathode showed a capacity a retention of 77.6% after 300 cycles at 0.2C. It is remarkable that these good results have

been obtained despite the fact that PVP is not conducting (the same situation met with TiO_2). The acetylene has insured the conductivity. In the same way, a graphene oxide (GO)-sulfur composite with a PANI layer has been proposed. Since neither GO nor S are conductive, the results, are expected are very bad. A simple PANI layer improves the performance, but the results are still mitigate. However, cross-linking the PANI by heating is accompanied by an increase of electrical conductivity. As a result, the cross-linked (i.e. highly conductive) PANI layer deposited uniformly on GO-S composite by a layer-by-layer method gave very good results [208]. 80.6% of capacity retention was achieved after 100 cycles, and further, an excellent Coulombic efficiency of 98.7% was also attained at 0.5C cycling. Even at 1C, a high capacity retention of 80.4% as well as 97.5% of the average coulombic efficiency were obtained, over 500 cycles. The claim that the conducting nature of the polymer seems subsidiary, even dispensable in [209] should then be softened as it is true only if the use of the cell is restricted to applications that do not require high power, i.e. high C-rate. On another hand, hollow structure is very important to obtain good electrochemical properties even at low C-rate. This is best illustrated by the direct comparison of these properties between the core-shell S/PANI composite (without hollow), and the same composite, but in the yolk-shell structure (with hollow) [210]. In situ polymerization of pyrrole on the surface of carbon nanotubes also helps in the contact of sulfur with the carbon framework [211]. A new cathode was obtained by infiltration of sulfur inside hollow carbon nanofiber@polydopamine (HCNF@PDA) micro-nanostructure based on the micron-sized hollow carbon nanofiber in length and nano-sized polydopamine grafted on the outer surfaces of the HCNFs with homogeneously distribution of sulfur [212]. This cathode delivered a capacity of 381 mAh g^{-1}/electrode at 0.5C and 290 mAh g^{-1}/electrode at 2C. After 200 cycles, a high discharge capacity of 334 mAh g^{-1}/electrode was still remained.

3.3. Polyacrylonitrile

Polyacrylonitrile (PAN) was also used for the preparation of carbon–sulfur composites [213-214], when doping the PAN-derived carbon with PF_6^- ions. To improve the rate capability and reduce the weight of conductive additives, carbon nanotubes [215] and graphene sheets [216] were used as the conductive backbones of the sulfur PAN-derived composites. The rate performance of such composites can be improved by increasing the synthesis temperature from 330 to 550 °C, but is is at the expense of the capacity [217]. The methodology made use of interactions between lithium ions in solution and the nitrile groups uniformly distributed along the chain backbone of the PAN precursor to control the

distribution of lithium sulfide [218]. The resulting Li_2S-carbon composite delivered a good capacity, but only 20 cycles were investigated. On another hand, free-standing carbon paper supported Li_2S@C integrated cathode retained 52% of its initial capacity after 100 cycles at 0.1C [219]. Freestanding sulfur/dehydrogenated polyacrylonitrile/multiwalled carbon nanotube composite (S/DPAN/MWCNT) as a binder/current collector-free composite cathode exhibited a high capacity at 0.2C, 64% of it being retained at 2C rate [220]. This performance is due to the fact that PAN has high electrochemical performance due to the dipole interactions between nitrile groups -C≡N in PAN and Li^+ ions in the electrolytes. Sulfur/carbon (S/C) nanocomposite-filled polyacrylonitrile (PAN) nanofibers demonstrates a high reversible capacity at a current rate of 200 mA g^{-1}, a high coulombic efficiency of 100% after a few cycles, a good rate capability with 60% capacity retention over 400 cycles at 4.0 A g^{-1} [221]. Pyrolyzed porous spherical composites of polyacrylonitrile-Ketjenblack carbon and sulfur (PAN-KB/S) with a high sulfur content (ca. 72%) (pore volume: 1.42 cm^3 g^{-1}; BET surface area: 727 m^2 g^{-1}) exhibited a high capacity retention and rate capability over 100 cycles at 0.5C, with high sulfur loading (ca. 4.4 mg_{sulfur} cm^{-2}) [222]. A cyclized-polyacrylonitrile-cast carbon nanofiber (CP@CNF) film as an interlayer in Li–S batteries assembled with bare sulfur cathodes deliver superior rate capability and cycle stability over 200 cycles at 0.3C and up to 2C rate [223]. The improved performance are attributed to both the abundant pyridine groups in the cyclized polyacrylonitrile matrix, which can entrap polysulfides by strong interatomic attraction, and the three-dimensional porous conductive network composed of the carbon nanofiber skeleton and conjugated polymer matrix, giving rise to highly effective transfer pathways for electrons and ions.

3.4. Other polymers

Huang et al. introduced the electroactive polymer poly(N-vinyl carbazole) (PVK) into the lithium–sulfur system as a conductive matrix and sulfur reservoir. A core–shell sulfur quantum dot/PVK (SQD/PVK) nanocomposites in which a large number of SQDs (about 5 nm in size) with plenty of internal high capacity over 600 cycles at 0.5C, and at 0.75C over 500 cycles [224].

Anchoring polar polymer Triton X-100 on the surface of carbon materials was efficient to improve the performance of this host for sulfur, owing to the oxygen containing functional groups (hydroxyl and ether group) of Triton X-100. After areal mass loading of 2.5 mg cm^{-2} in sulfur, this electrode showed a capacity retention of 76% after 50 cycles at a rate of 0.2C, and at a rate of 0.5C the capacity decay was 0.3% per cycle over 100 cycles [225]. Sulfur−carbon cathodes based on ethering polyethylenimine

(PEI) polymers bearing large numbers of amine groups in every molecular unit to hydroxyl- and carboxyl-functionalized multiwall carbon nanotubes was also a good strategy, as the incorporation of CNT-PEI hybrids in a sulfur cathode stabilized it by both kinetic and thermodynamic processes [226]. After deep cycling of such a composite with loading of 70% in sulfur, the electrode showed a high capacity retention of ~79% after 300 cycles at 0.5C.

Poly(ethylene oxide) (PEO)/poly-(acrylic acid) (PAA) multilayers on a single poly(allylamine hydrochloride) (PAH)/PAA priming bilayer, deposited on the S_8 cathodes by layer-by-layer deposition. As a result, PAH/PAA/$(PEO/PAA)_3$ multilayer-coated cathodes exhibited the highest capacity retention (806 mAh g^{-1}) after 100 cycles at 0.5C, as well as the high C-rate capability up to 2C. Furthermore, the multilayer coating effectively mitigated the polysulfide shuttle effect in the absent of $LiNO_3$ additives in the electrolyte [227]. In the same spirit, a 7 layer membrane was assembled by sequential absorption of poly diallyldimethylammonium chloride (PDADMAC) and poly(3,4-ethylenedioxythiophene) (PEDOT): poly(styrenesulfonate) (PSS) by the layer-by-layer technique to impede the migration of polysulfides [228]. The capacity fade was reduced to a 33% loss at cycle 500 at 2C rate with a sulfur loading of 1 mg cm^{-2} and 65% sulfur loading by mass in the finished cathode. PEDOT was also shown to improve the performance of the cells in different works [229-230], but was not tested on many cycles.

A new approach that gave promising results consisted in the synthesis of flexible sulfur wires (Flex-SWs) by electrospinning in the form of pressed pellets [231]. The electrospinning procedure yields wires (diameter: 6 mm) which are in-effect encapsulated in a polymer matrix (polystyrene), in proportion 30 wt.% sulfur content and 70 wt.% polystyrene. The polystyrene thus directly addressed the primary problem of polysulfide dissolution. The pressing procedure ensures the formation of a carbon coating which solves the problem of the electrical conductivity. Then, these Flex-SWs have been coated with lithium orthosilicate (Li_4SiO_4), a lithium ion conductor, to further ensure surface polysulfide entrapment and prevent initial capacity fade. This Li_4SiO_4 layer consisted of macroscopic particles fused together as a result of the mechanical pressing process consisting of macroscopic pores ideal for liquid electrolyte percolation. As a result, this multi-composite showed a fade rate of 0.003% over 135 cycles after stabilization but the authors failed to mention how the C-rate.

Finally, polymers of intrinsic microporosity featuring electrophilic 1,4-dicyanooxanthrene moieties were shown to be susceptible to nucleophilic attack by lithium polysulfides, which results in aging. This undesirable chemically was recently mitigated by cross-linking the membranes, showing that the

relationship between membrane chemical reactivity and selectivity are critical for developing membranes for the next generation of Li-S batteries [232]. Other conductive polymers can be used as a shell, like polythiophene (Pth) [233]. Recently, Kim et al. [234] fabricated directly a Nafion nanoweb deposited onto a sulfur cathode to stabilize the polysulfures by electrostatic repulsion, leading to an increase of the cycling life and rate capability

4. Sulfur-inorganic material composite electrodes

As soon as 2005, the role of hydrophilic groups that can absorb the polysulfide to suppress the internal shuttle has been recognize [235]. In particular, the hydrophilicity of the ceramic particles has motivated their insertion as additive in the cathode of Li-S batteries. In an early work, 50 nm-thick $Mg_{0.6}Ni_{0.4}O$ nanoparticles have been introduced, with satisfy partly the purpose as it reduced the diffusion of polysulfides into the electrolyte by 45% [236]. The results suggest the existence of a critical concentration of polysulfides in the electrolyte to activate the internal shuttle phenomenon. Al_2O_3 particles have a similar effect: in concentration 10 wt.% in the sulfur electrode, the capacity was stabilized over 25 cycles (current density of 100 mA g_{sulfur}^{-1}) [237]. Since then, may other inorganic composites were proposed.

As a matter of fact, the progress in the sulfur electrode has been concomitant with that of the Li-ion electrodes [38] and the same recipes applied: in both kinds of electrodes, nanosized particles of metal oxides and ceramics have been used as an additive to the electrode. In the particular case of the cathode of Li-S cells, the best results were obtained with $Mg_{0.6}Ni_{0.4}O$, $Mg_{0.8}Cu_{0.2}O$, Al_2O_3, TiO_2, La_2O_3 [238-243], and recently Nb_2O_5 [244]. The hydrophilicity of the ceramic particles can also improve the wetting behaviors [241]. The advantage of these 30-50 nm-thick particles in this particular case of the Li-S battery is that they reduce the agglomeration of polysulfides by trapping them, which is beneficial to the cycling life. This trapping is more efficient when the effective surface of these particles is larger, the reason why the size of the particles has been decreased to the nanorange.

4.1. Oxides

Mesoporous SiO_2 (SBA-15) is effective as it retains the soluble polysulphides due to its high surface area, large pore volume, bi-connected porous structure and highly hydrophilic surface properties [245]. In the same way, silicon/silica (Si/SiO_2) cross-link with hierarchical porous carbon spheres ($Si/SiO_2/C$), as uses as a new and efficient sulfur host to prepare Si/SiO_2@C-S porous spheres. [246]. The best

results were obtained with 15.5 wt.% of Si/SiO_2, in which case, the initial capacity at 0.5C was large, 61% of which could be retained after 500 cycles at 2C (capacity decay rate is only 0.063% per cycle).

On another hand, the incorporation of manganese into the zeolite silicalite-1 (MnS-1) framework as additive generates Mn^{3+} extra-framework where manganese is in the form of manganese oxide (Mn_2O_3) nanoparticles [247]. Then, manganese modified zeolite silicalite-1 (MnS-1) with a cathode composite containing SBA-15 additive combined highly ordered microporous silica structure within the individual zeolite particles together with nanosized Mn_2O_3 particles to improve the properties of the electrolyte [248]. More recently, ultrafine CeO_2 particles nanoparticles have been used to decorate a sulfur-carbon deposit. 89% of the initial capacity was retained after 100 cycles at 0.2C, and 55% at 5C [249]. ZnO-wrapped sulfur/carbon nanotubes delivered a large capacity at a charge/discharge rate of 160 mA g^{-1}, 42% of which could be retained after 200 cycles at current density of 1600 mA g^{-1} [250]. In a different geometry, a porous bifunctional Nafion/γ-Al_2O_3 membrane was found efficient to stabilize the polysulfides: 54% of the high initial discharge was preserved after 200 cycles at 1C [251]. The best results that have been reported, however, have been obtained recently with S/MnO_2 nanosheets that exhibit a remarkable improvement of the cycling life: 2000 cycles tested with capacity fading rate of only 0.036% [252]. This performance was attributed to a unique mechanism: An active polythionate complex served as an anchor to curtail the dissolution of polysulfides, and a transfer mediator to control the deposition of Li_2S_2 /Li_2S. This outstanding cycleability associated to MnO_2 nanosheets has also been evidenced in [253]. Drawback of the addition of these metal oxides is that their weight is about the same as that of the sulfur, thus reducing by a factor two the energy density.

Another route is the use of composite architecture with void space like in anodes for Li-ion anodes (see [38] for a review), since the void space is used to accommodate the volume change during cycling, even if the volume change is much smaller here than in the case of Li insertion in silicon for example. For example, a S-C yolk-shell cathode delivered 560 mAh per gram of electrode or 1400 mAh per gram of sulfur [254], which, however, decreases significantly as a function of the number of cycles. An $S-TiO_2$ cathode with a yolk-shell architecture showed a coulombic efficiency of 98.4% over 1000 cycles at 0.5C [255] (Fig. 6). Therefore, the TiO_2 shell was very efficient to alleviate the migration of the polysulfides and suppress the shuttle effect, which is corroborated by the ability of mesoporous TiO_2 additives to a C–S composite to improve the cycle life and the capacity retention [53,256]. With the addition of 20 cycle atomic layer deposited TiO_2 on a N-doped graphene used as a host for impregnation of 59 wt.% sulfur, 67% of the initial capacity measured at 0.1C was retained after

500 cycles at 1C with an average coulombic efficiency of about 99.7% [257]. Whether it is used as an additive or a framework, TiO_2 is insulating which limits its role to that of an absorber, implying that the performance of these electrodes at high rate is poor, unless conductive additive is present. However, adding the conductive graphene to TiO_2 solves the problem: coating the surface of a C–S cathode with a graphene/TiO_2 film, which accounted for only ≈7.8 wt.% of the whole cathode enabled the porous carbon nanotubes (PCNTs)–S cathode to exhibit ultrahigh cycling abilities, with a capacity degradation rate of 0.01% and 0.018% per cycle, measured over 1000 cycles at 2C and 3C, respectively [258]. In the same way, hierarchical TiO_2 sphere–sulfur frameworks assisted with graphene showed a capacity loss of only 0.04% per cycle in the prolonged charge–discharge processes at 1C [259]. Other forms of carbon were also used, like an activated carbon (OSAC) obtained from olive stones in a cell with very good results at 2C [260]. In particular, a composite was made by infiltration of sulfur in a TiO_2-grafted carbon paper membrane constructed of interlaced circuitous carbon fibers and TiO_2 nanoparticles distributed on/in the void among the carbon fiber, with good electrochemical performance over 200 cycles at 0.5C and at 5C [261]. The synergistic effects from TiO_2 (polysulfide chemisorption material) and activated carbon fibers (ACF) (electronically conductive material) have been employed to design a hybrid cathode, consisted of S-infused ACF cloth and a thin TiO_2 wrapping layer with a high S-loading of about 3.0 mg cm^{2}, which showed a capacity retention of 77% after 100 cycles at 0.2C, and rate ability at 5C [262]. Recently it has been demonstrated that one reason for the remarkable improvement of the electrochemical performance induced by TiO_2 is the large increase of the diffusion coefficient of Li-ions due to the Ti-S chemical bonding during charge/discharge process [263]. TiO_2 nanotubes decorated with PPy provide a highly ordered conductive framework for Li^+ ion diffusion and reaction with sulfur. The as-designed S/PPy/TiO_2 nanotube cathode had an average coulombic efficiency of 96% after 100 cycles at 0.1C [264].

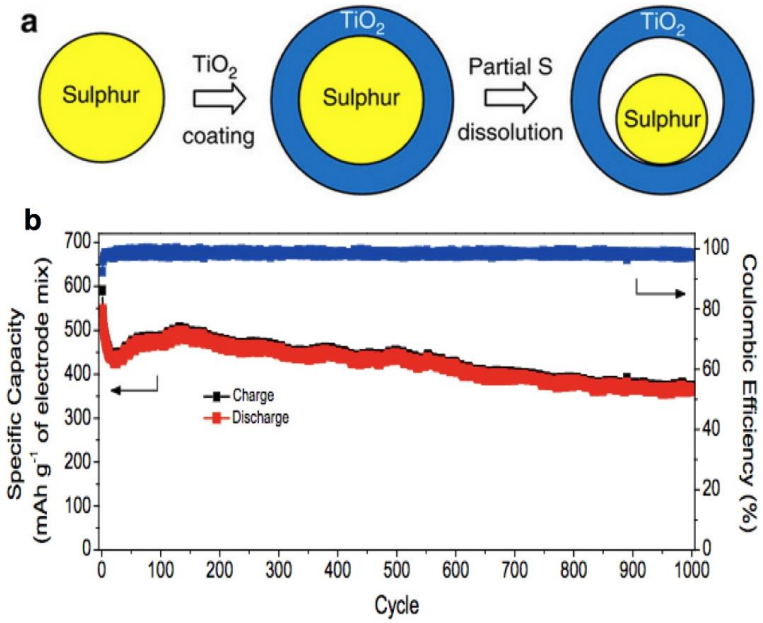

Figure 6. (a) Schematic of the synthetic process that involves coating of sulfur nanoparticles with TiO_2 to form sulfur–TiO_2 core–shell nanostructures, followed by partial dissolution of sulfur in toluene to achieve the yolk–shell morphology. (b) Charge/discharge capacity and Coulombic efficiency of sulfur–TiO_2 yolk–shell nanostructures over 1000 cycles at 0.5C [255]. Reproduced with permission from the Nature Publishing Group.

4.2. Nitrides

Instead of metal oxide, metal nitrides have been proposed: TiN [265-268], VN [269], Mo_2N [270-271], Ni_3N [272], NbN [273]. Recently, another metal nitride has recently been proposed: with porous carbon aerogels modified with VN as the sulfur host, 78% of the initial discharge capacity was retained after 100 cycles at 0.2C. At a higher rate of 1C, maintained at 62% at 1C rate [274]. S/CoS_2 nanoparticles-embedded N-doped carbon polyhedrons exhibited an enhanced cycling stability at 0.5C over 250 cycles, and a good rate capability up to 2C [275]. This result can be compared with another good result obtained with porous CoS_2/carbon paper placed as an interlayer between the separator and the S/rGO cathode [276], which confirms the ability of CoS_2 to trap the polysulfides.

5. Other composite electrodes

5.1. Metal organic frameworks

To improve the rate capability and as an alternative to porous carbon, porous metal organic frameworks (MOF) have been used with success provided they have a chemical formula that makes them stable [277-279], for two reasons. First, the contact between the MOF and the sulfur is very good, which insures a good conductivity, thus improving the rate capability. Second, the interaction between the MOF and the polysulfides is strong so that they cannot migrate into the electrolyte, which improves the cycling life. For example, the chromium trimesate MIL-100(Cr) MOF approximately the same surface area than mesoporous carbon, but outperforms it as a host for sulfur [280]. Increasing the surface are up to 5000 $m^2 g^{-1}$, this MIL-100(Cr)/S composite used as a cathode showed 80% capacity retention after 100 cycles at 0.1C. At rate 0.8 C, 70% of the initial capacity was retained and decreased only by 19.9% over 300 cycles [281]. Modified with reduced graphene oxide (rGO), MIL-100(Cr)/S@rGO gave similar results [282]. As already pointed out, on a general basis, graphene alone is not as efficient as expected in Li-S batteries; its association with polymers is much more efficient. For example, PEG-modified sulfur wrapped by graphene gives better results, because the PEG on the sulfur provides a flexible cushion between the sulfur and the graphene sheet to buffer the volume changes during cycling [283]. In addition to this Cr-based MOF, Ni-based MOF also works, since the bonding between the Lewis acidic Ni^{2+} and basic S^{2-} immobilizes the polysulfides [284]. Nickel fibers/sulfur composites have also been proposed, but the tests have been made on 50 cycles only [285]. Good results have also been obtained recently with a new type of MOF-derived sulfur host containing cobalt and N-doped graphitic carbon (Co–N-GC) [286]. In these different cases, however, the initial capacity is not large, mainly because the electrical conductivity is not high, a problem that affects importantly the rate capability. The term “metal organic” is somewhat misleading, because even if a transition metal is in the chemical formula, the bonds inside the organic material have an ionic component. More recently, a new MOF has been proposed, Ti_4O_7, which has a much better conductivity (2000 S cm^{-1}), and still fixes the polysulfides owing to their strong interaction with the low-coordinated Ti atoms at the surface [287-288]. The Ti_4O_7/S composite as a cathode delivered a large initial capacity retained by 99% after running for 100 cycles at 0.1C, and even at high rate of 2C, 70% of the initial capacity was retained. A novel Zn(II) MOF based separator proved to be able to play an efficient role as an ionic sieve for the soluble polysulfide ions, as it decreased the capacity decay to 0.041% per cycle at 1C over 1000 cycles [289]. Recently, reduced graphene oxide (RGO) wrapped MOFs with cobalt-doped porous carbon polyhedrons used for sulfur immobilizers. This RGO/C–Co–S cathode exhibited greatly improved electrochemical performance, showing excellent capacity at 300^{th} cycle at a current density 0.3 A g^{-1}

[290].

5.2. Other additives

Coating the cathode with a mixed ionic electronic conductor also improved the electrochemical properties by rapid removal of the precipitates on the cathode produced during the discharge [291]. Additives with N-O bonds are also efficient [292] owing to their reaction with the anode surface or with other species in the electrolyte and the salt, which forms a protective film comprising Li_xNO_y and/or Li_xSO_y [293].

Recently, Pan et al. have found that sepiolite, a porous mineral, is an excellent matrix and absorbing material for lithium-sulfur batteries due to its ion transmission channels and large pore volume. Indeed, the sepiolite-sulfur cathode delivered a high capacity at 0.2C rate, 63% of which was retained after 300 cycles. Under 1C current density, the first discharge capacity was still 84% of the initial value at0.2C, and the capacity fading was 0.1% per cycle over 500 cycles [294].

A cobalt hydroxide-covered sulfur/conductive carbon black (CCB) electrode, where the sublimed sulfur is anchored in the CCB, followed by a uniform coating of $Co(OH)_2$ nanosheets, showed a high rate capability. After 200 cycles at 1C, a capacity retention of 71.2% was obtained. These results are much better than those obtained in absence of the $Co(OH)_2$ coat, giving evidence that the $Co(OH)_2$ layer helped to inhibit the shuttle diffusion of the polysulfides [295].

5.3. Other modifications

Mixtures of Li_2S and Fe [296], or Co [297], or Cu [298-300] were proposed as positive electrodes. The MS_x phase (M =Fe, Co, Cu) is formed during the charge process, so that these electrodes have the same defects as any electrode based on a conversion mechanism [38], including large polarization effect, low coulombic efficiency during the first cycles. Another possibility is to use prelithiated sulfur composite as a cathode, to prepare the battery in a discharged state, which permits to get rid of the lithium metal and avoid the problems associated to it (high reactivity, formation of dendrites, safety concern). Alternative anodes that have been proposed include graphite [301-302]. An alternative was the use of $Li_2S–P_2S_5$ [303-304] known to be a very good lithium ion conductor. However, these modifications did not give results that are competitive with respect to the other strategies reported in this review, and in practice, they have been abandoned since 2010.

6. The binders

Conventional binders like polyvinylidene difluoride (PVdF) have been used for Li-S like in Li-ion batteries to bind the active particles. However, some alternative binders have been found, in order to accomodate the large change in volume of the sulfur during cycling, and reduce as much as possible the dissolution and migration of the polysulfides [305-306]. The addition of polyvinylpyrrolidone and polyethyleneimine to the binder inhibit at least partly the formation of agglomerates on the cathode [307]. The use of gelatin as a binder with a S/active carbon nanospheres makes possible to reach the full capacity at the initial stage [308], but the capacity fading was large [309]. Improved transport owing to internal macropores raised the initial capacity but failed to solve the problem of the capacity fading [310].

A dual binder made of cationic polyelectrolyte binder, poly(acrylamide- co-diallyldimethylammonium chloride) (AMAC) plus poly(acrylonitrile–methyl methacrylate) (ANMMA), was used with high-loading sulfur electrodes (sulfur content of 80 wt.%) [311]. The second binder, ANMMA, is used to avoid the corrosion of the aluminum current collector. The electrodes with the AMAC binder retained a porous and complete structure during cycling. Other binders are also used to insure the stability of the electrode, and also mitigate the aggregation of the sulfur [312-314].

The poly(ethylene oxide) (PEO) and its derivatives can also be used as a binder [315]. It dissolves or swells in the liquid electrolyte. The ether-modified solvent interface delays the precipitation of insoluble discharge products and hence affords an improvement in the reutilization of the active material, thus improving the cycling life [316-317]. The amphiphilic Pluronic F-127 block copolymer can partially replace the PVdF binder to provide a polysulfide-retention capability [318]. The reason is that it contains a hydrophobic poly(propylene oxide) (PPO) middle block used to adhere to the hydrophobic sulfur, and two hydrophilic PEO end blocks that create a chemical gradient that limits the diffusion of polysulfides out of the cathode. Owing to these properties, the structure of the electrode is maintained during cycling and the dissolution of polysulfides is reduced, so that the capacity retention is increased. In addition, PEO can facilitate Li^+-ion transference by an electrostatic coordination of Li ions with ether oxygen atoms [319], which increases the rate capability. Cathodes using a 10 wt.% Pluronic F-127 copolymer achieve an excellent electrochemical stability at high 1C and 2C rates.

The Nafion that is used in separators can also be used in binders. A binder composed of Li^+-

Nafion, polyvinylpyrrolidone, and nano silica (employed to enhance polysulfide adsorption and Li^+ conduction) gave very good results when coupled with a macroporous carbon/sulfur composite cathode (Fig. 7) [320].

Poly(acrylic acid) (PAA) swells slightly and dissociates poorly in the organic liquid electrolyte. These features have made it suitable as a water-based binder of the sulfur cathode [321-322]. Poly(ethylene oxide) (PEO) and poly(vinyl alcohol) (PVA-*x*) with different degrees of saponification (*x*%) were recently used as binders to prepare the composite cathodes. Decreasing the degree of saponification leads to increased electrolyte uptake by the PVA-*x* binder, increasing the charge and discharge capacities of Li-S cell. The rate capability of Li-S cell is also enhanced by the partial swelling of the PVA-*x* binder. The enhanced performance of Li-S cell containing PVA-x was attributed to the lowering of resistance of Li^+ ion transport in the composite cathode [323].

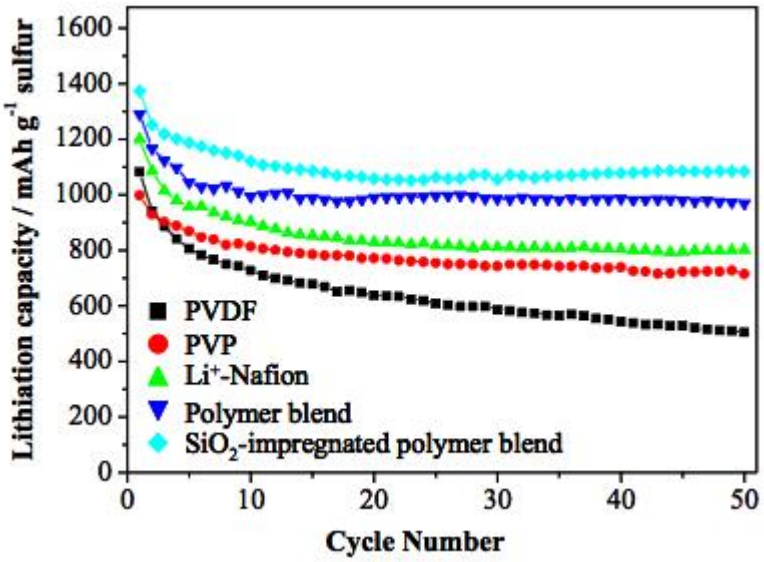

Figure 7. Cycling performance of a cell where macroporous carbon (MPC) is employed for sulfur retention in cathode, using different binders: PVDF, polyvinylpyrrolidone (PVP), Li^+-Nafion, polymer blend of Li^+-Nafion with PVP, and SiO_2-impregnated polymer blend as the binder at 25 °C [320]. Reproduced with permission from Elsevier.

7. The electrolyte

"All liquid" battery refers to a configuration were additives in the electrolyte are used to maintain solubility of the polysulfides aiming to increase the fraction of species electrochemically active [324].

In addition, the ionic conductivity of such cells is very high, but the life of the battery is reduced. Moreover, the reduction of polysulfides on the Li anode necessitates the use of an interfacial ion-conductive membrane as an inhibitor. A solid electrolyte interface (SEI) can be formed by reaction of the lithium with the electrolyte [325]. A protecting polymer layer [326], or amorphous glass, or metal alloy [327-328] layer can also be formed.

Using a solid electrolyte (SE) can alleviate the shuttle problem because both electrolyte types do not dissolve lithium polysulfide and greatly improve cycle performance [329-330]. Among SEs, Li_2S-P_2S_5, Li_2S-P_2S_5-LiI, Li_2S-P_2S_5 -$LiBH_4$, and Li_2S-GeS_2-P_2S_5 systems possess high ionic conductivities exceeding 10^3 S cm^{-1} at room temperature [331-334]. A composite cathode prepared using P_2S_5 combined with another SE, namely $0.82(Li_{1.5}PS_{3.3})\cdot 0.18(LiI)$, showed energy densities at the cell level (18650) of 540 Wh kg^{-1} and 990 Wh L^{-1} estimated from the equivalent structure of a current lithium-ion battery [335]. The gel-polymer electrolytes, however, were more investigated.

In a cell where Sn/C composite was proposed as the anode instead of lithium metal [336], the common liquid organic electrolyte was replaced with a gel-type polymer membrane, formed by trapping an ethylene carbonate/dimethylcarbonate lithium hexafluorophosphate (EC:DMC $LiPF_6$) solution saturated with lithium sulfide in a polyethylene oxide lithium trifluoromethanesulfonate (PEO/$LiCF_3SO_3$) polymer matrix, plus dispersed zirconia ceramic filler to enhance the mechanical properties of the gel. The results were very promising, opening the route to all-solid Li-S batteries. Since then, a variety of polymer electrolytes have been proposed, based on polyethylene oxide (PEO) [337], polyethylene glycol-dimethoxyethane (PEGDME) [338], or tetraethylene glycol-dimethoxyethane (TEGDME) [339-340] with ionic liquids. The polymers are not good conductors, the reason why the working temperature of lithium metal/polymer batteries is raised to 70 °C. A PEO–MIL-53(Al)–LiTFSI thin film electrolyte was used to inhibit polysulfide dissolution [341]. At 80 °C, the discharge capacities at 0.2C was close to theoretical, and 21% of it was retained in the 1000^{th} cycle at 4C (Fig. 8).

$LiNO_3$ is added to the electrolyte, because it participates in the formation of a stable passivation film on the anode that protects it against the attack of the polysulfides [342], and potentially suppresses the gas generation [343]. The passivation of the Li electrode comes from the fact that $LiNO_3$ oxidizes the sulfides to Li_xSO_y species [344], and thus prevents the continuous transport of electrons from Li to polysulfides in the electrolyte. In addition, $LiNO_3$ is capable of catalyzing the conversion of high soluble PS to slightly soluble elemental sulfur near the end of charging process, and that the

combination of a soluble nitrate in the electrolyte and an insoluble nitrate in the sulfur cathode leads to synergetic improvement [343, 345]. For these reasons, $LiNO_3$ is consider as a key additive in the electrolyte for Li-S batteries [346]. However, it can be reduced on the cathode side, which irreversibly affects the sulfur cathode below 1.6 V vs. Li^+/Li [347-348]. In addition, the effect of $LiNO_3$ decomposition on the activation process is revealed to be minimal early on, but in the long term causes enough resistance to deactivate the process [349]. Because of the incompatibility of reduced sulfur species with conventional carbonate-based solvents [350-351], Li-S battery commonly uses an ether solvent 1,3-dioxolane (DOL), although polymerization could occur during cycling with high contents of this cyclic ether as solvent [352]. Tetraethyleneglycol dimethyl ether (TEGDME) is often combined with it [353-355] to take advantage of its good solvation ability, but the reduction of the shuttle effect and the dissolution of the sulfur species is only partial. Recently, a new ether derivative with partially fluorinated structure, ethyl 1,1,2,2-tetrafluoroethyl ether (ETFE) was proposed as an electrolyte solvent [356] in partial or total substitution to TEGDME in DOL/ TEGDME. This resulted in improved results, and the positive role of ETFE to participate to the formation of a passivation layer on the anode, and the dissolution of polysulfides was clearly demonstrated, but it brings polarization particularly in initial cycles, which still needs to be addressed, in particular at high-C rates.

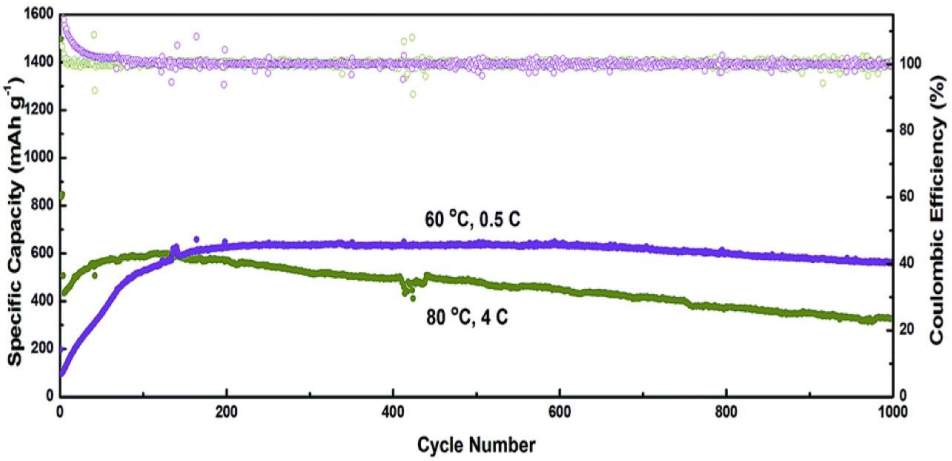

Figure 8. Discharge capacity (solid circle) and coulombic efficiencies (open circle) at 80 °C, 4C (dark yellow, after a three-cycle activation at 80 °C, 0.2C) and at 60 °C, 0.5C (purple), for a battery in which the cathode was fabricated from a slurry of PANI@C/S, carbon black (SuperP) and a binder (80:10:10 by weight). The electrolyte was a PEO–MIL-53(Al)–LiTFSI 60 μm-thick film [341]. Reproduced with permission from the Royal Society of Chemistry.

Recently, acrylate-based hierarchical electrolyte (AHE) for Li-S batteries have been proposed to realize the controllable polymer channels and maximize polysulfide trapping with the minor sacrifice of electrolyte conductivity [357-358]. In particular, a binder-free AHE assembled by integrating a PPETEA GPE with a polymethyl methacrylate (PMMA)-based electrospun fiber network was reported to be a low-cost and effective way to enhance the performance of current Li-S batteries.

A gel polymer electrolyte (GPE) prepared by trapping 1 mol dm^{-3} solution of lithium bistrifluoromethanesulfonamide in tetraethylene glycol dimethyl ether in a polymer matrix composed of poly(vinylidene fluoride-co-hexafluoropropylene)/poly(methylmethacrylate)/silicon dioxide (PVDF-HFP/PMMA/SiO_2) was found to increase the performance [359]. A version of this electrolyte in which SiO_2 was replaced by montmorillonite nanoclay (MMT) was also published [360]. Ahn et al. further improved the performance of a Li-S battery, by introducing a MMT ceramic protective film to form an ion selective separator [361]. The discharge capacity and cycle life obtained with the MMT coated separator in a sulfur–MWCNT composite cathode was retained 67% of the initial capacity after 200 cycles at a current density of 100 mA g^{-1}.

The addition of ionic liquids (IL) improves the conductivity; however, they are usually expensive, a drawback for massive production. Moreover, the solubility of the polysufides in IL is small, so that their addition is less promising than in electrolytes for lithium metal polymer batteries [362-363]. Nevertheless, an ionic liquid, 1-ethyl-3-methylimidazolium bis(tri□uoromethylsulfonyl)imide (EMITFSI), was used successfully as the electrolyte solvent, in which lithium bistri□uoromethanesulfonimidate (LiTFSI) was dissolved to form a 1 mol L^{-1} LiTFSI–EMITFSI electrolyte that improved mesopous carbon/sulfur composite electrode [363]. The addition of DOXL and TEGDME to lower the viscosity raised the initial discharge capacity of the Li-S battery, but the cycling life was poor [364]. Recently, a new electrolyte based on ionic liquid of (N-methoxyethyl-N-methylpyrrolidinium-bis (trifluoromethanesulfonyl)-imide, $P_{1,201}$TFSI) and co-solvents of TEGDME with LiTFSI as lithium salt was proposed [365]. The electrolyte provides a counterbalance between shuttle suppression and solubility of lithium polysulfides by combining the ionic liquid and TEGDME in the optimum mass ratio of 7:3. The 0.4 mol kg^{-1} LiTFSI-$P_{1,201}$TFSI/(30 wt.%) TEGDME electrolyte exhibits good ion transport (room temperature ionic conductivity of 4.3 mS cm^{-1}) and safety (self-extinguishing time of 4.8 s g^{-1}). In addition, it could also operate at 80 °C. Lithium difluoro(oxalate)borate (LiODFB) introduced for the modification to obtain $Pyr_{1,201}$TFSI/TEGDME

electrolyte with LiTFSI/LiODFB binary lithium salts in the optimized mole ratio of 6:4 was reported [366]. The results are very good at 0.1C. No test has been reported at higher rate, however. The introduction of LiODFB is reported to increase significantly the viscosity.

Recently, ionic liquids of the N-methyl-N-propylpiperidinium bis (trifluoromethanesulfonyl) imide (PP13TFSI)-based electrolytes with the $LiNO_3$ additive have been recommended [367]. It is anticipated that the weakly Lewis acidic/basic nature of PP13TFSI induces decreased coordination ability with a Lewis acidic cation of Li^+, and thereby the solubility and mobility of Li_2S_x is successfully controlled.

A strategy to mitigate the polysulfide shuttle is to protect the Li anode from reaction with polysulfides by forming a passivation layer on the Li metal surface [368-370] or a hybrid anode structure [371].Recent experiments have shown that alphalipoic acid (ALA), a unique antioxidant in the human body and commercially available in bulk quantities as a dietary supplement, forms a dense and uniform layer of poly(ALA) at the cathode–electrolyte interface under cathodic conditions prior to the electrochemical reduction of sulfur [372]. Owing to the Donnan potential difference between the sulfur cathode and the poly(ALA) layer imparted by the carboxylate anions attached to poly(ALA), the rejection of the polysulfide anion at the sulfur cathode interface is realized. As a result, alphalipoic acid as an electrolyte additive forms a polysulfide rejection layer on the cathode. In addition, the SEI layer additionally prevents the chemical reaction of the polysulfide and Li metal anode.

8. Lithium salts

Two salts, LiTFSI and LiTf, both at 1 mol L^{-1} concentration, totally dominate the Li–S literature [373], especially LiTFSI because its use almost doubles the electrolyte conductivity compared to LiTf [374-375]. Both these Li-salts are not viable for LIBs as Al (current collector) corrosion starts at ca. 2.8 V vs. Li^+/Li [376]. Some Li-salts that we can foresee to be employed for Li–S batteries in the near future [377]: LiFSI (even more conductive than LiTFSI), if the concerns on the stability of this salt vs. Li–metal anodes [378-379] can be solved; $Li[B(OCH_2CF_3)_4]$ borate salt newly tested, but only on 40 cycles [380]. Kim et al. [381] studied four Li-salts in the same solvent; $LiPF_6$, LiTFSI, LiTf, and LiBETI and Gao et al. [382] did the same for three salts: LiTf, $LiPF_6$, and $LiClO_4$. Both these studies used standard Li–S battery electrolyte solvents DME/DOL (4:1) and tetraglyme, respectively, and a salt concentration of 1 mol. Generally, the linear DME offers higher polysulfide solubility and faster polysulfide reaction kinetics while being more reactive with Li metal, whereas the cyclic DOL forms a more stable solid electrolyte interface on the Li surface while providing lower polysulfide solubility

and slower polysulfide reaction kinetics. Therefore, the combination of DME and DOL leads to synergetic effects on the specific capacity and capacity retention of sulfur compared to their individual use. On the other hand, a remarkable cycleability enhancement of the Li–polysulfide battery is observed with the long-chain, ether-based tetraglyme (TEGDME) solvent [383]. In the work of Kim et al. the winners are LiTFSI (first) and LiBETI (second). Gao et al. [382] claimed to find no significant effect on Li–S cell performance, but only 10 cycles were used in the tests. A study as a function of the LiTFSI concentration led Barchasz et al. [194,195] to recommend a concentration of 1 mol as the best compromise between cost and performance. However, less dissolution of PS and better coulombic efficiency were observed at the higher concentrations of 5 mol [384] and at 7 mol (close to the saturation limit), the polysulfide dissolution was negligible and uniform Li–metal anode plating and stripping was demonstrated [385]

9. The separators

In any battery the separator, which has a microporous functional polymeric membrane, plays a significant job to separate the positive and negative ends avoiding the chance of short circuit occurrence. Another property required for the separators is more specific to the Li-S batteries, namely their ability to inhibit polysulfide migration [386].

9.1. Carbon-modified separators

All kinds of carbon materials have been used to modify the separators, leading to much improved cycle life and capability, provided the carbon is porous and conductive like in [387]. Conductive carbon powder (Super P-Timcal) has been coated on one face of the commercial Celgard 2320, the carbon particles being interconnected by PVDF binder [388]. 72% of the initial capacity was retained after 100 cycles at the rate of 0.5C. Replacing P-Timcal by Ketjen black (KB) layer, Zhao et al. obtained an initial capacity close to theoretical at 0.1C, and 62% capacity was retained after 100 cycles at 1C [389], which is better than the results with an activated carbon (AC) matrix obtained from sisal fibers impregnated of sulfur [390].

Functional sulfonated acetylene black (AB-SO_3) coated separator was proposed recently [391]. The AB-SO_3 coated separator was a highly perm-selective to lithium ions against polysulfide anions, and the coating could function as a secondary current collector. 76% of the initial capacity was retained after 100 cycles at 0.1C.

Coating the commercial separator with a Ketjen black (KB)-MnO composite where KB encapsulated the MnO nanoparticles also increases importantly the performance of the separator [392], because it added the benefit of the conductive carbon and of the metal oxide that we have already discussed on the occasion of their use as host for sulfur in the cathode. The commercial separator modified by porous N-doped carbon nanowires gave excellent results, with 0.08% capacity fading per cycle at 0.5C [393].

N- and O- co-doped graphene sheets (NSG) deposited on a polyethylene separator stabilized the lithium electrode in lithium metal batteries by effectively suppressing dendrite growth and maintaining a uniform ionic flux on the metal surface [394], and for this purpose, the NSG coating was placed near the lithium anode. A Celgar 2400 separator with nitrogen-doped porous hollow carbon sphere (NHC) coating gave excellent electrochemical performance. A good initial discharge capacity at 0.2C was reported recorded, with a low fading rate of 0.11% per cycle within 500 cycles at 1C [395]. Actually, this device makes use simultaneously of the three pertinent parameters that were determined form the works on the carbon as a composite element for the cathode: porosity, hollow-structuration, N-doping.

As an alternative to N-doping, boron-functionalized reduced graphene oxide (B-rGO) layer (only 0.2–0.3 mg cm^2) coated on a separator was demonstrated to improve the electrochemical properties of the Li-S cells [396]. Boron also proved its efficiency on a B-doped multiwalled carbon nanotube coated separator that created a polysulfide trap between the pure sulfur cathode and the polymeric separator and increased importantly the cycleability [397]. This work thus confirms that boron can enhance the binding with polysulfides, which helps suppress the shuttle reactions, and boron doped into the graphene matrix can improve the electrical conductivity of the coating layer. The same effect had been observed with the boron and oxygen dually doped multi-walled carbon nanotubes as the host material for sulfur [398].

An activated carbon nanofiber filters attached onto a polypropylene membrane as separator demonstrated a boost of the performance and capacity fading of 0.13% per cycle after 200 cycles at 0.1C [399]. The surface modification of the commercial polypropylene separator with a nitrogen-doped mesoporous carbon enhanced the initial discharge capacity at 0.2C, and notable cycling stability with high reversible capacity and negligible degradation rate of 0.037% after 1200 cycles at 0.5C [400]. It is not always possible to make a comparison between different results obtained on different separators, because the experiments published in different papers are not made on cells with the same cathode. In the present case, however, the authors used of a simple-mixed sulfur-carbon black cathode with high-

sulfur loading of 3.95 mg cm^2, and the cell with a hybrid separator delivers a high areal capacity of ~3 mAh cm^2. So the remarkable performance of this cell with N-doped carbon with respect to the previous one [395] without doping is attributable to the unique physical and interfacial chemical properties of the N-doping.

A bi-functional separator consisting of a layer of multiwalled carbon nanotubes (MWCNTs) (0.17 mg cm-2) coated on the cathode-side of a Celgard polypropylene sheet could intercept/absorb the migrating polysulfide and suppress the polysulfide diffusion as well [401]. As a result very capacities were obtained at 0.2C and 1C, and the fading rates at both rates was only 0.19 ± 0.03% per cycle after 300 cycles.

A custom single-wall carbon nanotube (SWCNT)-modulated separator could suppress the polysulfide migration. Meanwhile, the conductive carbon scaffold continuously reactivated and reutilized the trapped active material, so that very good results were obtained even at high sulfur loadings [402].

We have already reported in the section devoted to graphene the example of few sandwich structures that improved the performance of the battery. Another sandwich structure was made with one graphene membrane used as a current collector (GCC) with sulfur coated on it as the active material, and the other graphene membrane was coated on a commercial polymer separator [403]. At current density of 1.5 A g^{-1}, the battery retained a capacity of 680 mAh g^{-1} after 300 cycles.

A mesoporous cellular graphene framework (CGF)/polypropylene membrane used as a separator was able to reactivate the shuttling-back polysulfides (and was thus named the Janus separator). The resultant battery retained the capacity after 250 cycles at 0.2C that was 40% higher than with the routine polypropylene membrane [404]. Coating the commercial polypropylene separator with a conductive mesoporous carbon layer boosted the initial capacity and reduced the degradation rate to only 0.081% per cycle after 500 cycles at 0.5C for the same reason why such a coat is also efficient as a component of the cathode (trapping of the polysulfides, large room provided by the porous framework to accommodate the volume change), but in addition, the conducting coat served as a secondary current collector [405].

Reduced graphene oxide (rGO) layer for the separator was also used to take advantage of the chemical absorption of the polysulfides by the functional units of the rGO and the other benefits due to the porosity and conductivity. With this modified separator, 82% of the initial discharge capacity was maintained after 100 cycles at 0.2C and 66% of the capacity was maintained at 2C [406].

A layered MWCNT/SiO_2/MWCNT nanomaterial coated on a polypropylene separator (Celgard 2500) by a layer-by-layer Langmuir Blodgett process created in a clip-like configuration, with gravimetric areal coverage of 130 μg cm^{-2} and a thickness of 3 μm, which efficiently intercepted and reutilized dissolved lithium polysulfides for improving electrochemical performances of lithium sulfur batteries [407].

9.2. Polymer-modified separators

The use of sulfonated tetrafluoroethylene based fluoropolymer-copolymer (Li-Nafion) membrane to separate lithium anode from sulfur cathode successfully reduced the internal shuttle effect [408-411] because polysulfide was blocked by Li-Nafion membrane while Li^+ was not. A Celgard 2400 coated with Nafion also reduced the shuttle effect [412-413]. The improvements, however, were limited, because of the low power of solvation. With a Nafion/super P-modified dual functional separator, a cathode with 70% S-content showed only 0.22% capacity fade per cycle over 250 cycles at 0.5C [414]. Zhuang et al. [415] prepared a ternary-layered separator consisting of a macroporous polypropylene (PP) layer, graphene oxide (GO) barrier layer and Nafion. PP can be regarded as the matrix and provide the high strength, ultrathin layer of GO can block the macropores of PP matrix and further decrease the charge-transfer resistance, and a dense ion selective Nafion layer is attached as a retarding layer to suppress the polysulfide transportation, reducing the capacity fade to 0.18% per cycle within 200 cycles. Therefore, Nafion has become increasingly popular among the cation-selective gel-polymer electrolyte coated on the cathode of Li-S cells. However, the high cost of Nafion limits its use for large scale applications. Also, we have noted that DOL is an essential solvent for Li-S electrolytes, and the strong acidity of Nafion could potentially initiate the ring-opening polymerization of the DOL, if the H^+-form Nafion polymer is used.

The PEO polymer can be acted as a surfactant during the phase inversion to improve the porous structure and enhance the electrolyte uptake [416-417]. A PEO-S composite coated commercial polyolefin separator was used in a Li-S battery to deliver a capacity that increases in the first cycles to reach the maximum only in the 25^{th} cycle, because the PEO-S coat also served as a secondary source of sulfur [418]. A multifunctional separator that combines the properties of Nafion and PEO was prepared by Cai et al. [419]. Super-P was added to the Nafion/PEO membrane to decrease the charge transfer resistance. With this separator, a high initial discharge capacity was delivered at 0.2C, and still 52% of it was delivered at 10C rate. The degradation rate was less than 0.1% per cycle over 300 cycles at 1C.

A polyvinylidene fluoride-carbon (PVDF-C) layer coated on the commercial separator formed a uniform porous network, raising the capacity of the battery after the first 20 discharge cycles at a current density of 0.5C with a coulombic efficiency of more than 90% [420]. A sandwiched gel polymer electrolyte: polyvinylidene fluoride/ polymethyl methacrylate/polyvinylidene fluoride(PVDF/PMMA/PVDF) used as separator solely improved the performance of the Li-S batteries with respect to the commercial binders [421]. The outer PVDF layers are porous, which contributes to ether- based electrolyte to pass through and then enhance Li^+ transfer; the inner PMMA layer is a solid film, which has a good compatibility with ether-based electrolyte and trap the dissolved Li_2S_x ($4 \leq x \leq 8$).

PEG is already used to modify carbon on the cathode side, because it creates a chemical gradient that retards diffusion of the polysulfides into the electrolyte. Advantage has been taken of this property to also modify the surface of the separator with PEG [422-423], which improved the electrochemical performance of lithium-sulfur cells, also by turning the surface of the separator from conventional hydrophobic to hydrophilic to increase the amount of electrolyte uptake, and the hydrophilic surface also reduced the charge transfer resistance of the lithium-sulfur battery.

As seen in the section on polymer additives, polydopamine has been proposed to enter the composition of new cathodes for Li-S batteries, but it is routinely used as a coating layer to enhance the hydrophilic surface properties of the separators [424-425]. The capacity reached with such a modified separator improved the performance by 77% compared with the cells using conventional separators [425] and 59% of the initial capacity measured at 0.2C was still retained after 600 cycles at 0.6C rate [426]. Zhang et al. coated a commercial PP/PE/PP separator (Celgard 2320) by simple immersion in polydopamine. The Li-S battery equipped with this polydopamine-coated separator showed excellent rate performance from 0.5 to 2C [427].

Chitosan, a nitrogenous polysaccharide with abundant hydroxyl groups and amine groups, shows great hydrophilic properties and has a strong affinity to lithium polysulfide which potentially minimizes their loss into the electrolyte [428]. As an additive for cathodes and separators it has also been proven to be an effective polysulfide trapping agent. Li-S batteries with separators that are coated with a carbon/chitosan layer showed a capacity fading of 0.11% per cycle over 200 cycles at 1C [429].

Comparing modified separators, Ma et al. reported that the adsorption effect of polypyrrole(PPy) to lithium polysulfides is stronger compared to that of rGO, and the wettability of the PPy modified separators towards the electrolyte is much better. To illustrate their conclusion, they showed that a Li-S cell with 2.5–3 mg cm^2 sulfur loading using the PPy nanotube modified separator retains 72% of its

initial capacity after 300 cycles at 0.5C [430] (See Fig. 9).

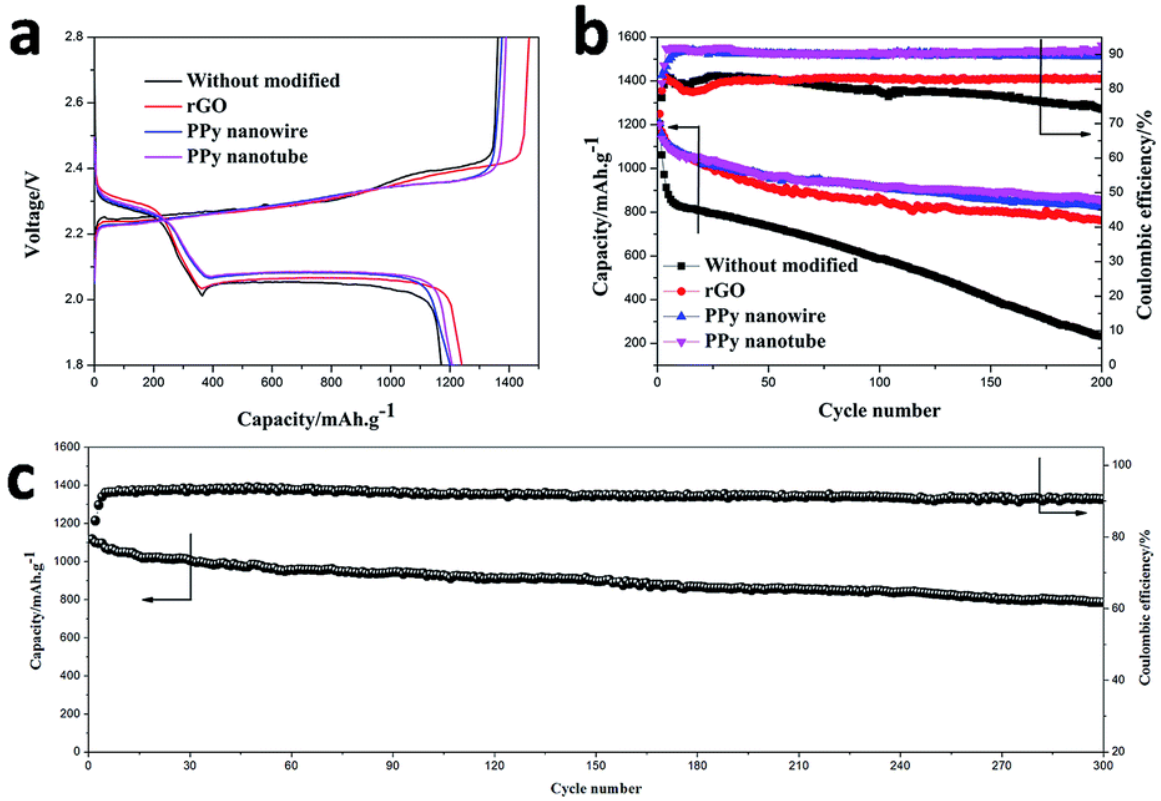

Figure 9. Effect of the modification of the separator with polypyrrole (PPy) nanotubes, PPy nanowires and reduced graphene oxide (rGO) [432]. a) The initial charge–discharge profiles; (b) the cycle performance and coulombic efficiencies of Li–S batteries with different separators at 0.2C; (c) the cycle performance and coulombic efficiencies of Li–S batteries with PPy nanotube modified separators at 0.5C. Reproduced with permission from the Royal society of Chemistry.

9.3. Inorganic material-modified separator

Al_2O_3 particles, already currently used as additive in the cathodes of Li-ion and Li-S batteries, has been also considered for separators. Al_2O_3-coated separator with developed porous channels for lithium-sulfur battery were proposed in [431], with moderate performance. On another hand, a layer of conducting $W_{18}O_{49}$ nanowires deposited on a commercial separator gave very good results, but the tests were limited to 50 cycles [432]. A Li-S cell with a few-layered Ti_3C_2 nanosheet layer covered glass fiber membrane composite separator retained 88% of its initial capacity at a current density of 0.5 A g^{-1} after 100 cycles [433]. This efficiency of Ti_3C_2 confirmed the good results obtained with layered Ti_3C_2 with an accordion-like structure: after loading with sulfur (57.6 wt.%) to form a S/L-Ti_3C_2 composite,

this cathode showed a high initial discharge capacity and an excellent capacity retention of 75% after 100 cycles [434]. With a nanoparticle-embedded mesoporous carbon-coated (RuO_2-MPC) separator, a Li-S cell demonstrated a high initial discharge capacity and a long-term cycling stability over 300 cycles at 0.1C, and a very good capacity retention (at decay rate of 0.022% per cycle, over 200 cycles at 0.5C) [435]. This remarkable performance is due to the synergetic effect of a catalytic behavior of RuO_2 redox reaction of migrating polysulfides, leading to their early adsorption and trapping for further re-utilization, while the MPC insures the electrical conductivity.

9.4. Multi-modified separators

Multi-modified separators have also been built to take benefit of the different positive effects of their three components. They include a three layer carbon nanotube (CNT)/polypropylene/Al_2O_3 separator [436]. The highly porous CNT is here for its high conductivity, and host for sulfur. The hydrophilic Al_2O_3 layer prevented CNT from penetrating the separator and improved the electrolyte intake. Even better results were obtained with graphene/polypropylene/Al_2O_3 separator when graphene and Al_2O_3 were coated on the different side of polypropylene (PP) separator. The graphene layer was in contact with the cathode and considered as an electrolyte reservoir, which was extremely favorable for the electron and ion transportation. The Al_2O_3 layer enhanced the thermal stability, safety and prevented the lithium dendrites. With this modified separator, a high capacity was reached at the rate of 0.2C, 75% of which was retained after 100 cycles [437]. With a thin coated layer composed of the mixture of the electronic conductive carbon and lithium aluminum germanium phosphate (LAGP) to modify the commercial separator for lithium-sulfur battery, 66% of the initial capacity of the Li-S cell was retained after 150 extended cycles at 0.5C rate [438]. The commercial polypropylene separators were also modified with a highly porous, conductive, nitrogen-rich carbon material (TNC) layer and a nitrogen-doped mesoporous carbon layer [439-440]. The initial discharge capacity was close to theoretical at 0.2C, the cyclic stability was excellent, with a degradation rate of 0.037% after 1200 cycles at 0.5C [440]. The lithium-sulfur battery with ultralight weight polyaniline nanofiber/multiwall carbon nanotube (PANiNF/MWCNT) layer to modify the commercial separator separators had high reversible capacities even at 1C rate after 100 cycles [441]. $Ca(OH)_2$–carbon framework derived from crab shells was successfully used to design a modified separator for Li–S batteries, resulting in high initial capacity, 72% of which was retained after 250 cycles at a rate of 0.5C [442].

We have mentioned in a section devoted to the cathodes the remarkable properties of the

sulfur/dehydrogenated polyacrylonitrile/multiwalled carbon nanotube composite (S/DPAN/MWCNT) as a binder/current collector-free composite cathode [220], owing to the interactions between nitryle groups -C≡N in PAN and Li^+ ions in the electrolytes. In the same spirit, PAN separators were proposed. First, the nitryle-Li^+ interaction is also used in these separators, but in addition, the viscoelastic polymer can mechanically suppress the dendrite formation on the anode side. Zhu et al. [443] made polyacrylonitrile/graphene oxide (PAN/GO) nanofiber membrane with high porosity, large number of nitryle and Li_2S/polysulfides and excellent resistance to oxidative degradation. Enormous improvement of the electrochemical properties of Li-S batteries have been with this separator that showed an excellent wettability and good ionic conductivity. The same group prepared a multi-functional separator by coating a super thin layer of multi-walled carbon nanotube sheet on one side of a PAN nanofiber membrane, acting as both a conductive layer and an electrolyte reservoir mitigating the diffusion of the polysulfides to the anode, and the silica particles on the other side, to improve thermal stability and safety [444]

A multilayered membrane (polyetherimide(PEI), poly-anion sodium poly (styrene sulfonate)-polycation poly (dimethyldiallylammonium chloride)$_2$ (PSS-PDADMA)$_2$) was also used recently to improve the performance of Li-S batteries [445]. Polyethylene oxide (PEO)-based polymer separator also gave good results [446].

9.5. Ceramic separators

Owing to their highly porous structure, superior thermal stability, low cost, excellent electrolyte wettability, ceramic glasses can be used as separators n Li-S cells. One of them was used to achieve a good performance at 0.2C [447]. Carbon-coating is of the face on the cathode side, not only because the coat can act as a secondary collector for the current, enabling for an outstanding high-rate response up to 4 C, but also because it serves as a strong absorbent and an effective barrier to trap the diffusion of polysulfides, increasing the cycleability [448]. Melamine formaldehyde-modified glass fiber composite separator showed enhanced thermo-stability [449]. Graphitic carbon nitride (g-C_3N_4) with enriched polysulfide adsorption sites of pyridinic-N was coated on a separator to achieve its functionalization at the molecular level. Besides the conventional pyridinic−N-Li bond formed in the vacancies of g-C_3N_4, the C−S bond between g- C_3N_4 and Li_2S endowed g-C_3N_4 with an inherent adsorption capacity for polysulfides. As a result, an excellent reversible capacity was retained at 0.5C after 400 cycles for a pure sulfur electrode at a current density of 1 C, and the cell still delivered a

stable capacity after 500 cycles. Increasing the sulfur loading to 5 mg cm^{-2}, a high areal capacity of 5.11 mAh cm^{-2} was insured [450]. In addition, g-C_3N_4 is nontoxic and mass produced, so that this modified separator is scalable for industrial use.

Nanofiber membranes have also been considered as separators that can efficiently suppress the formation of the Li_2S_2/Li_2S layer on the cathode [113-115]. Many of them have recently been made owing to electrospinning process; they have been reviewed in [451].

10. Hybrid materials and sandwich architecture

Yang et al. proposed a sulfur-doped microporous carbon (SMPC), which is subsequently rolled into an SMPC interlayer that acts as the polysulfide diffusion inhibitor between a sulfur cathode and separator in a Li–S battery [452]. The SMPC had large specific surface area (3211 m^2 g^{-1}), high pore volume (1.72 cm^3 g^{-1}), good electrical conductivity (1.89 S cm^{-1}) and in situ S-doping (2.72 at.%). Li–S batteries containing the SMPC interlayer delivered a high initial reversible capacity close to theoretical at 0.2C), superior rate capability at 5C, and excellent cycling stability (over 500 cycles at 2C with 0.057% capacity fading per cycle).

N, S-co-doped graphene (NSG) sponge as electroactive interlayer with sulfur cathode showed remarkable performance since an additional contribution of ca. 30% was available from active NSG [453]. As a result, high energy density of 418 Wh kg^{-1} could be released at the power density of 4.55 kW kg^{-1} (6C) based on the total mass of the sulfur cathode and interlayer. The capacity retention was increased by coaxially wrapping graphene over sulfur-coated carbon nanofibers taking advantage of the possibility to coat graphene on carbon nanofibers owing to their difference in zeta-potential by adjusting the pH [454]. The capacity decay was reduced to 0.043% per cycle over 1500 cycles, but it was at the expense of the energy density per gram of sulfur, and the sulfur content of the cathode was limited to 33%. The sulfur content was raised to 49% in case sulfur-coated carbon nanotubes were sandwiched inside the interlayer of graphene sheets [455].

Protruding carbon nanotubes covalently anchored on the graphene sheets inhibited not only the stacking of graphene but also the entanglement of carbon nanotubes [456]. The outstanding conductivity of this graphene-carbon nanotube hybrid, 3130 S cm^{-1}, enabled the operation of the battery without the need of any conducting additive. The retention capacity was very good over 100 cycles at 5C [456].

A sheet-like carbon sandwich, which contained a graphene layer as the conductive filling with N-

doped porous carbon layers uniformly coated on both sides, was obtained by hydrothermal process [457]. This carbon sandwich was about 50–70 nm in thickness and had a high specific surface area (2677 m^2 g^{-1}) and a large pore volume (1.8 cm^3 g^{-1}). At a 2C rate, the capacity fading was only 0.13% per cycle over 200 cycles at 2C rate. Most important, tightly stacked coating on an electrode sheet, guaranteed a volumetric capacity as high as 350 mAh cm^{-3}.

A graphene/carbon nanotube (CNT)/sulfur (denoted GCS) hybrid with interconnected structure with a loading of sulfur of 70% showed a capacity loss of 0.3% per cycle over 100 cycles at 0.3C and the capacity was reduced by 65% only after 450 cycles at 1C [458]. Carbon nanotube-grafted/graphene, with Ni nanoparticles scattered on the graphene sheet showed a high capacity at 0.1C, only reduced by 29% at 30C [459]. Activated carbon introduced in the graphene-carbon nanotube hybrid enables the sulfur content to be increased up to 77 wt.% (sulfur content on the electrode: 69%) [460]. Experimental performance of the cell, extended to the battery at the package level would give an energy density of 400 Wh kg^{-1} for a power density of 10000 W kg^{-1}. Even if these sp^2 -hybridized carbon scaffolds gave the best results, a sandwich-type porous carbon-graphene was able to deliver a high capacity after 100 cycles at 1C [461].

Some additives were also put in sandwich between the electrodes. With a bifunctional microporous carbon paper between the cathode and separator, a significant improvement of the electrochemical properties were observed, increasing the initial capacity to a value close to theoretical even at 1C rate, 73% of which was retained after 100 cycles [462]. Comparable results were obtained by inserting a flexible activated carbon nanofiber interlayer with tunable porosity between the sulfur cathode and the separator [463]. Interestingly, the results were not as good when the microporous carbon was replaced by multi-walled carbon nanotubes (MWCNTs) [464], indicating that the conductivity is not the only parameter: we recover the fact that the porous form of carbon is more efficient to absorb/adsorb more dissolved sulfur species from the electrolyte than the non-porous (MWCNT) form. The Li−S cells fabricated with self-assembled MWCNT interlayer and a high loading of 3 mg cm^{-2} sulfur retained 95.8% of the capacity at 0.5C rate after 100 cycles [465]. On another hand, reduced graphene oxide-based film sandwiched between the sulfur cathode and the separator, effectively acted as a shuttle inhibitor [466]. The lithium–sulfur cell with such a configuration retained 71% of the initial capacity after 100 cycles. A lightweight multifunctional porous sulfur–nitrogen dual-doped graphene (SNGE) interlayer coupled with a porous-CNT/S cathode enables the Li-S battery to deliver a reversible specific capacity close to theoretical at 0.25C and a much higher rate performance, up to 40C. Critically, these

cathodes exhibited ultrahigh cycleability when cycled at 8C for 1000 cycles, exhibiting a capacity degradation rate of 0.01% per cycle [467] (See Fig. 10).

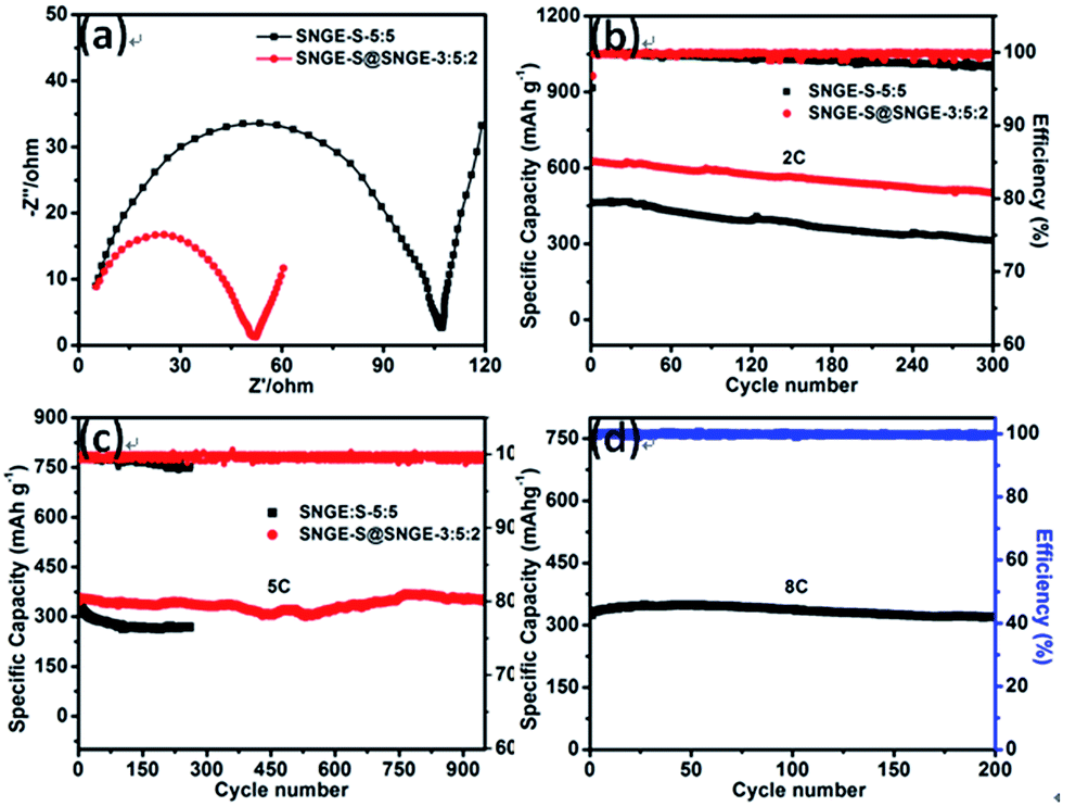

Figure 10. Effect of porous sulfur–nitrogen dual-doped graphene (SNGE) interlayer coupled to a porous-carbon nanotube/S cathode (PCNT–S) [469]. (a) Nyquist curves from EIS measurements; (b) cycling performance and their corresponding galvanostatic discharge–charge profiles at 2C; (c) cycling performance of SNGE–S-5:5 and SNGE–S@SNGE 3:5:2 cathodes at 5C; (d) cycling performance of SNGE–S@SNGE 3:5:2 cathode at elevated rate of 8C. Reproduced with permission from the Royal society of Chemistry.

We have already mentioned that PAA possesses carboxyl groups throughout the chain, which was shown to be effective in suppressing the polysulfide shuttling effect by forming hydrogen bonds [468]. It is also known for its hydrophilic properties [469]. That is why this polymer now enters into the composition of interlayers. Taking advantage of these properties, an ultrathin poly(acrylic acid) coated single-walled carbon nanotube (PAA-SWNT) film was used as an interlayer between the cathode and

the separator with the coat on the cathode side. This interlayer lowered the charge transfer resistance by the support of the upper current collector, but also localized the dissolved polysulfides within the cathode part by the aid of a physical blocking and chemical bonding [470]. As a result, the sulfur cathode with a PAA-SWNT interlayer maintained higher capacity retention over 200 cycles and achieved better rate retention: 57% retention of the initial capacity at 1C rate after 200 cycles. A gel obtained by adding the liquid electrolyte with porous PAA membrane chemically blocked the out-diffusion of polysulfide anions by forming hydrogen bonds between the carboxyl groups in the gelled PAA [471]. Such an interlayer placed between the cathode and a Celgard 3401 separator improved importantly the performance of the Li-S cell and increases the cycle life from 100 cycles to 300 cycles [472]. A porous CoS_2/carbon paper placed as an interlayer between the separator and the S/rGO cathode with a sulfur content of 70.5% retained 66% of its initial capacity at 0.2C after 200 cycles [276].

The chemical polysulfide-trapping capability of an alcohol–alkaline/thermally-treated porous Torey carbon paper was studied in [473]. In addition to the properties of porous carbon, the paper introduces hydroxyl functional groups onto the interlayer, enhancing its hydrophilicity. The beneficial effects of the hydrophilic functional groups have already been described when discussing the advantage of PEO as a binder: create chemical gradients that chemically limit the diffusion of polysulfides and increase the transference of the Li^+-ions. As a result, the initial discharge capacity was 1651 mAh g^{-1}, and a capacity retention of 85% was retained up to 1C rate. In a unique natural approach, inherent water-locking film of carbonized tree leaves was used to block the migrating polysulfides. The micro/mesoporous adsorption sites of the carbonized leaf interlayer not only intercept/trap the migrating polysulfides, but also facilitate their reutilization. Long term cycleability over 150 cycles with a low capacity fading rate of 0.18% per cycle [474].

Three-dimensional carbonized bacterial cellulose was used as an interlayer between the cathode and the separator [475]. A capacity of 525 mAh per gram of cathode plus interlayer was retained after 400 cycles at current density 400 mA g^{-1}. Note the high specific capacity with respect to the total mass of the cathode, due to the fact that the sulfur content was as high as 81%, and the fact that the cell did not require any metal current collector, conducting additive and binder.

A hierarchical carbon nanotube-loaded glass-filter composite (GF/CNT) paper interlayer which offers a high degree of electrolyte uptake as well as superior conductivity for the reactivation of dissolved polysulfides was used between the separator and the cathode to build a cell that retained 72%

of the initial discharge capacity of 803 mAh g^{-1} at 0.2C rate after 230 cycles [476]. A polypyrrole nanotube film (PNTF) was used as a functional interlayer between the cathode and the separator in cells that retained 65% of the initial capacity after 300 cycles at 0.5C [477-478].

A novel interlayer made from Fe_3C/carbon nanofiber webs placed between the separator and the sulfur cathode plays many synergistic roles, offering (i) a number of macropores within the nanofiber web to facilitate ion transport and electrolyte penetration, (ii) nitrogen containing functional groups that entrap soluble polysulfides by strong interatomic attraction, and (iii) much enhanced electron/ion transfer due to the high electrical conductivity of the carbon nanofiber web. As a result, the battery maintained 76% of its initial capacity at 0.1C rate [479].

The best results, however, were obtained with a three-dimensional carbon fiber cloth (CFC) placed between the separator [480]. At 1C, this interlayer increased the performance, so that the capacity degradation rate was reduced to 0.025% per cycle over 1000 cycles at 5C. The ultrafast and long-life cycling stability obtained owing to this interlayer is very promising for the development of the Li-S battery in the near future.

With another architecture, 0.5 nm thick layer of Al_2O_3 conformably coated onto highly porous carbon cloth by atomic layer deposition (ALD) and then assembled between the separator and Li anode increased the specific discharge capacity by 25% at the 1st cycle, and by 114% at the 40th cycle [481], but the authors fail to specify the C-rate. A porous Al_2O_3 protective layer was also fabricated on the surface of the metallic lithium anode by using a spin-coating method [482]. The lithium anode can also be coated with a Li_3N protection layer to suppress the shuttle effect [483]. Owing to this protection, the 70% of the initial discharge capacity was retained after 500 cycles at 0.5C, with an average coulombic efficiency of 92.3% in the electrolyte without $LiNO_3$, while the sulfur loading of the simple sulfur cathode was 2.5–3 mg cm^{-2}. Coating the metallic lithium with PPy was not as efficient as coating with Li_3N [484].

11. Alternative electrodes

11.1. Alternative cathodes

Instead of pure sulfur, other cathodes have been tested. They are polysulfides [485-489], poly(acrylonitrile)-sulfur composite [215, 217, 490-494], lithium superionic sulfide by coating nano-structured lithium sulfide (nanoLi_2S) with lithium phosphorus sulfide (Li_3PS_4) [495]. An alternative

was the use of $Li_2S–P_2S_5$ [496-497] known to be a very good lithium ion conductor. Other tested cathodes include lithium polysulfidophosphates [498] and poly(sulfurrandom- 1,3-diisopropenylbenzene) (poly(S-r-DIB) [499-500]. Among polysulfide-based cathodes, the 3D Li_2S/graphene cathode, binder-free and without metallic current collectors or conducting additives, exhibited a high capacity retention of 87.7% after 300 cycles at 0.2C, and high-rate capacity up to 4C [501]. The same cathode with reduced graphene oxide instead of graphene did not give as good results [502], which illustrates the advantage of graphene, owing to its remarkable conductivity. Li_2S has several advantages. It is compatible with metal-free anodes; moreover, there are no large volumetric expansion in the lithiation/delithiation process of the Li_2S electrode, which is different from the sulfur electrode [503-505]. That is why many works are done on the Li_2S@C cathode, and we guide the reader to a recently published review on all-solid-state cells based on Li_2S cathodes [506] for a more exhaustive report.

S/Bi_2S_3/ porous carbon composites were prepared, where Bi_2S_3 formed in-situ in excess of melt sulfur atmosphere was homogeneously distributed with S and C [507]. The cutoff voltage of the cathodes was set as 1.8 V with the purpose of avoid electrochemical reaction of Bi_2S_3 at lower potential [508-510]. As a result, the capacity was stable at 0.5C over 400 cycles, with 91% capacity retention and high coulombic efficiency.

The inverse vulcanization of sulfur using divinylbenzene (DVB) was used to create a sulfur/organic polymer network with good chemical stability [511]. The Li-poly (S-DVB) cell demonstrated an extremely low degradation rate of 0.04% per cycle achieving over 1600 cycles at C/2 current rate. With the amorphous state of a NiS_2 host, a Li-S battery showed a very high initial specific capacity close to theoretical at 0.1 A g_{sulfur}^{-1} and could retain 77% of the initial capacity after 1200 cycles at 0.5 A g_{sulfur}^{-1} [512].

A sandwiched cathode configuration composed of pristine Li_2S powder in between two layers of self-weaving, binder-free carbon nanotube (CNT) electrodes gave good results, but only with low loading (23%) of sulfur [513]. Three-dimensional reduced graphene oxide supported Li_2S/carbon composite is an alternative cathode retained 50% of the initial capacity at 0.1C after 100 cycles at 1C [514]. Coating of graphene interlayer onto Li_2S proposed as a cathode exhibited a capacity retention of above 60% over 300 cycles at 5C [515].

11.2. Alternative anode: example of Si

The problems of lithium metal are known: strong reactivity, formation of dendrites, safety concerns, so that recent attempts have been made to replace Li by another anode, chosen among the anodes already used in Li-ion batteries. We have recently reviewed such anodes [38], and simply guide the reader to this book for details. The particular case of the silicon-based anode, however, merits a special attention in the context of the sulfur-based cathode. The reason is that it is necessary to have an anode with a large capacity if we want to take benefit of the large capacity of the sulfur cathode, otherwise, the capacity of the battery will be limited by the cathode. Except the lithium itself, the material that has the highest theoretical capacity is silicon, which also has a small redox potential versus Li^+/Li. That is why efforts have been made to choose alloy-type silicon anodes for Li-S batteries. In first attempts, lithiated amorphous silicon film as anode and sulfur/carbon black composite as cathode was proposed. [516]. Results were improved by adding ionic liquid in the electrolyte [517]. The poor cycleability, however, was disappointing. Actually, Si suffers of a low conductivity, so that it must be coupled to a conductive agent like carbon, in an open structure that enables the huge variation of volume of silicon during cycling. Fortunately, important improvements have been made in the recent years to prepare Si-based anodes for Li-ion batteries [38], which are now beneficial to the Li-S battery. Of course, since we need a reservoir of lithium somewhere we need either to have lithiated sulfur in anode, or a lithiated silicon in anode. A major improvement has been made by choosing as the anode silicon lithiated up to a Li concentration that keeps the Si stable, coupled with hollow carbon spheres/sulfur composite as the cathode [518]. This full cell sustained 100 cycles. With lithiated Nafion-coated porous Si as anode and sulfur as cathode, a stable capacity was retained over 100 cycles [519]. Si nanowires coupled with Li_2S–mesoporous carbon as the cathode delivered a reversible capacity corresponding to an energy density of 630 Wh kg^{-1} for 100 cycles [520] based on the total weight of the electrodes. Si(lithiated)-S full cells using lithiated Nafion-coated porous Si as anode and sulfur as cathode achieved energy density more than 2 times higher than commercially available lithium-ion batteries [521].

12. Concluding remarks

The confinement of the sulfur into the meso- and microporous carbon initiated by the group of Nazar has greatly improved the performance of Li-S batteries through the years. Moreover, strategies have been developed to suppress the internal shuttle effect by using additives that fix the polysulfides. As a consequence, the cycle life of the Li-S batteries exceeds 1000 cycles with a good coulombic efficiency. This outstanding progress was mainly obtained between 2010 and 2013, but the price to be paid was a

rather small energy density, because of the important concentration of carbon or polymers in the electrode that limited the loading of the sulfur. Then, the efforts since 2014 have been more focused on the increase of the power density, and of the energy density. Progress in this area has been obtained owing to a combination of strategies: Control the porosity of the carbon, use the most conductive forms of carbon, in particular graphene sheets, since graphene can act as a current collector. It reduces weight of the cell and increases the power density since it is highly conductive. The control of the porosity of carbon is sufficient to solve the problem of the internal shuttle that reduced the cycling life of the Li-S batteries. Owing to its hierarchical micro-, meso- and macropore structure, the performance of a carbide-derived/S cathodes is demonstrated over 4100 cycles with sulfur content of 69.7 wt.% per total electrode [61]. To improve the rate capability, doping the carbon is a first solution. In particular, N-doping helps immobilizing the sulfur. Nitrogen and oxygen dual-doped porous carbon that possesses a hierarchical porous structure serving as a host for 64.5 wt.% sulfur content shows good electrochemical performance over 600 cycles at rate of 1C (based on the sulfur) [76]. It would be interesting to look at the effect of doping on the performance of an optimized form of carbon such as the carbide-derived carbon after doping. Different examples mentioned in this review show that the advances in the development of carbon substrates under different forms have increased the discharge capacity to a value corresponding to the use of almost 100% of the sulfur at low cycle rate and an enhancement in cycle life to 1000 cycles, with good electrochemical properties up to typically 0.5C for electrodes containing 60-70% of sulfur.

To increase the performance at higher C-rates, one has to play with the form of carbon that is used. Functionalized carbon nanotubes (CNTs) showed a low capacity decay rate (0.025% per cycle) at C/3 rate over 1300 cycles. Even for 1000 cycles at 2C and 5C for charge and discharge, a substantial capacity retention of 75.8% capacity retention was maintained [117]. The drawback, however, is that the synthesis includes many steps, which also means a major difficulty to make it scalable.

Another form of carbon that is to be considered is graphene oxide. One difficulty met with graphene oxide is that it is insulating, like sulfur, so that the addition of conductive agents is unavoidable and can weight typically 20 wt.%, so that graphene is usally believed to be more promising. However, a cationic surfactant (cetyltrimethyl ammonium bromide) insures a uniform deposition of sulfur on graphene oxide [140] so that the content in sulfur can reach 80%. In this case, there is 56 wt.% of sulfur in the electrode, and even though the capacity is divided by approximately two when the total weight of the electrode is taken into account, it is superior to the weight density

available with the Li-ion technology. Graphene foams have the advantage of being much more conductive than graphene oxide and they also can host a high sulfur loading, provided an essential parameter that it has the appropriate porosity. A graphene foam electrode with 10.1 mg cm^{-2} sulfur loading could deliver a high areal capacity of 13.4 mAh cm^{-2} and preserve stable cycling performance with 0.07% capacity decay per cycle over 1000 cycles [172,173]. If even better cycling performance is needed, one can take advantage of the stabilizing effect of TiO_2 on the polysulfides. The drawback is the increase in the weight of the electrode, but a compromise can be found: coating the surface of a C-S cathode with a graphene/TiO_2 film accounting for only ≈7.8 wt.% of the whole cathode is sufficient to enable a porous carbon nanotubes (PCNTs)–S cathode to reduce the capacity degradation rate of 0.01% and 0.018% per cycle, measured over 1000 cycles at 2C and 3 C.

The carbon is useful not only for the cathode, but also for the separator. Improvements of the electrochemical performance of the Li-S cells has been systematically observed upon coating the commercial separators with carbon, preferentially N-doped with the appropriate porosity. The most promising strategy, however, is to add interlayers. In particular, a remarkable improvement was obtained by inserting a three-dimensional carbon fiber cloth [480] or carbonized bacterial cellulose (CBC) [475] between the separator and the sulfur cathode. In the last case, the intrinsic macroporous structure of CBC contributed to a high sulfur loading of 81 wt.%, so that the capacity was 525 mAh per gram of cathode plus interlayer after 400 cycles, and the ultralight interlayer does not result in any weight penalty.

For electrolytes, efforts have been made to improve the performance of the Li-S cells with respect to the popular combination DOL/TEGDME and LiTFSI salt with or without $LiNiO_3$. An acrylate-based hierarchical electrolyte assembled by integrating PPETEA with a polymethyl methacrylate (PMMA)-based electrospun fiber network was reported to be a low-cost and effective way to enhance the performance of current Li-S batteries [357,358].

These results show that the stabilization of the polysulfides have been obtained by coating the electrodes and/or the separator and/or by introducing functional interlayers that are of nano-size, and thus very light. Capacities per gram of sulfur have increased and are now not far from the theoretical value, but in addition, the loading in sulfur has significantly increased up to 70-80 wt.%, against 50 wt.% few years ago. The lithium-sulfur battery has thus fully benefited from the progress that has been made in nanoscience, making possible “nano-painting” with functional products that have been efficient to suppress the shuttle effect without penalty on the weight. At this point, the best results make

the Li-S battery competitive with most of the Li-ion batteries at the laboratory scale. Attention should now be more focused on the scalability of the synthesis process. Nanotubes or even graphene are still difficult to synthesize at the industrial scale and most of the synthesis processes that give the best results are still probably too expensive to access the market. The trends in the recent years also show that the progress will come from a combination of optimized synthesis of all the elements of the cell: electrodes, electrolyte and separator since their properties are correlated and play an important role in the overall performance of the cells. So far, however, almost all the works that have been reported in the literature mention the capacities of the cells per gram of sulfur. Among the exceptions, a capacity for the whole cathode electrode (including the conductive additive and the binder) was reported at 877 mAh $g_{electrode}^{-1}$ [179]. Now that all the Li-S cells that have been published the two last years have in common the property that almost all the sulfur in the cell can be used, with capacities that are stable over hundreds or even thousands of cycles, the problem is different: What is the energy density and power density per gram of the full cell? This is the only useful information needed to make a comparison between the cells in order to optimize the different combinations of the different elements in the cell, and this is the information that should now be reported in the next works to be published. It is also the only way to make a true comparison with respect to other chemistries such as Li-ion cells and prove that the hope we put in the future of the Li-S battery is justified. There is one result where such data have been reported: a composite cathode prepared using P_2S_5 combined with a solid electrolyte to form an all-solid-state Li-S battery working at room temperature showed energy densities at the cell level (18650-type) of 540 Wh kg^{-1} and 990 Wh L^{-1} at 25 °C, estimated from the equivalent structure of a current lithium-ion battery [335]. This is indeed encouraging, since this is sufficient to electric vehicles, provided the cycle life extends to thousands of cycles (only 100 cycles have been tested in this particular case).

References

[1] K. Zaghib, A. Mauger, C.M. Julien, *Rechargeable Lithium Batteries for Energy Storage in Smart Grids*, Chap. 12 in: Rechargeable Lithium Batteries, Woodhead Publishing Series in Energy, vol. 81, Elsevier (2015).

[2] D. Peramunage, S. Licht, Science 261 (1993) 1029.

[3] D. Herbert, J. Ulam, U.S. Patent 3,043,896 (1962) accessed July 10.

[4] M.L.B. Rao, U.S. Patent 3,413,154 (1968) accessed November 28; D. Nole, V. Moss, U.S. Patent 3,532,543 (1970) accessed October 6.

[5] Lange's Handbook of Chemistry, ed. J. A. Dean, 3rd ed., McGraw-Hill, New York, 1985, pp.

3–5.

[6] X. Ji, L. F. Nazar, J. Mater. Chem. 20 (2010) 9821.

[7] L. Nazar, M. Cuisinier, Q. Pang, MRS Bulletin 39 (2014) 436.

[8] X. Fang, H. Peng, Small (2014) DOI: 10.1002/smll.201402354.

[9] G. Xu, B. Ding, J. Pan, P. Nie, L. Shen, X. Zhang, J. Mat. Chem. A 2 (2014) 12662.

[10] D. Bresser, S. Passerini, B. Scrosati, Chem. Commun. 49 (2013) 10545.

[11] D.-W. Wang, Q. Zeng, G. Zhou, L. Yin, F. Li, H.-M. Cheng, I. R. Gentle, G. Q. M. Lu, J. Mat. Chem. A 1 (2013) 9382.

[12] R. Van Noorden, Nature 507 (2014) 26.

[13] C. Li, H. Zhang, L. Otaegui, G. Singh, M. Armand, L. M. Rodriguez-Martinez, J. Power Sources 326 (2015) 1.

[14] B. Yan, X. Li, Z. Bai, X. Song, D. Xiong, M. Zhao, D. Li, S. Lu, J. Power Sources 338 (2016) 34.

[15] H. Yamin, E. Peled, J. Power Sources 9 (1983) 281.

[16] K. Kumaresan, Y. Mikhaylik, R. E. White, J. Electrochem. Soc. 155 (2008) A576.

[17] J.-I. Yamaki, S.-I. Tobishima, Y. Sakurai, K.-I. Saito, K. Hayashi, J. Appl. Electrochem. 28 (1998) 135.

[18] L. Yuan, X. Qiu, L. Chen, W. Zhu, J. Power Sources 189 (2009) 127.

[19] S. Walus, C. B archasz, J.-F. Colin, J.-F. Martin, E. Elkaim, J.-C. Lepretre, F. Alloin, Chem. Commun. 49 (2013) 7899.

[20] B. M. L. Rao, J. A. Shropshire, J. Electrochem. Soc. 128 (1981) 942.

[21] Y. V. Mikhaylik, J. R. Akridge, J. Electrochem. Soc. 151 (2004) A1969.

[22] Y.X. Ren, T.S. Zhao, M. Liu, P. Tan, Y.K. Zeng, J. Power Sources 336 (2016) 115.

[23] T. Danner, G. Zhu, A. F.Hofmann, A. Latz, Electrochim. Acta 184 (2015) 124.

[24] V. Knap, D.-I. Stroe, M. Swierczynski, R. Purkayastha, K. Propp, R. Teodorescu, E. Schaltz, J. Power Sources 336 (2016) 325.

[25] S.M. Al-Mahmoud, J.W. Dibden, J.R. Owen, G. Denuault, N. Garcia-Araez, J. Power Sources 306 (2016) 3230.

[26] B. H. Jeon, J. H. Yeon, K. M. Kim, I. J. Chung, J. Power Sources 109 (2002) 89.

[27] C. Barchasz, J.C. Leprêtre, F. Alloin, S. Patoux, J. Power Sources199 (2012) 322.

[28] J. Zheng, M. Gu, C. Wang, P. Zuo, P. K. Koech, J. Zhang, J. Liu, J. Xiao, J. Electrochem. Soc. 160 (2013) A1992.

[29] S. S. Zhang, Electrochem. Commun. 31 (2013) 10.

[30] Y. Diao, K. Xie, S. Xiong, X. Hong, J. Electrochem. Soc. 159 (2012) A421.

[31] J. Nelson, S. Misra, Y. Yang, A. Jackson, Y. Liu, H. Wang, H. Dai, J. C. Andrews, Y. Cui, M. F. Toney, J. Am. Chem. Soc. 134 (2012) 6337.

[32] H. Marceau, C.-S. Kim, A. Paolella, S. Ladouceur, M. Lagacé, M. Chaker, A. Vijh, A. Guerfi,

C.M. Julien, A. Mauger, M. Armand, P. Hovington, K. Zaghib, J. Power Sources 319 (2016) 247.

[33] M. U. M. Patel, R. Demir-Cakan, M. Morcrette, J. M. Tarascon, M. Gaberscek, R. Dominko, ChemSusChem 6 (2013) 1177.

[34] A. Paolella, W. Zhu, H. Marceau, C.-su Kim, Z. Feng, D. Liu, C. Gagnon, J. Trottier, G. Abdelbast, P. Hovington, A. Vijh, G. P. Demopoulos, M. Armand, K. Zaghib, J. Power Sources 325 (2016) 641.

[35] Y. Su, Y. Fu, T. Cochell, A. Manthiram, Nat. Commun. 4 (2013) 2985.

[36] E. Peled, A. Gorenshtein, M. Segal, Y. Sternberg, J. Power Sources 26 (1989) 269.

[37] J. Wang, L. Liu, Z. Ling, J. Yang, C. Wan, C. Jiang, Electrochim. Acta 48 (2003) 1861.

[38] C.M. Julien, A. Mauger, A. Vijh, K. Zaghib, *Lithium Batteries*, Ed. by Springer (2016).

[39] S.-C. Han, M.-S. Song, H. Lee, H.-S. Kim, H.-J. Ahn, J.-Y. Lee, J. Electrochem. Soc. 150 (2003) A889.

[40] W. Zheng, Y. W. Liu, X. G. Hu, C. F. Zhang, Electrochim. Acta, 51 (2006) 1330.

[41] Y.-J. Choi, K.-W. Kim, H.-J. Ahn, J.-H. Ahn, J. Alloys Compd. 449 (2008) 313.

[42] L. Yuan, H. Yuan, X. Qiu, L. Chen, W. Zhu, J. Power Sources, 189 (2009) 1141.

[43] X. Ji, K. T. Lee, L. F. Nazar, Nat. Mater. 8 (2009) 500.

[44] Y. Yang, G. Yu, J. J. Cha, H. Wu, M. Vosgueritchian, Y. Yao, Z. Bao, Y. Cui, ACS Nano 5 (2011) 9187

[45] X. Y. Zhao, J. P. Tu, Y. Lu, J. B. Cai, Y. J. Zhang, X. L. Wang, C. D. Gu, Electrochim. Acta 113 (2013) 256.

[46] X. Zhou, J. Xie, J. Yang, Y. Zou, J. Tang, S. Wang, L. Ma, Q. Liao, J. Power Sources 243 (2013) 993.

[47] Q. Li, C. Zhou, Z. Ji, B. Han, L. Feng, J. Wu, J. Mater. Chem. A 3 (2015) 724.

[48] C. Lai, X. P. Gao, B. Zhang, T. Y. Yan, Z. Zhou, J. Phys. Chem. C 113 (2009) 4712.

[49] X. Li, Y. Cao, W. Qi, L. V. Saraf, J. Xiao, Z. Nie, J. Mietek, J. Zhang, B. Schwenzer, J. Liu, J. Mater. Chem. 21 (2011) 16603

[50] J. Zheng, M. Gu, M. J. Wagner, K. A. Hays, X. Li, P. Zuo, C. Wang, J. Zhang, J. Liu, J. Xiao, J. Electrochem. Soc. 160 (2013) A1624.

[51] G. He, X. L. Ji, L. Nazar, Energy Environ. Sci. 4 (2011) 2878.

[52] H. Ye, Y.-X. Yin, Y.-G. Guo, Electrochim. Acta 185 (2015) 62.

[53] J. Schuster, G. He, B. Mandlmeier, T. Yim, K. T. Lee, T. Bein, L. F. Nazar, Angew. Chem. Int. Ed. 51 (2012) 3591.

[54] Y.-S. Su, Y.-Z. Fu, B. Guo, S. Dai, A. Manthiram, Chem. Eur. J. 19 (2013) 8621.

[55] J. Y. Koh, S. Kim, M.-S. Park, H. J. Yang, T. H. Yang, Y. Jung, Electrochim. Acta 212 (2016) 212.

[56] C. Liang, N. J. Dudney, J. Y. Howe, Chem. Mater. 21 (2009) 4724.

[57] D. Wang, A. Fu, H. Li, Y. Wang, P. Guo, J. Liu, X. S. Zhao, J. Power Sources 285 (2015) 469.

[58] Y.-J. Choi, Y.-D. Chung, C.-Y. Baek, K.-W. Kim, H.-J. Ahn, J.-H. Ahn, J. Power Sources 184 (2008) 548.

[59] C. Wang, J. J. Chen, Y. N. Shi, M. S. Zheng, Q. F. Dong, Electrochim. Acta 55 (2010) 7010.

[60] K. Li, B. Wang, D. Su, J. Park, H. Ahn, G. Wang, J. Power Sources 202 (2012) 389.

[61] S. Thieme, J. Brückner, A. Meier, I. Bauer, K. Gruber, J. Kaspar, A. Helmer, H. Althues, M. Schmuck, S. Kaskel, J. Mater. Chem A 3 (2015) 3808.

[62] M. Adam, P. Strubel, L. Borchardt, H. Althues, S. Dörfler, S. Kaskel, J. Mater. Chem. A 3 (2015) 24103.

[63] G. Ren, S. Li, Z.-X. Fan, J. Warzywoda, Z. Fan, J. Mater. Chem. A. 4 (2016) 16507.

[64] A. Jozwiuk, H. Sommer, J. Janek, T. Brezesinski, J. Power Sources 296 (2015) 454.

[65] Z. Sun, S. Wang, L. Yan, M. Xiao, D. Han, Y. Meng, J. Power Sources 324 (2016) 547.

[66] Y. Wei, Y. Tao, C. Zhang, J. Wan, W. Qiao, L. Ling, D. Long, Electrochim. Acta 188 (2016) 385.

[67] J. Guo, J. Zhang, F. Jiang, S. Zhao, Q. Su, Gaohui Du, Electrochim. Acta 176 (2015) 853.

[68] W. Zhai, W. Tu, Y. Liu, H. Gao, J. Yu, Y. Zhao, G. Li, Electrochim. Acta 219 (2016) 143.

[69] F. Nitze, K. Fossum, S. Xiong, A. Matic, A. E.C. Palmqvist, J. Power Sources 317 (2016) 112.

[70] Q. Sun, B. He, X.-Q. Zhang, A.-H. Lu, AS Nano 9(8) (2015) 8504.

[71] J. Song, T. Xu, M. L. Gordin, P. Zhu, D. Lv, Y.-B. Jiang, Y. Chen, Y. Duan, D. Wang, Adv. Funct. Mater. 24 (2014) 1243.

[72] P. Zhu, J. Song, D. Lv, D. Wang, C. Jaye, D. A. Fischer, T. Wu, Y. Chen, J. Phys. Chem. C 118 (2014) 7765.

[73] Z. Geng, Q. Xiao, D. Wang, G. Yi, Z. Xu, B. Li, C. Zhang, Electrochim. Acta 202 (2016) 131.

[74] H. Wu, J. Mou, L. Zhou, Q. Zheng, N. Jiang, D. Lin, Electrochim. Acta 212 (2016) 1021.

[75] Q. Li, Z. Zhang, Z. Guo, K. Zhang, Y. Lai, J. Li, J. Power Sources 274 (2015) 338.

[76] F. Chen, J. Yang, T. Bai, B. Long, X. Zhou, Electrochim. Acta 192 (2016) 99.

[77] S. Zheng, F. Yi, Z. Li, Y. Zhu, Y. Xu, C. Luo, J. Yang, C. Wang, Adv. Funct. Mater. 2014, 24, 4156.

[78] C. Erhardt, S. Sörgel, S. Meinhard, T. Sörgel, J. Power Sources 296 (2015) 70.

[79] X. Li, J. Liang, K. Zhang, Z. Hou, W. Zhang, Y. Zhu, Y. Qian, Energy Environ. Sci. 8 (2015) 3181.

[80] B. Ding, C. Yuan, L. Shen, G. Xu, P. Nie, X. Zhang, Chem. Eur. J. 19 (2013) 1013.

[81] S. Zhao, C. Li, W. Wang, H. Zhang, M. Gao, X. Xiong, A. Wang, K. Yuan, Y. Huang, F. Wang, J. Mater. Chem. A 1 (2013) 3334.

[82] S.-H. Chung, Electrochem. Commun. 38 (2013) 91.

[83] S.-H. Chung, A. Manthiram, J. Mater. Chem. A 1 (2013) 9590.

[84] Z. Li, Y. Jiang, L. Yuan, Z. Yi, C. Wu, Y. Liu, P. Strasser, Y. Huang, ACS Nano 8 (2014) 9295.

[85] Z. Li, L. Yuan, Z. Yi, Y. Sun, Y. Liu, Y. Jiang, Y. Shen, Y. Xin, Z. Zhang, Y. Huang, Adv. Energy Mater. 4 (2014) 1301473.

[86] T. A. Zegeye, C.-F. J. Kuo, A. S. Wotango, C.-J. Pan, H.-M. Chen, A. M. Haregewoin, J.-H. Cheng, W.-N. Su, B.-J. Hwang, J. Power Sources 324 (2016) 239.

[87] S. Chen, B. Sun, X. Xie, A. K. Mondal, X. Huang, G. Wang, Nano Energy 16 (2015) 268-280.

[88] B. Zhang, X. Qin, G. R. Li, X. P. Gao, Energy Environ. Sci. 3 (2010) 1531.

[89] D.-W. Wang, G. Zhou, F. Li, K.-H. Wu, G. Q. Lu, H.-M. Cheng, I. R. Gentle, Phys. Chem. Chem. Phys. 14 (2012) 8703.

[90] R. Sahore, L. P. Estevez, A. Ramanujapuram, F. J. DiSalvo, E. P. Giannelis, J. Power Sources 297 (2015) 188.

[91] J. Yang, S. Wang, Z. Ma, Z. Du, C. Li, J. Song, G. Wang, G. Shao, Electrochim. Acta 158 (2015) 8.

[92] S. Xiao, S. Liu, J. Zhang, Y. Wang, J. Power Sources 293 (2015) 119.

[93] N. Jayaprakash, J. Shen, S. S. Moganty, A. Corona, L. A. Archer, Angew. Chem., Int. Ed., 50 (2011) 5904.

[94] C. Zhang, H. B. Wu, C. Yuan, Z. Guo, X. W. Lou, Angew. Chem., Int. Ed. 51 (2012) 9592.

[95] Y. An, Q. Zhu, L. Hu, S. Yu, Q. Zhao, B, Xu, J. Mater. Chem. A 4 (2016) 15605.

[96] Y. Xie, L. Fang, H. Cheng, C. Hu, H. Zhao, J. Xu, J. Fang, X. Lu, J. Zhang, J. Mater. Chem. A 4 (2016) 15612.

[97] L. Ji, M. Rao, S. Aloni, L. Wang, E. J. Cairns, Y. Zhang, Energy Environ. Sci. 4 (2011) 5053 – 5059

[98] M. Rao, X. Song, E. J. Cairns, J. Power Sources 205 (2012) 5053.

[99] X. Cheng, J. Huang, Q. Zhang, H. Peng, M. Zhao, F. Wei, Nano Energy 4 (2014) 65.

[100] W. Wei, J. Wang, L. Zhou, J. Yang, B. Schumann, Y.N. Li, Electrochem. Commun. 13 (2011) 399.

[101] L. Wang, Y. Zhao, M.L. Thomas, H.R. Byon, Adv. Funct. Mater. 2014, 24, 2248

[102] L. Ji, M. Rao, H. Zheng, L. Zhang, Y. Li, W. Duan, J. Guo, E. J. Cairns, Y. Zhang, J. Am. Chem. Soc. 133 (2011) 18522.

[103] C. Zu, A. Manthiram, Adv. Energy Mater. 3 (2013) 1008.

[104] T. Lin, Y. Tang, Y. Wang, H. Bi, Z. Liu, F. Huang, X. Xie, M. Jiang, Energy Environ. Sci. 6 (2013) 1283.

[105] H. Kim, H.-D. Lim, J. Kim, K. Kang, J. Mater. Chem. A 2 (2014) 33.

[106] H. Ye, Y.-X. Yin, S. Xin, Y.-G. Guo, J. Mater. Chem. A 1 (2013) 6602.

[107] Z. Zhang, Z. Li, F. Hao, X. Wang, Q. Li, Y. Qi, R. Fan, L. Yin, Adv. Funct. Mater. 24 (2014) 2500.

[108] W.-C. Du, Y.-X. Yin, X.-X. Zeng, J.-L. Shi, S.-F. Zhang, L.-J. Wan, Y.-G. Guo, ACS Appl. Mater. Interfaces 8 (2016) 3584.

[109] R. Elazari, G. Salitra, A. Garsuch, A. Panchenko, D. Aurbach, Adv. Mater. 23 (2011) 5641.

[110] J.-J. Chen, Q. Zhang, Y.-N. Shi, L.-L. Qin, Y. Cao, M.-S. Zheng, Q.-F. Dong, Phys. Chem. Chem. Phys. 14 (2012) 5376.

[111] S. Dor□er, M. Hagen, H. Althues, J. Tubke, S. Kaskel, M. J. Hoffmann, Chem. Commun. 48 (2012) 4097.

[112] J. Yan, X. Liu, X. Wang, B. Li, J. Mater. Chem. A 3 (2015) 10127.

[113] J. Guo, Y. Xu, C. Wang, Nano Lett. 11 (2011) 4288.

[114] G. Zheng, Y. Yang, J. J. Cha, S. S. Hong, Y. Cui, Nano Lett. 11 (2011) 4462.

[115] Z. Zhang, H.-K. Jing, S. Liu, G.-R. Li, X.-P. Gao, J. Mater. Chem. A 3 (2015) 6827.

[116] G. Zheng, Q. Zhang, J. J. Cha, Y. Yang, W. Li, Z. W. Seh, Y. Cui, Nano Lett. 13 (2013) 1265.

[117] S. Moon, Y. H. Jung, W. K. Jung, D. S. Jung, J. W. Choi, D. K. Kim, Adv. Mater. 25 (2013) 6547.

[118] S. C. Jung, Y.-K. Han, J. Power Sources 325 (2016) 495.

[119] S. Zhang, Q. Zhang, J. Huang, X. Liu, W. Zhu, M. Zhao, W. Qian, F. Wei, Particle Particle Syst. Charact. 30 (2013) 158.

[120] H. Peng, T. Hou, Q.Zhang, J. Huang, X. Cheng, M. Guo, Z. Yuan, L. He, F. Wei, Adv. Mater. Interfaces 1 (2014) 1400227, DOI: 10.1002/admi.201400227.

[121] G. Zhou, D.-W.Wang, F. Li, P.-X. Hou, L. Yin, C. Liu, G. Q. Lu, I. R. Gentle, H.-M. Cheng, Energy Environ. Sci. 5 (2012) 8901.

[122] Y. Su, Y. Fu, A. Manthiram, Phys. Chem. Chem. Phys. 14 (2012) 14495.

[123] K. Jin, X. Zhou, L. Zhang, X. Xin, G. Wang, Z. Liu, J. Phys. Chem. C 117 (2013) 21112.

[124] L. Sun, M. Li, Y. Jiang, W. Kong, K. Jiang, J. Wang, S. Fan, Nano Lett. 14 (2014) 4044.

[125] H. S. Kang, Y. K. Sun, Adv. Func. Mater. 26 (2016) 1225.

[126] M. Cinke, J. Li, B. Chen, K. Wignarajah, S. Pisharodi, J. Fisher, L. Delzeit, M. Meyyappan, M. Partridge, K. Klark, 2003 SAE International https://ntrs.nasa.gov/archive/nasa/casi.ntrs.nasa.gov/20040013502.pdf.

[127] Z. Xiao, Z. Yang, H. Nie, Y. Lu, K. Yang, S. Huang, J. Mater. Chem. A 2 (2014) 8683.

[128] S. Xin, L. Gu, N. Zhao, Y. Yin, L. Zhou, Y. Guo, L. Wan, J. Am. Chem. Soc. 134 (2012) 18510.

[129] Y. Zhao, W. Wu, J. Li, Z. Xu, L. Guan, Adv. Mater. 26 (2014) 5113.

[130] K. Mi, Y. Jiang, J. Feng, Y. Qian, S. Xiong, Adv. Func. Mater. 26 (2016) 1571.

[131] J. Rong, M. Ge, X. Fang, C. Zhou, Nano Lett. 14 (2014) 473.

[132] H. Wu, Y. Huang, M. Zong, H. Fu, X. Sun, Electrochim. Acta 163 (2015) 24.

[133] X. Duan, Y. Han, L. Huang, Y. Li, Y. Chen, J. Mater. Chem. A 3 (2015) 8015.

[134] L. Zhang, L. W. Ji, P. A. Glans, Y. G. Zhang, J. F. Zhu, J. H. Guo, Phys. Chem. Chem. Phys. 14 (2012) 13670.

[135] L. Q. Lu, L. J. Lu, Y. Wang, J. Mater. Chem. A 1 (2013) 9173.

[136] C. Zhang, W. Lv, W. Zhang, X. Zheng, M. Wu, W. Wei, Y. Tao, Z. Li, Q. Yang, Adv. Energy Mater. 4 (2014) 1301565.

[137] W. Zhou, H. Chen, Y. Yu, D. Wang, Z. Cui, F. J. DiSalvo, H. D. Abruna, ACS Nano 7 (2013)

8801.

[138] L. Wang, D. Wang, F. Zhang, J. Jin, N ano Lett. 13 (2013) 4206.

[139] Y. Deng, H. Xu, Z. Bai, B. Huang, J. Su, G. Chen, J. Power Sources 300 (2015) 386.

[140] M. Song, Y. Zhang, E. J. Cairns, Nano Lett. 13 (2013) 5891.

[141] Y. Qiu, W. Li, W. Zhao, G. Li, Y. Hou, M. Liu, L. Zhou, F. Ye, H. Li, Z. Wei, S. Yang, W. Duan, Y. Ye, J. Guo, Y. Zhang, Nano Lett. 14 (2014) 4821.

[142] M. Shaibani, A. Akbari, P. Sheath, C.D. Easton, P.C. Banerjee, K. Konstas, A. Fakhfouri, M. Barghamadi, M.M. Musameh, A.S. Best, T. Rüther, P.J. Mahon, M.R. Hill, A.F. Hollenkamp, M. Majumder, ACS Nano 10 (2016) 7768.

[143] M. Yu, R. Li,a Y. Tong, Y. Li, C. Li, J.-D. Hong, G. Shi, J. Mater. Chem. A 3 (2015) 9609.

[144] X. D. Huang, B. Sun, K. F. Li, S. Q. Chen, G. X. Wang, J. Mater. Chem. A 1 (2013) 13484.

[145] J. Jin, Z. Wen, G. Ma, Y. Lu, Y. Cui, M. Wu, X. Liang, X. Wu, RSC Adv. 3 (2013) 2558.

[146] S. Thieme, J. Bruckner, I. Bauer, M. Oschatz, L. Borchardt, H. Althuesa, S. Kaskel, J. Mater. Chem. A 1 (2013) 9225.

[147] J.-Q. Huang, H.-J. Peng, X.-Y. Liu, J.-Q. Nie, X.-B. Cheng, Q. Zhang, F. Wei, J. Mater. Chem. A 2 (2014) 10869.

[148] L. Zeng, F. Pan, W. Li, Y. Jiang, X. Zhong, Y. Yu, Nanoscale 6 (2014) 9579.

[149] Z. Yuan, H.-J. Peng, J.-Q. Huang, X.-Y. Liu, D.-W. Wang, X.-B. Cheng, Q. Zhang, Adv. Funct. Mater. 24 (2014) 6105.

[150] M. Wei, P. Yuan, W. Chen, J. Hu, J. Mao, G. Shao, Electrochim. Acta 178 (2015) 564.

[151] J. Z. Wang, L. Lu, M. Choucair, J. A. Stride, X. Xu, H. K. Liu, J. Power Sources 196 (2011) 7030.

[152] F.-F. Zhang, X.-B. Zhang, Y.-h. Dong, L.-M. Wang, J. Mater. Chem. 22 (2012) 11452.

[153] S. Evers, L. F. Nazar, Chem. Commun. 48 (2012) 1233.

[154] M.-S. Park, J.-S. Yu, K. J. Kim, G. Jeong, J.-H. Kim, Y.-N. Jo, U. Hwang, S. Kang, T. Woo, Y.-J. Kim, Phys. Chem. Chem. Phys. 14 (2012) 6796.

[155] Y. Cao, X. Li, I. A. Aksay, J. Lemmon, Z. Nie, Z. Yang, J. Liu, Phys. Chem. Chem. Phys. 13 (201) 7660.

[156] N. W. Li, M. B. Zheng, H. L. Lu, Z. B. Hu, C. F. Shen, X. F. Chang, G. B. Ji, J. M. Cao, Y. Shi, Chem. Commun. 48 (2012) 4106.

[157] S. Li, M. Xie, J. B. Liu, H. Wang, H. Yan, Electrochem. Solid-State Lett. 14 (2011) A105 ; Y. X. Wang, L. Huang, L. C. Sun, S. Y. Xie, G. L. Xu, S. R. Chen, Y. F. Xu, J. T. Li, S. L. Chou, S. X. Dou, S. G. Sun, J. Mater. Chem. 22 (2012) 4744.

[158] B. Wang, K. Li, D. Su, H. Ahn, G. Wang, Chem.–Asian J. 7 (2012) 1637.

[159] H. Sun, G.-L. Xu, Y.-F. Xu, S.-G. Sun, X. Zhang, Y. Qiu, S. Yang, Nano Res. 5 (2012) 726.

[160] Z.-K. Wei, J.-J. Chen, L.-L. Qin, A.-W. Nemage, M.-S. Zheng, Q.-F. Dong, J. Electrochem. Soc. 159 (2012) A1236.

[161]. D. Usachov, O. Vilkov, A. Grüneis, D. Haberer, A. Fedorov, V. K. Adamchuk, A. B. Preobrajenski, P. Dudin, A. Barinov, M. Oehzelt, C. Laubschat, D. V. Vyalikh, Nano Lett. 11 (2011) 5401.

[162]. C. Tang, Q. Zhang, M.-Q. Zhao, J.-Q. Huang, X.-B. Cheng, G.-L. Tian, H.-J. Peng, F. Wei, Adv. Mater. 26 (2014) 6100.

[163] J. Song, Z. Yu, M. L. Gordin, D. Wang, Nano Lett. 16 (2016) 862.

[164] X. Jia, C. Zhang, J. Liu, W. Lv, D.-W. Wang, Y. Tao, Z. Li, X. Zheng, J.-S. Yu, Q.-H. Yang, Nanoscale 8 (2016) 44472.

[165] Z. Meng, Y. Xie, T. Cai, Z. Sun, K. Jiang, W.-Q. Han, Electrochim. Acta 210 (2016) 8292.

[166] X. Yu, J. Zhao, R. Lv, Q. Liang, C. Zhan, Y. Bai, Z.-H. Huang, W. Shen, F. Kang, J. Mater. Chem. A 3 (2015) 184002.

[167] J. Xu, D. Su, W. Zhang, W. Bao, G. Wang, J. Mater. Chem. 4 (2016) 173812.

[168] L. Zhang, H. Huang, H. Yin, Y. Xia, J. Luo, C. Liang, Y. Gan, X. Tao, W. Zhang, J.Mater. Chem. A 3 (2015) 16513.

[169] B. Ding, C. Yuan, L. Shen, G. Xu, P. Nie, Q. Lai, X. Zhang, J. Mater. Chem. A 1 (2013) 1096.

[170] X. Yang, L. Zhang, F. Zhang, Y. Huang, Y. Chen, ACS Nano 8 (201) 5208.

[171] T. Xu, J. Song, M. L. Gordin, H. Sohn, Z. Yu, S. Chen, D. Wang, ACS Appl. Mater. Interfaces 5 (2013) 11355.

[172] G. Zhou, L. Li, C. Ma, S. Wang, Y. Shi, N. Koratkar, W. Ren, F. Li, H.-M. Cheng, Nano Energy 11 (2015) 356.

[173] H.-J. Peng, J. Liang, L. Zhu, J.-Q. Huang, X.-B. Cheng, X. Guo, W. Ding, W. Zhu, Q. Zhang, ACS Nano 8 (2014) 11280.

[174] G. Zhou, L. Li, D.-W. Wang, X.-Y. Shan, S. Pei, F. Li, H.-M. Cheng, Adv. Mater. 27 (2015) 641.

[175] M. Zhao, Q. Zhang, J. Huang, G. Tian, J. Nie, H. Peng, F. Wei, Nat. Commun. 5 (2014) 3410.

[176] Z. Peng, W. Fang, H. Zhao, J. Fang, H. Cheng, T. N. L. Doan, J. Xu, P. Chen, J. Power Sources 282 (2015) 70.

[177] M. Nagao, K. Suzuki, Y. Imade, M. Tateishi, R. Watanabe, T. Yokoi, M. Hirayama, T. Tatsumi, R. Kanno, J. Power Sources 330 (2016) 120.

[178] S. Liu, K. Xie, Z. Chen, Y. Li,a X. Hong, Jing Xu, L. Zhou, J. Yuan, C. Zheng, J. Mater. Chem. A 3 (2015) 11395

[179] Z. Zheng, H. Guo, F. Pei, X. Zhang, X. Chen, X. Fang, T. Wang, N. Zheng, Adv. Func. Mater. (2016) DOI: 10.1002/adfm.201601897.

[180] J. He, Y. Chen, P. Li, F. Fu, Z. Wang, W. Zhang, J. Mater. Chem. A 3 (2015) 18605.

[181] L. Sun, W. Kong, Y. Jiang, H. Wu, K. Jiang, J. Wang, S. Fan, J. Mater. Chem. A 3 (2015) 5305.

[182] W. Weng, H. Lin, X. Chen, J. Ren, Z. Zhang, L. Qiu, G. Guan, H. Peng, J. Mater. Chem. A 2 (2014) 9306.

[183] S. Chen, X. Huang, H. Liu, B. Sun, W. Yeoh, K. Li, J. Zhang, G. Wang, Adv. Energy Mater. 4 (2014) 1301761.

[184] W. Deng, A. Hu, X. Chen, S. Zhang, Q. Tang, Z. Liu, B. Fan, K. Xiao, J. Power Sources 322 (2015) 138.

[185] C. Wang, K. Su, W. Wan, H. Guo, H. Zhou, J. Chen, X. Zhang, Y. Huang, J. Mater. Chem. A 2 (2014) 5018.

[186] Y. Li, Z. Li, Q. Zhang, P. K. Shen, J. Mater. Chem. A 2 (2014) 4528.

[187] C. Xu, Y. Wu, X. Zhao, X. Wang, G. Du, J. Zhang, J. Tu, J. Power Sources 275 (2015) 22.

[188] J. Feng, X. Qin, Z. Ma, J. Yang, W. Yang, G. Shao, Electrochim. Acta 190 (2016) 426.

[189] Z. Li, X. Li, Y. Liao, X. Li, W. Li, J. Power Sources 334 (2016) 23.

[190] K. Zhang, F. Qin, Y. Lai, J. Li, X. Lei, M. Wang, H. Lu, J. Fang, ACS Appl. Mater. Interfaces 8 (2016) 6072.

[191] J. L. Wang, J. Yang, J. Y. Xie, N. X. Xu, Adv. Mater. 14 (2002) 963.

[192] J. Wang, J. Yang, C. Wan, K. Du, J. Xie, N. Xu, Adv. Funct. Mater. 13 (2003) 487.

[193] J.E. Hyun, P.C. Lee, I. Tatsumi, Electrochim. Acta 176 (2015) 887.

[194] J. Wang, J. Chen, K. Konstantinov, L. Zhao, S. H. Ng, G. Wang, Z. Guo, H. K. Liu, Electrochim. Acta 51 (2006) 4634.

[195] G. Ma, Z. Wen, J. Jin, M. Wu, X. Wu, J. Zhang, J. Power Sources 267 (2014) 542.

[196] X. Liang, Y. Liu, Z. Wen, L. Huang, X. Wang, H. Zhang, J. Power Sources 196 (2011) 6951.

[197] X. Liang, Z. Wen, Y. Liu, X. Wang, H. Zhang, M. W. Huang, Solid State Ionics 192 (2011) 347.

[198] G. Ma, Z. Wen, J. Jin, Q. Wang, J. Power Sources 273 (2015) 511.

[199] Y. Fu, A. Manthiram, RSC Adv. 2 (2012) 5927.

[200] N. Nakamura, T. Yokoshima, H. Nara, T. Momma, Tetsuya Osaka, J. Power Sources 274 (2015) 1263.

[201] G. Ma, Z. Wen, J. Jin, Y. Lu, X. Wu, M. Wu, C. Chen, J. Mater. Chem. A 2 (2014) 10350.

[202] K. Ding, Y. Bu, Q. Liu, T.i Li, K. Meng, Y. Wang, J. Mater. Chem. A 3 (2015) 8022.

[203] X. Li, M. Rao, H. Lin, D. Chen, Y. Liu, S. Liu, Y. Liao, L. Xing, M. Xu, W. Li, J. Mater. Chem. A 3 (2015)18098 .

[204] Y. Sun, S. Wang, H. Cheng, Y. Dai, J. Yu, J. Wu, Electrochim. Acta 158 (2015) 143.

[205] H. Gao, Q Lu, N. Liu, X. Wang, F. Wang, J. Mater. Chem. 3 (2015) 7215.

[206] S. Sen, D. Dutta, A. J. Bhattacharyya, J. Mater. Chem. 3 (2015) 20958.

[207] W. Li, G. Zheng, Y. Yang, Z. W. Seh, N. Liu, Y. Cui, Proc. Natl. Acad. Sci. USA 110 (2013) 7148.

[208] S. Moon, Y. H. Jung, D. K. Kim, J. Power Sources 294 (2015) 386.

[209] X. Fang, H. Peng, Small 11(13) (2015) 1488.

[210] W. Zhou, Y. Yu, H. Chen, F. J. DiSalvo, H. D. Abruna, J. Am. Chem. Soc. 135 (2013) 16736.

[211] C. Wang, W. Wan, J. Chen, H. Zhou, X. Zhang, L. Yuan, Y. Huang, J. Mater. Chem. A 1 (2013) 1716.

[212] Z. Zhang, Q. Li, K. Zhang, Y. Lai, J. Li, Electrochim. Acta 152 (2015) 53.

[213] J. L. Wang, J. Yang, J. Y. Xie, N. X. Xu, Adv. Mater. 14 (2002) 963.

[214] J. L. Wang, J. Yang, C. R. Wan, K. Du, J. Y. Xie, N. X. Xu, Adv. Funct. Mater. 13 (2003) 487.

[215] L. C. Yin, J. L. Wang, J. Yang, Y. N. Nuli, J. Mater. Chem. 21 (2011) 6807.

[216] L. C. Yin, J. L. Wang, F. J. Lin, J. Yang, Y. Nuli, Energy Environ. Sci. 5 (2012) 6966.

[217] J. Fanous, M. Wegner, J. Grimminger, M. Rolff, M. B. M. Spera, M. Tenzer, M. R. Buchmeiser, J. Mater. Chem. 22 (2012) 23240.

[218] J. Guo, Z. Yang, Y. Yu, H. D. Abruna, L. A. Archer, J. Am. Chem. Soc. 135 (2012) 763.

[219] D.H. Wang, D. Xie, T. Yang, Y. Zhong, X.L. Wang, X.H. Xia, C.D. Gu, J.P. Tu, J. Power Sources 331 (2016) 475.

[220] A. Mentbayeva, A. Belgibayeva, N. Umirov, Y. Zhang, I. Taniguchi, I. Kurmanbayeva, Z. Bakenov, Electrochim. Acta 217 (2016) 242.

[221] J. Ye, F. He, J. Nie, Y. Cao, H. Yang, X. Ai, J. Mater. Chem. A 3 (2015) 7406.

[222] H. Sohn, M. L. Gordin, M. Regula, D. H. Kim, Y. S. Jung, J. Song, D. Wang, J. Power Sources 302 (2016) 70.

[223] Q. Li, M. Liu, X. Qin, J. Wu, W. Han, G. Liang, D. Zhou, Y.-B. He, B. Li, F. Kangab, J. Mater. Chem. A 4 (2016) 12973.

[224] L. Huang, J. Cheng, X. Li, D. Yuan, W. Ni, G. Qu, Q. Guan, Y. Zhang, B. Wang, J. Mater. Chem. A 3 (2015) 4049.

[225] M. Chen, X. Wang, S. Cai, Z. Ma, P. Song, A. C. Fisher, J. Mater. Chem. 4 (2016) 16148.

[226] L. Ma, H. L. Zhuang, S. Wei, K. E. Hendrickson, M. S. Kim, G. Cohn, R. G. Hennig, L. A. Archer, ACS Nano 10 (2016) 1050.

[227] E. T. Kim, J. Park, C. Kim, A. G. Simmonds, Y.-E. Sung, J. Pyun, K. Char, ACS Macro Lett. 5 (2016) 471.

[228] C. B. Bucur, J. Muldoon, A. Lita, Energy Environ. Sci. 9 (2016) 992.

[229] H. Chen, W. Dong, J. Ge, C. Wang, X. Wu, W. Lu, L. Chen, Sci. Rep. 3 (2013) 1910.

[230] J. Song, H. Noh, J. Lee, I.-W. Nah, W.-I. Cho, H.-T. Kim, J. Power Sources 332 (2016) 72.

[231] P. J. Hanumantha, B. Gattu, P. M. Shanthi, S. S. Damle, Z. Basson, R. Bandi, M. K. Datta, S. Park, P. N. Kumta, Electrochim. Acta 212 (2016) 286.

[232] S.E. Doris, A.L. Ward, P.D. Frischmann, L. Li, B.A. Helms, J. Mater. Chem. A 4 (2016) 16946.

[233] F. Wu, J. Chen, R. Chen, S. Wu, L. Li, S. Chen, T. Zhao, J. Phys, Chem. C 115 (2011) 6057.

[234] J.H. Kim, J. Choi, J. Seo, J. Kwon, U. Paik, J. Mater. Chem. A 4 (2016) 11203.

[235] A. Gorkovenko, T.A. Skotheim, Z.-S. Xu, U.S. Patent 6,878,488 (2005) accessed April 12.

[236] M.S. Song, S.C. Han, H.S. Kim, J.H. Kim, K.T. Kim, Y.M. Kang, H.J. Ahn, S.X. Dou, J.Y. Lee, J. Electrochem. Soc. 151 (2004) A791.

[237] Y.J. Choi, B.S. Jung, D.J. Lee, J.H. Jeong, K.W. Kim, H.J. Ahn, K.K. Cho, H.B. Gu, Phys. Scr.

T129 (2007) 62.

[238] W. Zheng, X.G. Hu, C.F. Zhang, Electrochem. Solid-State Lett. 9 (2006) A364.

[239] Y. Zhang, X. Wu, H. Feng, L. Wang, A. Zhang, T. Xia, H. Dong, Int. J. Hydrogen Energy 34 (2009) 1556.

[240] Y.J. Choi, B.S. Jung, D.J. Lee, J.H. Jeong, K.W. Kim, H.J. Ahn, K.K. Cho, H.B. Gu, Phys. Scr. 129 (2007) 62.

[241] K. Dong, S. Wang, H. Zhang, J. Wu, Mater. Res. Bull. 48 (2013) 2079.

[242] B. Ding, L. Shen, G. Xu, P. Nie, X. Zhang, Electrochim. Acta 107 (2013) 78.

[243] Q. Li, Z. Zhang, K. Zhang, L. Xu, J. Fang, Y. Lai, J. Li, J. Solid State Electrochem. 17 (2013) 2959.

[244] Y. Tao, Yanju Wei, Y. Liu, J. Wang, W. Qiao, L. Ling, D. Long, Energy Environ. Sci. 9 (2016) 3230.

[245] X. Ji, S. Evers, R. Black, L.F. Nazar, Nat. Commun. 2 (2011) 325.

[246] S. Rehman, S. Guo, Y. Hou, Adv. Mater. 28(6) (2016) 3167.

[247] D. Maucec, Diploma thesis, Ljubljana (2008) pp. 20-78.

[248] V. Lapornik, N. N. Tusar, A. Ristic, R. Chellappan, D. Foix, R. Dedryvere, M. Gaberscek, R. Dominko, J. power sources 274 (2015) 1239.

[249] X. Li, L. Pan, Y. Wang, C. Xu, Electrochim. Acta 190 (2016) 548.

[250] X. Gu, C.-J. Tong, B. We, L.-M. Liu, C. Lai, S. Zhang, Electrochim. Acta 196 (2016) 369.

[251] X. Liu, Z. Shan, K. Zhu, J. Du, Q. Tang, J. Tian, J. Power Sources 274 (2015) 85.

[252] Q. Pang, D. Kundu, M. Cuisinier, L.F. Nazar, Nature Communications 5 (2014) 4759.

[253] X. Wang, G. Li, J. Li, Y. Zhang, A. Wook, A. Yu, Z. Chen, Energy Environ. Sci. 9 (2016) 2533.

[254] N. Ding, Y. Lum, S. Chen, S. W. Chien, T.S.A. Hor, Z. Liu, Y. Zong, J. Mater. Chem. A 3 (2015) 1853.

[255] Z.W. Seh, W. Li, J.J. Cha, G. Zheng, Y. Yang, M.T. McDowell, P. C. Hsu, Y. Cui, Nat. Commun. 4 (2013) 1331.

[256] S. Evers, T. Yim, L. F. Nazar, J. Phys. Chem. C 116 (2012) 19653.

[257] M. Yu, J. Ma, H. Song, A. Wang, F. Tian, Y. Wang, H. Qiu, R. Wang, Energy Environ. Sci. 9 (2016) 1495.

[258] Z. Xiao, Z. Yang, L. Wang, H. Nie, M. Zhong, Q. Lai, X. Xu, L. Zhang, S. Huang, Advanced Materials 27 (2015) 2891.

[259] L. Gao, M. Cao, Y. Q. Fu, Z. Zhong, Y. Shen, M. Wang, J. Mat. Chem. A 4 (2016) 16454.

[260] N. Moreno, A. Caballero, J. Morales, E. Rodrigues-Castellon, J. Power Sources 313 (2016) 21.

[261] Z. Zhang, Q. Li, K. Zhang, W. Chen, Y. Lai, J. Li, J. Power Sources 290 (2015) 159.

[262] K. Xie, K. Zhang, Y. Han, K. Yuan, Q. Song, J.-G. Wanga, C. Shen, X. Liu, B. Wei, Electrochim. Acta 210 (2016) 415.

[263] C. Li, Z. Li, Q. Li, Z. Zhang, S. Dong, L. Yin, Electrochim. Acta 215 (2016) 689.

[264] Y. Zhao, W. Zhu, G. Z. Chen, E. J. Cairns, J. Power Sources 327 (2016) 447.

[265] X. Lu, G. Wang, T. Zhai, M. Yu, S. Xie, Y. Ling, C. Liang, Y. Tong, Y. Li, Nano Lett. 12 (2012) 5376.

[266] N. Mosavati, V. R. Chitturi, S. O. Salley, K.Y. S. Ng, J. Power Sources 321 (2016) 87.

[267] Z. Hao, L. Yuan, C. Chen, J. Xiang, Y. Li, Z. Huang, P. Hu, Y. Huang, J. Mater. Chem. A 4 (2016) 17711.

[268] Z. Cui, C. Zu, W. Zhou, A. Manthiram, J. B. Goodenough, Adv. Mater. 28(32) (2016) 6926.

[269] Q. Sun, Z.-W. Fu, Electrochim. Acta 54 (2008) 403.

[270] D.K. Nandi, U.K. Sen, D. Choudhury, S. Mitra, S.K. Sarkar, ACS Appl. Mater Interfaces 6 (2014) 6606.

[271] H.-C. Park, K.-H. Lee, Y.-W. Lee, S.-J. Kim, D.-M. Kim, M.-C. Kim, K.-W. Park, J. Power Sources 269 (2014) 534.

[272] F. Gillot, J. Oro-Sole, M.R. Palacín, J. Mater. Chem. 21 (2011) 9997.

[273] D. Choi, P.N. Kumta, J. Am. Ceram. Soc. 94 (2011) 2371.

[274] X. Li, R. Tang, K. Hu, L. Zhang, Z. Ding, Electrochim. Acta 210 (2016) 734.

[275] J. Zhou, N. Lin, W. l. Cai, C. Guo, K. Zhang, J. Zhou, Y. Zhu, Y. Qian, Electrochim. Acta 218 (2016) 243.

[276] Z. Ma, Z. Li, K. Hu, D. Liu, J. Huo, S. Wang, J. Power Sources 325 (2016) 71.

[277] G. de Combarieu, M. Morcrette, F. Millange, N. Guillou, J. Cabana, C. P. Grey, I. Margiolaki, G. Férey, J. M. Tarascon, Chem. Mater. 21 (2009) 1602

[278] G. Férey, F. Millange, M. Morcrette, C. Serre, M. L. Doublet, J. M. Grenèche, J. M. Tarascon, Angew. Chem. Int. Ed. 46 (2007) 3259.

[279] J. Zhou, R. Li, X. Fan, Y. Chen, R. Han, W. Li, J. Zheng, B. Wang,X. Li, Energy Environ. Sci. 7 (2014) 2715.

[280] R. Demir Cakan, M. Morcrette, F. Nouar, C. Davoisne, T. Devic, D. Gonbeau, R. Dominko, C. Serre, G. Férey, J. M. Tarascon, J. Am. Chem. Soc. 13 (2011) 16154.

[281] Z. Zhao, S. Wang, R. Liang, Z. Li, Z. Shi, G. Chen, J. Mater. Chem. A 2 (2014) 13509.

[282] W. Bao, Z. Zhang, Y. Qu, C. Zhou, X. Wang, J. Li, J. Alloys Compd. 582 (2014) 334.

[283] H. Wang, Y. Yang, Y. Liang, J. T. Robinson, Y. Li, A. Jackson, Y. Cui, H. Dai, Nano Lett. 11 (2011) 2644.

[284] J. Zheng, J. Tian, D. Wu, M. Gu, W. Xu, C. Wang, F. Gao, M. H. Engelhard, J. Zhang, J. Liu, J. Xiao, Nano Lett. 14 (2014) 2345.

[285] H. Tang, S. Yao, M. Jing, X. Wu, J. Hou, X. Qian, D. Rao, X. Shen, X. Xi, K. Xiao, Electrochim. Acta 176 (2015) 442.

[286] Y.-J. Li, J.-M. Fan, M.-S. Zheng, Q.-F. Dong, Energy Environ. Sci. 9 (2016) 1998.

[287] Q. Pang, D. Kundu, M. Cuisinier, L. F. Nazar, Nat. Commun. 5 (2014) 4759.

[288] X. Tao, J. Wang, Z. Ying, Q. Cai, G. Zheng, Y. Gan, H. Huang, Y. Xia, C. Liang, W. Zhang, Y. Cui, Nano Lett. 14 (2014) 5288.

[289] S. Bai, K. Zhu, S. Wu, Y. Wang, J. Yi, M. Ishida, H. Zhou, J. Mater. 4 (2016) 16812.

[290] Z. Li, C. Li, X. Ge, J. Ma, Z. Zhang, Q. Li, C. Wang, L. Yin, Nano Energy 23 (2016) 15

[291] S. J. Visco, M. Y. Chu, U.S. Patent 6,210,832 (2001) accessed April 3.

[292] Y. V. Mikhaylic, U.S. Patent 7,354,680 (2008) accessed April 8.

[293] D. Aurbach, E. Pollak, R. Elazari, G. Salitra, C. S. Kelley, J. Affinito, J. Electrochem. Soc. 156 (2009) A694.

[294] J. Pan, C. Wu, J. Cheng, Y. Pan, Z. Ma, S. Xie, J. Li, J. Power Sources 293 (2015) 527.

[295] X.-Q. Niu, X.-L. Wang, D.-H. Wang,a Y. Li,a Y.-J. Zhang, Y.-D. Zhang, T. Yang, T. Yu, J.-P. Tu, J. Mater. Chem. A 3 (2015) 17106.

[296] M. N. Obrovac, J. R. Dahn, Electrochem. Solid-State Lett. 5 (2002) A70.

[297] Y. Zhou, C. Wu, H. Zhang, X. Wu, Z. Fu, Electrochim. Acta 52 (2007) 3130.

[298] A. Hayashi, T. Ohtomo, F. Mizuno, K. Tadanaga, M. Tatsumisago, Electrochem. Commun. 5 (2003) 701.

[299] A. Hayashi, R. Ohtsubo, T. Ohtomo, F. Mizuno, M. Tatsumisago, J. Power Sources 183 (2008) 422.

[300] L.-J. Liu, Y. Chen, Z.-F. Zhang, X.-L. You, M. D. Walle, Y.-J. Li, Y.-N. Liu, J. Power Sources 325 (2016) 301.

[301] X. He, J. Ren, L. Wang, W. Pu, C. Wan, C. Jiang, Ionics 15 (2009) 477.

[302] X. He, J. Ren, L. Wang, W. Pu, C. Jiang, C. Wan, J. Power Sources 190 (2009) 154.

[303] A. Hayashi, R. Ohtsubo, T. Ohtomo, F. Mizuno, M. Tatsumisago, J. Power Sources 183 (2008) 422.

[304] T. Kobayashi, Y. Imade, D. Shishihara, K. Homma, M. Nagao, R. Watanabe, T. Yokoi, A. Yamada, R. Kanno, T. Tatsumi, J. Power Sources 182 (2008) 621.

[305] A. Manthiram, Y. Fu, S.-H. Chung, C. Zu, Y.-S. Su, Chem. Rev. 114 (2014) 11751.

[306] L. Chen, L. L. Shaw, J. Power Sources 267 (2014) 770.

[307] Y. Jung, S. Kim, Electrochem. Commun. 9 (2007) 249.

[308] Y. Huang, J. Sun, W. Wang, Y. Wang, Z. Yu, H. Zhang, A. Wang, K. Yuan, J. Electrochem. Soc. 155 (2008) A764.

[309] J. Sun, Y. Huang, W. Wang, Z. Yu, A. Wang, K. Yuan, Electrochim. Acta 53 (2008) 7084.

[310] J. Sun, Y. Huang, W. Wang, Z. Yu,A. Wang, K. Yuan, Electrochem. Commun. 10 (2008) 930.

[311] M.M. Rao, X.Y. Geng, X.P. Li, S.J. Hu, W.S. Li, J. Power Sources 212 (2012) 179.

[312] L. Wang, Z. Yao, C.-W. Monroe, J. Yang, Y. Nuli, Adv. Funct. Mater. 23 (2013) 1194.

[313] H. Schneider, A. Garsuch, A. Panchenko, O. Gronwald, N. Janssen, P. Novák, J. Power Sources 205 (2012) 420.

[314] M. He, L.-X. Yuan, W.-X. Zhang, X.-L. Hu, Y.-H. Huang, J. Phys. Chem. C 115 (2011) 15703.

[315] M. J. Lacey, F. Jeschull, K. Edstrom, D. Brandell, Chem. Commun. 49 (2013) 8531.

[316] S.-M. Zhang, Q. Zhang, J.-Q. Huang, X.-F. Liu, W. Zhu, M.-Q. Zhao, W.-Z. Qian, F. Wei, Part. Part. Syst. Char. 30 (2013) 158.

[317] J.-Q. Huang, Q. Zhang, S.-M. Zhang, X.-F. Liu, W. Zhu, W.-Z. Qian, F. Wei, Carbon 58 (2013) 99.

[318] Y.-Z. Fu, Y.-S. Su, A. Manthiram, ACS Appl. Mater. Interfaces 4 (2012) 6046.

[319] P. G. Bruce, C. A. Vincent, J. Chem. Soc. Faraday Trans. 89 (1993) 3187.

[320] G. Li, W. Cai, B. Liu, Z. Li, J. Power Sources 294 (2015) 187.

[321] Z. Zhang, W. Bao, H. Lu, M. Jia, K. Xie, Y. Lai, J. Li, ECS Electrochem. Lett. 1 (2012) A34.

[322] J.T. Lee, Y. Zhao, S. Thieme, H. Kim, M. Oschatz, L. Borchardt, A. Magasinski, W. I. Cho, S. Kaskel, G. Yushin, Adv. Mater. 25 (2013) 4573.

[323] T. Nakazawa, A. Ikoma, R. Kido, K. Ueno, K. Dokko, M. Watanabe, J. Power Sources 307 (2016) 746.

[324] Y.V. Mikhaylik, U.S. Patent 7,354,680 (2008) accessed April 8.

[325] L.C. De Jonghe, S.J. Visco, U.S. Patent 4,917,974 (1990) accessed April 17.

[326] Y. M. Lee, N.-S. Choi, J. H. Park, J.-K. Park, J. Power Sources 119-121 (2003) 964.

[327] S. J. Visco, Y. S. Nimon, B. D. Katz, U.S. Patent 7,282,302 (2007) accessed October 16.

[328] Y. S. Nimon, M.-Y. Chu, S. J. Visco, U.S. Patent 6,955,866 B2 (2005) accessed October 18.

[329] M. Nagao, A. Hayashi, M. Tatsumisago, Electrochim. Acta 56 (2011) 6055.

[330] Z. Lin, C. Liang, J. Mater. Chem. A 3 (2015) 936.

[331] K. Minami, A. Hayashi, M. Tatsumisago, J. Ceram. Soc. Jpn. 118 (2010) 305.

[332] S. Ujiie, A. Hayashi, M. Tatsumisago, Solid State Ionics 211 (2012) 42.

[333] A. Yamauchi, A. Sakuda, A. Hayashi, M. Tatsumisago, J. Power Sources 244 (2013) 707.

[334] N. Kamaya, K. Homma, Y. Yamakawa, M. Hirayama, R. Kanno, M. Yonemura, T. Kamiyama, Y. Kato, S. Hama, K. Kawamoto, A. Mitsui, Nat. Mater 10 (2011) 682.

[335] H. Nagata, Y. Chikusa, J. Power Sources 329 (2016) 268.

[336] J. Hassoun, B. Scrosati, Angew. Chem. 49 (2010) 2371.

[337]. D. Marmorstein, T. H. Yu, K. A. Striebel, F. R. McLarnon, J. Hou, E. J. Cairns, J. Power Sources, 89 (2000) 219.

[338] J. Shim, K. A. Striebel, E. J. Cairns, J. Electrochem. Soc. 149 (2002) A1321.

[339] J. H. Shin, E. J. Cairns, J. Power Sources 177 (2008) 537.

[340] J. H. Shin, E. J. Cairns, J. Electrochem. Soc. 155 (2008) A368.

[341] C. Zhang, Y. Lin, J. Liu, J. Mater. Chem. A 3 (2015) 10760.

[342] X. Liang, Z. Wen, Y. Liu, M. Wu, J. Jin, H. Zhang, X. Wu, J. Power Sources 196 (2011) 9839.

[343] A. Jozwiuk, B.B. Berkes, T. Weiß, H. Sommer, J. Janek, T. Brezesinski, Energy & Environmental Science 9 (2016) 2603.

[344] M. Barghamadi, A. S. Best, A. I. Bhatt, A. F. Hollenkamp, P. J. Mahon, M. Musameh, T. Rüther, J. Power Sources 295 (2015) 212.

[345] S. S. Zhang, J. Power Sources 322 (2016) 99.

[346] R. Xu, J. C. M. Li, J. Lu, K. Amine, I. Belharouak, J. Mater. Chem. 3 (2015) 4170.

[347] S. S. Zhang, Electrochim. Acta 70 (2012) 344.

[348] S. S. Zhang, Electrochim. Acta 97 (2013) 226.

[349] J.-J. Kim, H. S. Kim, J. Ahn, K. J. Lee, W. C. Yoo, Y.-E. Sung, J. Power Sources 306 (2015) 617.

[350] J. Gao, M.A. Lowe, Y. Kiya, H.D. Abruña, J. Phys. Chem. C 115 (2011) 25132.

[351] T. Yim, M.S. Park, J.S. Yu, K.J. Kim, K.Y. Im, J.H. Kim, G. Jeong, Y.N. Jo, S.G.Woo, K. S. Kang, I. Lee, Y.J. Kim, Electrochim. Acta 107 (2013) 454.

[352] C. Barchasz, J.C. Leprêtre, S. Patoux, F. Alloin, Electrochim. Acta 89 (2013) 737.

[353] C. Barchasz, J.C. Lepretre, S. Patoux, F. Alloin, J. Electrochem. Soc. 160 (2013) A430.

[354] D.R. Changa, S.H. Leea, S.W. Kima, H.T. Kimb, J. Power Sources 112 (2002) 452.

[355] J.W. Choi, J.K. Kim, G. Cheruvally, J.H. Ahn, H.J. Ahn, K.W. Kim, Electrochim. Acta 52 (2007) 2075.

[356] H. Lu, K. Zhang, Y. Yuan, F. Qin, Z. Zhang, Y. Lai, Y. Liu, Electrochim. Acta 161 (2015) 55.

[357] M. Liu, D. Zhou, Y. He, Y. Fu, X. Qin, C. Miao, H. Du, B. Li, Q. Yang, Z. Lin, Nano Energy. 22 (2016) 278.

[358] M. Liu, H.R. Jianga, Y.X. Rena, D. Zhou, F.Y. Kang, T.S. Zhao, Electrochim. Acta 213 (2016) 871.

[359] Y. Zhang, Y. Zhao, Z. Bakenov, Nano. Res. Lett. 9 (2014) 137.

[360] Y.G. Zhang, Y. Zhao, Z. Bakenov, J. Solid State Electrochem. 18 (2014) 1111

[361] W. Ahn, S. Nam Lim, D. U. Lee, K.-B. Kim, Z. Chen, S.-H. Yeon, J. Mater. Chem. A 3 (2015) 9461.

[362] L. X. Yuan, J. K. Feng, X. P. Ai, Y. L. Cao, S. L. Chen, H. X. Yang, Electrochem. Commun. 8 (2006) 610.

[363] J. Wang, S. Y. Chew, Z. W. Zhao, S. Ashraf, D. Wexler, J. Chen, S. H. Ng, S. L. Chou, H. K. Liu, Carbon 46 (2008) 229.

[364] H.-S. Ryu, H.-J. Ahn, K.-W. Kim, J.-H. Ahn, K.-K. Cho, T.-H. Nam, J.-U. Kim, G.-B. Cho, J. Power Sources 201 (2006) 163.

[365] F. Wu, Q. Zhu, R. Chen, N. Chen, Y. Chen, L. Li, Electrochim. Acta 184 (2015) 356.

[366] F. Wu, Q. Zhu, R. Chen, N. Chen, Y. Chen, Y. Ye, J. Qian, L. Li, J. Power Sources 296 (2015) 10.

[367] L. Wang, J. Liu, S. Yuan, Y. Wang, Y. Xia, Energy Environ. Sci. 9 (2016) 224.

[368] S. S. Zhang, Electrochim. Acta 70 (2012) 344.

[369] Z. Lin, Z. Liu, W. Fu, N. J. Dudney, C. Liang, Adv. Funct. Mater. 23 (2013) 1064.

[370] J.-H. Song, J.-T. Yeon, J.-Y. Jang, J.-G. Han, S.-M. Lee, N.-S. Choi, J. Electrochem. Soc. 160 (2013) A873.

[371] C. Huang, J. Xiao, Y. Shao, J. Zheng, W.D. Bennett, D. Lu, L.V. Saraf, M. Engelhard, L. Ji, J. Zhang, X. Li, G.L. Graff, J. Liu, Nature Commun. 5 (2014) 3015.

[372] J. Song, H. Noh, H. Lee, J.-N. Lee, D. J. Lee, Y. Lee, C. H. Kim, Y. M. Lee, J.-K. Park, H.-T. Kim, J. Mater Chem. A3 (2015) 323.

[373] K. Xu, Chem. Rev. 104 (2004) 4303.

[374] J. T. Dudley, D. P. Wilkinson, G. Thomas, R. LeVae, S. Woo, H. Blom, C. Horvath, M. W. Juzkow, B. Denis, P. Juric, P. Aghakian, J. R. Dahn, J. Power Sources 35 (1991) 59.

[375] K. Xu, C. A. Angell, J. Electrochem. Soc. 149 (2002) A920.

[376] L. J.Krause, W. Lamanna, J. Summerfield, M. Engle, G. Korba, R. Loch, R. Atanasoski, J. Power Sources 68 (1997) 320.

[377] R. Younesi, G. M. Veith, P. Johansson, K. Edström, T. Vegge, Energy Environ. Sci. 8 (2015) 1905.

[378] J. Scheers, P. Johansson, P. Szczecinalski, W. Wieczorek, M. Armand, P. Jacobsson, J. Power Sources 195 (2010) 6081.

[379] P. Johansson, H. Nilsson, P. Jacobsson, M. Armand, Phys. Chem. Chem. Phys. 6 (2004) 895.

[380] M. Rohde, P. Eiden, V. Leppert, M. Schmidt, A. Garsuch, G. Semrau, I. Krossing, ChemPhysChem 16 (2015) 666.

[381] S. Kim, Y. Jung, S.-J. Park, Electrochim. Acta 52 (2007) 2116.

[382] J. Gao, M.A. Lowe, Y. Kiya, H.D. Abruna, J. Phys. Chem. C 115 (2011) 25132.

[383] C. Barchasz, F. Mesguich, J. Dijon, J.-C. Lepretre, S. Patoux, F. Alloin, J. Power Sources 211 (2012) 19.

[384] C. Barchasz, J.-C. Lepretre, S. Patoux, F. Alloin, J. Electrochem. Soc. 160 (2013) A430.

[385] X. Yu, A. Manthiram, Phys. Chem. Chem. Phys. 17 (2015) 2127.

[386] E. S. Shin, K. Kim, S. H. Oh, W. I. Cho, Chem. Commun. 49 (2013) 2004.

[387] L. Suo, Y.-S. Hu, H. Li, M. Armand, L. Chen, Nat. Commun. 4 (201) 1481.

[388] N. Deng, W. Kang, Y. Liu, J. Ju, D. Wu, L. Li, B. S. Hassan, B. Cheng, J. Power Sources 330 (2016) 132.

[389] U. Stoeck, J. Balach, M. Klose, D. Wadewitz, E. Ahrens, J. Eckert, L. Giebeler, J. Power Sources 309 (2016) 76.

[390] Z.Y. Zhang, Y.Q. Lai, Z.A. Zhang, J. Li, Solid State Ion. 278 (2015) 166.

[391] D. Zhao, X.Y. Qian, L.N. Jin, X.L. Yang, S.W. Wang, X.Q. Shen, S.S. Yao, D.W. Rao, Y.Y. Zhou, X.M. Xi, RSC Adv. 6 (2016) 13680.

[392] M. Raja, N. Angulakshmi, A. M. Stephan, RSC Adv. 6 (2016) 13772.

[393] F. Zeng, Z. Jin, K. Yuan, S. Liu, X. Cheng, A. Wang, W. Wang, Y.-S. Yang, J. Mater. Chem. A 4

(2016) 12319.

[394] X.Y. Qian, L. Jin, D. Zhao, X.L. Yang, S.W. Wang, X.Q. Shen, D.W. Rao, S.S. Yao, Y.Y. Zhou, X.M. Xi, Electrochim. Acta 192 (2016) 346.

[395] X.Y. Zhou, Q.C. Liao, J.J. Tang, T. Bai, F. Chen, J. Yang, J. Electroanal. Chem. 768 (2016) 55.

[396] W.K. Shin, A.G. Kannan, D.W. Kim, ACS Appl. Mater. Interfaces 7 (42) (2015) 23700.

[397] Z. Zhang, G. Wang, Y. Lai, J. Li, Z. Zhang, W. Chen, J. Power Sources 300 (2015) 157.

[398] F. Wu, J. Qian, R. Chen, Y. Ye, Z. Sun, Y. Xing, L. Li, J. Mater. A 4 (2016) 17033.

[399] S.-H. Chung, P. Han, A. Manthiram, ACS Appl. Mater. Interfaces, 8 (2016) 4709.

[400] C. Jin, W. Zhang, Z. Zhuang, J. Wang, H. Huang, Y. Gan, Y. Xia, C. Liang, J. Zhang, X. Tao J. Mat. Chem. A, DOI:10.1039/C6TA07620C.

[401] S.H. Chung, P. Han, R. Singhal, V. Kalra, A. Manthiram, Adv. Energy Mater 5 (2015) 1500738.

[402] J. Balach, T. Jaumann, M. Klose, S. Oswald, J. Eckert, L. Giebeler, J. Power Sources 329 (2016) 305.

[403] S.H. Chung, A. Manthiram, J. Phys. Chem. Lett. 5 (2014) 1978.

[404] C.H. Chang, S.H. Chung, A. Manthiram, Small 12 (2015) 174.

[404] G. Zhou, S. Pei, L. Li, D.W. Wang, S. Wang, K. Huang, L.C. Yin, F. Li, H. M. Cheng, Advanced Materials 26 (2014) 625.

[405] H.J. Peng, D.W. Wang, J.Q. Huang, X.B. Cheng, Z. Yuan, F. Wei, Q. Zhang, Adv. Sci. 3 (2016) 1500268.

[407] J. Balach, T. Jaumann, M. Klose, S. Oswald, J. Eckert, L. Giebeler, Adv. Funct. Mater 25 (2015) 5285.

[408] W. Lin, Y.F. Chen, P.J. Li, F. Fu, J. Electrochem. Soc. 162 (2015) A1624.

[409] M. S. Kim, L. Ma, S. Choudhury, S. S. Moganty, S. Wei, L. A. Archer, J. Mater. Chem. A 4 (2016) 14709.

[410] Z.Q. Jin, K. Xie, X.B. Hong, Z.Q. Hu, X. Liu, J. Power Sources 218 (2012) 163.

[411] Q.W. Tang, Z.Q. Shan, L. Wang, X. Qin, K.L. Zhu, J.H. Tian, X.S. Liu, J. Power Sources 246 (2014) 253.

[412] Z.J. Cai, Y.B. Liu, S.S. Liu, L. Li, Y.M. Zhang, Energy Environ. Sci. 5 (2012) 5690.

[413] X. Yu, J. Joseph, A. Manthiram, J. Mater. Chem. A 3 (2015) 15683.

[414] I. Bauer, S. Thieme, J. Brückner, H. Althues, S. Kaskel, J. Power Sources 251 (2014) 417.

[415] J.Q. Huang, Q. Zhang, H.J. Peng, X.Y. Liu, W.Z. Qian, F. Wei, Energy Environ. Sci. 7 (2014) 347.

[416] Z. Hao, L. Yuan, Z. Li, J. Liu, J. Xiang, C. Wu, R Zeng, Y. Huang , Electrochim. Acta 200 (2016) 197.

[417] T. Z. Zhuang, J.Q. Huang, H.J. Peng, L.Y. He, X.B. Cheng, C.M. Chen, Q. Zhang, Small 12 (2016) 381.

[418] C.H. Hsu, L.H. Chiena, P.L. Kuo, RSC Adv. 6 (2016) 18089.

[419] Q.Z. Xiao, X.Z. Wang, W. Li, Z.H. Li, T.J. Zhang, H.L. Zhang, J. Membr. Sci. 334 (2009) 117

[420] S.S. Zhang, D.T. Tran, J. Mater. Chem. A 2 (2014) 7383.

[421] W.L. Cai, G.R. Li, F. He, L.M. Jin, B.H. Liu, Z.P. Li, J. Power Sources 283 (2015) 524.

[422] H. Wei, J. Ma, B. Li, Y.X. Zuo, D.G. Xia, ACS Appl. Mater. Interfaces 6 (2014) 20276.

[423] W. Yang, W. Yang, J. Feng, Z. Ma, G. Shao, Electrochim. Acta 210 (2016) 71.

[424] A. Sabir, M. Shafiq, A. Islam, F. Jabeen, A. Shafeeq, A. Ahmad, M.T.Z. Butt, K.I. Jacob, T. Jamilb, Carbohyd. Polym. 36 (2016) 551.

[425] G.C. Wang, Y.Q. Lai, Z.A. Zhang, J. Li, Z.Y. Zhang, J. Mater. Chem. A 3 (2015) 7139.

[426] J.S. Kim, T.H. Hwang, B.G. Kim, J. Min, J.W. Choi, Adv. Funct. Mater 24 (2014) 53.

[427] G. C. Li, H. K. Jing, Z. Su, C. Lai, L. Chen, C. C. Yuan, H. H. Li, L. Liu, J. Mater. Chem. A 3 (2015) 11014.

[428] W. Zhou, X. Xiao, M. Cai, L. Yang, Nano Lett. 14 (2014) 5250.

[429] Z.A. Zhang, Z.Y. Zhang, J. Li, Y.Q. Lai, J. Solid State Electrochem. 19 (2015) 1709.

[430] H. J. Peng, T. Z. Hou, Q. Zhang, J. Q. Huang, X. B. Cheng, M. Q. Guo, F. Wei, Adv. Mater. Interfaces 1 (2014) 7.

[431] Y. Chen, N. Liu, H. Shao, W. Wang, M. Gao, C. Li, H. Zhang, A. Wang, Y. Huang, J. Mater. Chem. A 3 (2015) 15235.

[432] G. Ma, F. Huang, Z. Wen, Q. Wang, X. Hong, J. Jin, X. Wu, J. Mater. Chem. A 4 (2016) 16968.

[433] H. Xiang, J. Chen, Z. Li, H. Wang, J. Power Sources 196 (2011) 8651.

[434] W.K. Zhang, C. Lin, S. Cong, J.Y. Hou, B. Liu, F.X. Geng, J. Jin, M.H. Wua, Z.G. Zhao, RSC Adv. 6 (2016) 15234.

[435] C. Lin, W.K. Zhang, L. Wang, Z.G. Wang, W. Zhao, W.H. Duan, Z.G. Zhao, B. Liu, J. Jin, J. Mater. Chem. A 4 (2016) 5993.

[436] X. Zhao, M. Liu, Y. Chen, B. Hou, N. Zhang, B. Chen, N. Yang, K. Chen, J. Li, L. An, J. Mater. Chem. A 3 (2015) 7870.

[437] J. Balach, T. Jaumann, S. Muhlenhoff, J. Eckert, L. Giebeler, Chem. Commun. 52 (2016) 8134

[438] Q. Xu, G.C. Hu, H.L. Bi, H.F. Xiang, Ionics 21 (2015) 981.

[439] R.S. Song, R.P. Fang, L. Wen, Y. Shi, S.G. Wang, F. Li, J. Power Sources 301 (2016) 179.

[440] Q.S. Wang, Z.Y. Wen, J.H. Yang, J. Jin, X. Huang, X.W. Wu, J.D. Han, J. Power Sources 306 (2016) 347.

[441] U. Stoeck, J. Balach, M. Klose, D. Wadewitz, E. Ahrens, J. Eckert, L. Giebeler, J. Power Sources 309 (2016) 76.

[442] J. Balach, T. Jaumann, M. Klose, S. Oswald, J. Eckert, L. Giebeler, J. Power Sources 303 (2016) 317.

[443] C.H. Chang, S.H. Chung, A. Manthiram, J. Mater. Chem. A 3 (2015) 18829.

[444] H. Shao, B. Huang, N. Liu, W. Wang, H. Zhang, A. Wang, F. Wang, Y. Huang, J. Mater. Chem. A 4 (2016) 16627.

[445] J. D. Zhu, C. Chen, Y. Lu, J. Zang, M.J. Jiang, D. Kim, X.W. Zhang, Carbon 101 (2016) 272.

[446] J. D. Zhu, E. Yildirim, K. Aly, J. L. Shen, C. Chen, Y. Lu, M. J. Jiang, D. Kim, A. Tonelli, M. A. Pasquinelli, P. D. Bradford, X. Zhang, J. Mater. Chem. A 4 (2016) 13572.

[447] C.B. Bucur, J. Muldoon, A. Lita, J.B. Schlenoff, R.A. Ghostine, S. Dietz, G. Allred, Energy Environ. Sci. 6 (2013) 3286.

[448] M. Agostini, J. Hassoun, Sci. Rep. 5 (2015) 7591.

[449] J.D. Zhu, M. Yanilmaz, K. Fu, C. Chen, Y. Lu, Y.Q. Ge, D. Kim, X.W. Zhang, J. Membr. Sci. 504 (2016) 89.

[450] J.D. Zhu, Y.Q. Ge, D. Kim, Y. Lu, C. Chen, M.J. Jiang, X.W. Zhang, Nano Energy 20 (2016) 176.

[451] Q. Wang, Electrochim. Acta. 182 (2015) 334.

[452] C.Y. Fan, H.Y. Yuan, H.H. Li, H.F. Wang, W.L. Li, H.Z. Sun, X.L. Wu, J.P. Zhang, ACS Appl. Mater. Interfaces. 8 (2016) 16108.

[453] N. Deng, W. Kang, Y. Liu, J. Ju, D. Wu, L. Li, B. S. Hassan, B. Cheng, J. Power Sources 330 (2016) 132.

[454] J. Yang, F. Chen, C. Li, T. Bai, B. Long, X. Zhou, J. Mater. Chem. A 4 (2016) 14324.

[455] L.-B. Xing, K. Xi, Q. Li, Z. Su, C. Lai, X. Zhao, R. V. Kumar, J. Power Sources 303 (2016) 22.

[456] S. Lu, Y. Cheng, X. Wu, J. Liu, Nano Lett. 13 (2013) 2485.

[457] R. Chen, T. Zhao, J. Lu, F. Wu, L. Li, J. Chen, G. Tan, Y. Ye, K. Amine, Nano Lett. 13 (2013) 4642.

[458] M. Zhao, X. Liu, Q. Zhang, G. Tian, J. Huang, W. Zhu, F. Wei, ACS Nano 6 (2012) 10759 .

[459] S. Niu, W. Lv, C. Zhang, F. Li, L. Tang, Y. He, B. Li, Q.-H. Yang, F. Kang, J. Mater. Chem. A 3 (2015) 20218.

[460] S. Niu, W. Lv, C. Zhang, Y. Shi, J. Zhao, B. Li, Q.-H. Yang, F. Kang, J. Power Sources 295 (2015) 182.

[461] Q. Q. Wang, J. B. Huang, G. R. Li, Z. Lin, B. H. Liu, Z. P. Li, J. Power Sources 339 (2016) 20.

[462] H. Peng, J. Huang, M. Zhao, Q. Zhang, X. Cheng, X. Liu, W. Qian, F. Wei, Adv. Funct. Mater. 24 (2014) 2772.

[463] X. Chen, Z. Xiao, X. Ning, Z. Liu, Z. Yang, C. Zou, S. Wang, X. Chen, Y. Chen, S. Huang, Adv. Energy Mater. 4(13) (2014) 1301988

[464] Y. S. Su, A. Manthiram, Nat. Commun. 3 (2012) 1166.

[465] J. Wang, Y. Yang, F. Kang, Electrochim. Acta 168 (2015) 271.

[466] Y. S. Su, A. Manthiram, Chem. Comm. 48 (2012) 8817.

[467] H. M. Kim, J.-Y. Hwang, A. Manthiram, Y.-K. Sun, ACS Appl. Mater. Interfaces 8 (2016) 983.

[468] X. Wang, Z. Wang, L. Chen, J. Power Sources 242 (2013) 65.

[469] L. Wang, Z. Yang, H. Nie, C. Gu, W. Hua, X. Xu, X. Chen, Y. Chen, S. Huang J. Mater. Chem. A 4 (2016) 15343.

[470] S. S. Zhang, D. Tran, Z. C. Zhang, J. Mat. Chem A 2 (2014) 18288.

[471] S.S. Madaeni, S. Zinadini, V. Vatanpour, J. Membr. Sci. 380 (2011) 155 ; P. Daraei, S.S. Madaeni, N. Ghaemi, H. Ahmadi Monfared, M.A. Khadivi, Sep. Purif. Technol. 104 (2013) 32.

[472] J.H. Kim, J. Seo, J. Choi, D. Shin, M. Carter, Y. Jeon, C.W. Wang, L.B. Hu, U. Paik, ACS Appl. Mater. Interfaces 8 (2016) 20092.

[473] M. Safa, A. Chamaani, N. Chawla, B. El-Zahab, Electrochim. Acta 213 (2016) 587.

[474] S. S. Zhang, D. T. Tran, Z. C. Zhang, J. Mater. Chem. A 2 (2014) 18288.

[475] C. Zu, Y.-S. Su, Y. Fu, A. Manthiram, Phys. Chem. Chem. Phys. 15 (2013) 2291.

[476] S.-H. Chung, A. Manthiram, ChemSusChem 7 (2014) 1655.

[477] Y. Huang, M. Zheng, Z. Lin, B. Zhao, S. Zhang, J. Yang, C. Zhu, H. Zhang, D. Sun, Y. Shi, J. Mater. Chem. A 3 (2015) 10910.

[478] C.L. Lee, I.D. Kim, Nanoscale 7 (2015) 10362.

[479] G. Ma, Z. Wen, Q. Wang, C. Shen, P. Peng, J. Jin, X. Wu, J. Power Sources 273 (2015) 511.

[480] G. Ma, Z. Wen, J. Jin, M. Wu, X. Wu, J. Zhang, J. Power Sources 267 (2014) 542.

[481] J.-Q. Huang, B. Zhang, Z.-L. Xu, S. Abouali, M. A. Garakani, J. Huang, J.-K. Kim, J. Power Sources 285 (2015) 43.

[482] Y. Yang, W. Sun, J. Zhang, X. Yue, Z. Wang, K. Sun, Electrochim. Acta 209 (2016) 691.

[483] Y. Liu, H. Li, G. Rubloff, C. Wang, L. Hu, Nano Energy 2 (2013) 1197.

[484] H.-K. Jing, L.-L. Kong, S. Liu, G.-R. Li, X.-P. Gao, J. Mater. Chem. A 3 (2015) 12213.

[485] G. Ma, Z. Wen, M. Wu, C. Shen, Q. Wang, J. Jin, X. Wu, Chem. Commun. 50 (2014) 14209.

[486] S. J. Oh, W. Y. Yoon, Int. J. Precision Engin. Manu. 15(7) (2014) 1453.

[487] S. S. Zhang, J. A. Read, J. Power Sources 200 (2012) 77.

[488] R. Demir-Cakan, M. Morcrette, Gangulibabu, A. Gueguen, R. Dedryvere, J. M. Tarascon, Energy Environ. Sci. 6 (2013) 176.

[489] C. Zu, Y. Fu, A. Manthiram, J. Mater. Chem. A 1 (2013) 10362.

[490] Y. Fu, Y. S. Su, A. Manthiram, Angew. Chem. Int. Ed. 52 (2013) 30 6930.

[491] M. Nagao, A. Hayashi, M. Tatsumisago, T. Ichinose, T. Ozaki, Y. Togawa, S. Mori, J. Power Sources 274 (2015) 471.

[492] L. Yin, J. Wang, X. Yu, C. W. Monroe, Y. NuLi, J. Yang, Chem. Comm. 48 (2012) 7868.

[493] J. Fanous, M. Wegner, J. Grimminger, Ä. Andresen, M. R. Buchmeiser, Chem. Mater. 23 (2011) 5024.

[494] L. Wang, X. He, J. Li, M. Chen, J. Gao, C. Jiang, Electrochim.Acta 72 (2012) 114.

[495] T.N.L. Doan, M. Ghaznavi, Y. Zhao, Y. Zhang, A. Konarov, M. Sadhu, R. Tangirala, P. Chen, J. Power Sources 241 (2013) 61.

[496] J. Wang, L. Yin, H. Jia, H. Yu, Y. He, J. Yang, C. W. Monroe, ChemSusChem. 7 (2014) 563.

[497] M. Agostini, Y. Aihara, T. Yamada, B. Scrosati, J. Hassoun, Solid State Ionics 244 (2013) 48.

[498] A. Hayashi, R. Ohtsubo, T. Ohtomo, F. Mizuno, M. Tatsumisago, J. Power Sources 183 (2008) 422.

[499] T. Kobayashi, Y. Imade, D. Shishihara, K. Homma, M. Nagao, R. Watanabe, T. Yokoi, A. Yamada, R. Kanno, T. Tatsumi, J. Power Sources 182 (2008) 621.

[500] Z. Lin, Z. Liu, W. Fu, N. J. Dudney, C. Liang, Angew. Chem. Int. Ed. 125 (2013) 7608

[501] W. J. Chung, J. J. Griebel, E. T. Kim, H. Yoon, A. G. Simmonds, H. J. Ji, P. T. Dirlam, R. S. Glass, J. J. Wie, N. A. Nguyen, B. W. Guralnick, J. Park, Somogyiarpad, P. Theato, M. E. Mackay, Y.-E. Sung, K. Char, J. Pyun, Nat. Chem. 5 (2013) 518.

[502] A. G. Simmonds, J. J. Griebel, J. Park, K. R. Kim, W. J. Chung, V. P. Oleshko, J. Kim, E. T. Kim, R. S. Glass, C. L. Soles, Y. E. Sung, K. Char, J. Pyun, ACS Macro Lett. 3 (2014) 229-232.

[503] J. He, Y. Chen, W. Lv, K. Wen, P. Li, F. Qi, Z. Wang, W. Zhang, Y. Li, W. Qin, W. He, J. Power Sources 327 (2016) 474.

[504] D.H. Wang, D. Xie, T. Yang, Y. Zhong, X.L. Wang, X.H. Xia, C.D. Gu, J.P. Tu, J. Power Sources 313 (2016) 233.

[505] M. Agostini, J. Hassoun, J. Liu, M. Jeong, H. Nara, T. Momma, T. Osaka, Y.K. Sun, B. Scrosati, ACS Appl. Mater. Interfaces 6 (2014) 10924.

[506] J. Hassoun, B. Scrosati, Angew. Chem. Int. Ed. 49 (2010) 2371.

[507] J. Hassoun, Y.K. Sun, B. Scrosati, J. Power Sources 196 (2011) 343.

[508] S.-K. Lee, Y. J. Lee, Y.-K. Sun, J. Power Sources 323 (2016) 174.

[509] X. Li, J. Liang, Y. Lu, Z. Hou, W. Zhang, Y. Zhu, Y. Qian, J. Power Sources 329 (2016) 379.

[510] J. Ni, Y. Zhao, T. Liu, H. Zheng, L. Gao, C. Yan, L. Li, Adv. Energy Mater. 4 (2014) 79.

[511] H. Jung, C.M. Park, H.J. Sohn, Electrochim. Acta 56 (2011) 2135.

[512] Y. Zhao, D. Gao, J. Ni, L. Gao, J. Yang, Y. Li, Nano Res. 7 (2014) 765.

[513] I. Gomez, D. Mecerreyes, J. A. Blazquez, O. Leonet, H. Ben Youcef C. Li, J. L. Gomez-Camer, O. Bondarchuk, L. Rodriguez-Martinez, J. Power Sources 329 (2016) 72.

[514] Z. Liu, X. Zheng, S.-L Luo, S.-Q. Xu, N.-Y. Yuan, J.-N. Ding J. Mater. Chem. A 4 (2016) 13395.

[515] Y. Fu, Y.S. Su, A. Manthiram, Adv. Energy Mater. 4 (2014) 655.

[516] D.H. Wang, X.H. Xia, D. Xie, X.Q. Niu, X. Ge, C.D. Gu, X.L. Wang, J.P. Tu, J. Power Sources 299 (2015) 293.

[517] V.C. Hoang, V.D. Do, I.W. Nah, C. Lee, W.I. Cho, I.H. Oh, Electrochim. Acta 210 (2016) 1.

[518] R. Elazari, G. Salitra, G. Gershinsky, A. Garsuch, A. Panchenko, D. Aurbach, Electrochem. Commun. 14 (2012) 21.

[519] Y. Yan, Y. Yin, S. Xin, J. Su, Y. Guo, L. Wan, Electrochim. Acta 91 (2013) 58.

[520] J. Brückner, S. Thieme, F. Böttger-Hiller, I. Bauer, H. T. Grossmann, P. Strubel, H. Althues, S. Spange, S. Kaskel, Adv. Funct. Mater. 24 (2014) 1284.

[521] C. Shen, M. Ge, A. Zhang, X. Fang, Y. Liu, J. Rong, C. Zhou, Nano Energy 19 (2016) 68.

Figure captions

Fig. 1. Discharge–charge profiles of a Li–S cell, illustrating regions (I) conversion of solid sulfur to soluble polysulfides; (II) conversion of polysulfides to solid Li_2S_2; (III) conversion of solid Li_2S_2 to solid Li_2S.

Fig. 2. Electrochemical properties of carbon-sulfur electrodes. Cycling performance and corresponding discharge voltage profiles of DUT-107/S cathodes measured in a full cell setup [61]. The anode was made of prelithiated hard carbon anode (LiHC@GDL) with a stable areal capacity of ca. 3.0 mAh cm^{-2}, as a substitute for lithium metal. The electrolyte was 1 mol L^{-1} LiTFSI + 0.25 mil $LiNO_3$ in DME/DOL (a and b) and 0.8 mol LiTFSI + 0.25 mol $LiNO_3$ + 0.15 mol Li_2S_6 in DME/DOL (c and d), respectively. The amount of electrolyte was 12 mL per mg of sulfur (mg_{sulfur}). The insets in the cycling experiments compare the initial (cycles 1–24) and final (cycles 4076–4100) discharge capacities at 0.1C. CE= coulombic efficiency. Reproduced with permission from the Royal society of Chemistry.

Fig. 3. Electrochemical characterizations of carbonized porous aromatic framework (SCPAF) electrode [68]. (a) CV profiles of SCPAF electrode at a sweep rate of 0.2 mV s^{-1}, (b) galvanostatic charge/discharge curves of SCPAF electrode at different cycle at 0.2C, (c) charge/discharge curves of the SCPAF electrode at different rates, (d) rate capability of SCPAF composites, (e) cycling performance of SCPAF electrode at a rate of 0.5C. Reproduced with permission from Elsevier.

Fig. 4. Cycling performances of multi-chambered micro/mesoporous carbon nanocube encapsulated sulfur non-coated (CNC-S) and coated with PEDOT (P@CNC-S) at 1C for 1000 cycles (1C=1673 mA g^{-1}) and their corresponding coulombic efficiencies [87]. The working electrodes were made from 80 wt.% of active materials, 10 wt.% of carbon black, and 10 wt.% of the binder polyvinylidene fluoride (PVDF) dissolved in N-methyl-2- pyrrolidone (NMP). Reproduced with permission from Elsevier.

Fig. 5 (a) Schematic of the procedure for fabricating (S-PDMS/GF) electrodes from a sulfur

slurry (70 wt.% pure sulfur, 20 wt.% carbon black, and 10 wt.% polyvinylidene fluoride (PVDF)) filtered into graphene/poly(dimethyl siloxane). (b) Cycling performance and Coulombic efficiency of the S-PDMS/GF electrode with a 10.1 mg cm^{-2} sulfur loading at 1500 mA g^{-1} for 1000 cycles [172]. Reproduced with permission from Elsevier.

Fig. 6. (a) Schematic of the synthetic process that involves coating of sulfur nanoparticles with TiO_2 to form sulfur–TiO_2 core–shell nanostructures, followed by partial dissolution of sulfur in toluene to achieve the yolk–shell morphology. (b) Charge/discharge capacity and Coulombic efficiency of sulfur–TiO_2 yolk–shell nanostructures over 1000 cycles at 0.5C [255]. Reproduced with permission from Nature Publishing Group.

Fig. 7. Cycling performance of a cell where macroporous carbon (MPC) is employed for sulfur retention in cathode, using different binders: PVDF, polyvinylpyrrolidone (PVP), Li^+-Nafion, polymer blend of Li^+-Nafion with PVP, and SiO_2-impregnated polymer blend as the binder at 25 °C [320]. Reproduced with permission from Elsevier.

Fig. 8. Discharge capacity (solid circle) and coulombic efficiencies (open circle) at 80 °C, 4C (dark yellow, after a three-cycle activation at 80 °C, 0.2C) and at 60 °C, 0.5C (purple), for a battery in which the cathode was fabricated from a slurry of PANI@C/S, carbon black (SuperP) and a binder (80:10:10 by weight). The electrolyte was a PEO–MIL-53(Al)–LiTFSI 60 μm-thick film [341]. Reproduced with permission from the Royal society of Chemistry.

Fig. 9. Effect of the modification of the separator with polypyrrole (PPy) nanotubes, PPy nanowires and reduced graphene oxide (rGO) [430]. a) The initial charge–discharge profiles; (b) the cycle performance and coulombic efficiencies of Li–S batteries with different separators at 0.2C; (c) the cycle performance and coulombic efficiencies of Li–S batteries with PPy nanotube modified separators at 0.5C. Reproduced with permission from the Royal society of Chemistry.

Fig. 10. Effect of porous sulfur–nitrogen dual-doped graphene (SNGE) interlayer coupled to a porous-carbon nanotube/S cathode (PCNT–S) [467]. (a) Nyquist curves from EIS measurements; (b) cycling performance and their corresponding galvanostatic discharge–charge profiles at 2C;

(c) cycling performance of SNGE–S-5:5 and SNGE–S@SNGE 3:5:2 cathodes at 5C; (d) cycling performance of SNGE–S@SNGE 3:5:2 cathode at elevated rate of 8C. Reproduced with permission from the Royal society of Chemistry.